



**A University of Sussex PhD thesis**

Available online via Sussex Research Online:

<http://sro.sussex.ac.uk/>

This thesis is protected by copyright which belongs to the author.

This thesis cannot be reproduced or quoted extensively from without first obtaining permission in writing from the Author

The content must not be changed in any way or sold commercially in any format or medium without the formal permission of the Author

When referring to this work, full bibliographic details including the author, title, awarding institution and date of the thesis must be given

Please visit Sussex Research Online for more information and further details



**High-order compact finite difference  
schemes for option pricing in stochastic  
volatility jump-diffusion models**

Alexander Pitkin

Submitted for the degree of Doctor of Philosophy

University of Sussex

September 2019

# Abstract

This thesis focusses on the derivation and implementation of high-order compact finite difference schemes to price a variety of options under various stochastic volatility and jump models, with the inclusion of further studies relating to the derivatives of options and the practice of hedging.

First, we derive a implicit-explicit high-order compact finite difference scheme for pricing European options under the Bates model. The resulting scheme is fourth order accurate in space and second order accurate in time. In the numerical study this scheme is compared to both a second order finite difference scheme and high-order finite element methods, where it outperforms both in terms of convergence, computational speed and required memory allocation. A numerical stability study is conducted which indicates unconditional stability of the scheme.

Second, we introduce the practice of hedging and give examples of hedging strategies created from a combination of option payoffs, we show the important role the derivatives of the option price play in forming profitable strategies. We go on to complete a study of the convergence of derivatives of the option price, the so-called Greeks. We conduct studies into Delta, vega and gamma hedging, where the derived high-order compact scheme outperforms a second-order finite difference method. Examples are provided to display how this increase in computational efficiency may assist financial practitioners.

Third, we extend the high-order compact scheme to price European options under the stochastic volatility with contemporaneous jumps model. The derived scheme is fourth order accurate in space and second order accurate in time. We conduct numerical studies to test the new high-order compact schemes convergence, computational speed and required memory allocation against a second-order finite difference scheme, where the results show improvements in convergence at the expense of computational time. Further studies of numerical stability indicate unconditional stability of the high-order compact scheme.

# Declaration

I hereby declare that this thesis has not been and will not be submitted in whole or in part to another University for the award of any other degree.

Signature:

Alexander Pitkin

# Acknowledgements

First I would like to offer a huge thank you to my supervisor Bertram Düring for his support and advice throughout my studies, he is a wonderful friend and provided a relaxed and enjoyable environment to discuss, learn and most importantly produce work that I am extremely proud of. Both he and the University of Sussex deserve great credit for the wonderful tutelage they have provided over the many years I have spent with them.

I would also like to extend a thank you to my friends and fellow students, who through encouragement, distraction and belief helped enormously in the completion of this work. Particular thanks to Dr Ella Hodder and Dr Nima Shahroozi who continue to surprise me with their kindness and generosity.

Finally I would like to thank my family who have given me endless support and encouragement, without you this would not have been possible.

# Contents

<b>List of Tables</b>	<b>viii</b>
<b>List of Figures</b>	<b>x</b>
<b>1 Introduction</b>	<b>1</b>
1.1 The history of options . . . . .	1
1.2 Financial Background and Terminology . . . . .	2
1.3 Early mathematical modelling of options . . . . .	6
1.3.1 Bachelier’s theory of speculation . . . . .	7
1.3.2 Sprenkle’s warrant prices and indicators of expectation . . . . .	8
1.4 Modern mathematical modelling of options . . . . .	9
1.4.1 The Black-Scholes Equation . . . . .	10
1.4.2 Jump-diffusion models . . . . .	12
1.4.3 Stochastic volatility models . . . . .	14
1.4.4 Stochastic volatility models with jumps . . . . .	17
1.5 Numerical Methods . . . . .	21
1.5.1 Finite element method . . . . .	21
1.5.2 Finite difference method . . . . .	24
1.5.3 High-order compact finite difference method . . . . .	25
1.5.4 Time-stepping scheme . . . . .	26
1.6 Overview of the thesis . . . . .	29
1.6.1 Numerical methods for option pricing . . . . .	30
1.6.2 Thesis structure and contributions to knowledge . . . . .	31
<b>2 High-order compact finite difference scheme for option pricing in stochastic volatility jump models</b>	<b>34</b>
2.1 Bates’ model . . . . .	35
2.2 Transformation of the equation . . . . .	36

2.3	Implicit-explicit (IMEX) scheme . . . . .	36
2.3.1	High-order compact scheme for the differential operator . . . . .	37
2.3.2	Integral operator . . . . .	42
2.3.3	Time discretisation for IMEX method . . . . .	43
2.4	Initial condition and boundary conditions . . . . .	43
2.4.1	Initial condition . . . . .	43
2.4.2	Boundary conditions . . . . .	44
2.5	A finite element method for comparison . . . . .	44
2.6	Numerical experiments . . . . .	45
2.6.1	Numerical convergence . . . . .	47
2.6.2	Computational efficiency comparison . . . . .	47
2.6.3	Numerical stability analysis . . . . .	50
2.6.4	Feller Condition . . . . .	53
2.7	Summary of chapter . . . . .	54
<b>3</b>	<b>Efficient hedging in Bates model using high-order compact finite differ-</b>	
	<b>ences</b>	<b>55</b>
3.1	The Bates PIDE for a European call option . . . . .	56
3.1.1	Numerical approximation . . . . .	57
3.1.2	Numerical convergence . . . . .	57
3.2	Option trading strategies . . . . .	58
3.2.1	Straddles . . . . .	58
3.2.2	Butterfly Spread . . . . .	62
3.3	The Greeks . . . . .	65
3.3.1	Delta . . . . .	66
3.3.2	Vega . . . . .	68
3.3.3	Gamma . . . . .	72
3.4	Summary of chapter . . . . .	75
<b>4</b>	<b>High-order compact finite difference scheme for option pricing in stochastic</b>	
	<b>volatility with contemporaneous jump models</b>	<b>77</b>
4.1	The SVCJ Model . . . . .	78
4.1.1	Partial Integro-Differential Equation . . . . .	79
4.1.2	Implicit-explicit high-order compact scheme . . . . .	80
4.1.3	Two-dimensional integral operator . . . . .	80

4.2	Numerical Experiments . . . . .	85
4.2.1	Numerical convergence . . . . .	86
4.2.2	Computational efficiency comparison . . . . .	86
4.2.3	Numerical stability analysis . . . . .	88
4.2.4	Feller Condition . . . . .	89
4.3	Bates/SVCJ model selection . . . . .	91
4.4	Summary of chapter . . . . .	94
<b>5</b>	<b>Conclusion</b>	<b>96</b>
	<b>Bibliography</b>	<b>100</b>
<b>A</b>	<b>Derivation of the Black-Scholes partial differential equation</b>	<b>108</b>
<b>B</b>	<b>Derivation of the Heston partial differential equation</b>	<b>110</b>
<b>C</b>	<b>Derivation of the Bates partial integro-differential equation</b>	<b>113</b>
<b>D</b>	<b>Code</b>	<b>115</b>

# List of Tables

2.1	Default parameters for numerical simulations associated with Bates' model.	46
2.2	Performance results for the HOC, second-order FD and FEM ( $p = 1, 2$ ) schemes for Bates' model. Comparison for computational time and memory usage between the finite difference schemes (HOC and second-order) and the FEM schemes ( $p = 1, 2$ ) are only indicative since implementations are different . . . . .	51
2.3	Parameters for different regimes of the Feller condition. . . . .	53
2.4	Numerical convergence results for HOC scheme for Bates' model with varying Feller condition. . . . .	54
3.1	Volatility, price of XYZ and respective straddle price with $T = 0.47$ , $K = 100$ .	61
3.2	Price of XYZ at expiry and associated profit of butterfly spread . . . . .	63
3.3	Price of XYZ at $T = 0.25$ and associated profit of butterfly spread for given volatility. . . . .	65
3.4	Percentage error in the value of the Delta-hedged portfolio for a move down in the underlying. . . . .	68
3.5	Percentage error in the value of the Delta-hedged portfolio for a move up in the underlying. . . . .	69
3.6	Percentage error in vega hedge ratio . . . . .	71
3.7	Percentage error in gamma hedge ratio . . . . .	75
4.1	Default parameters for numerical simulations associated with the SVCJ model. . . . .	85
4.2	Performance results for the HOC and second-order FD schemes for the SVCJ model. . . . .	88
4.3	Numerical convergence results for HOC scheme for the SVCJ model with varying Feller condition. . . . .	91

# List of Figures

1.1	Typical finite element discretisation, a triangular grid of a rectangle . . . . .	24
1.2	Typical finite difference discretisation . . . . .	25
1.3	Nine-point compact stencil . . . . .	26
2.1	Price of a European put option under Bates' model. . . . .	46
2.2	$l_2$ -error in European put option price under Bates' model taken at mesh-sizes $h = 0.4, 0.2, 0.1, 0.05$ . . . . .	48
2.3	$l_\infty$ -error in European put option price under Bates' model taken at mesh-sizes $h = 0.4, 0.2, 0.1, 0.05$ . . . . .	49
2.4	Computational speed comparison for pricing algorithms for Bates' model taken at mesh-sizes $h = 0.4, 0.2, 0.1, 0.05$ . . . . .	50
2.5	Contour plot of the $l_2$ -error for the HOC scheme for Bates' model. . . . .	52
2.6	Contour plot of the $l_2$ -error for second-order scheme for Bates' model. . . . .	53
3.1	Price of a European call option under Bates' model. . . . .	58
3.2	$l_2$ -error in European call option price under Bates' model taken at mesh-sizes $h = 0.4, 0.2, 0.1, 0.05$ . . . . .	59
3.3	$l_\infty$ -error in European call option price under Bates' model taken at mesh-sizes $h = 0.4, 0.2, 0.1, 0.05$ . . . . .	60
3.4	Payoff for long and short straddle strategies . . . . .	60
3.5	Price of long straddle with strike $K = 100$ , $T = 0.5$ . . . . .	62
3.6	Payoff for long and short butterfly strategies, options strike $K = 90, 100, 110$ . . . . .	63
3.7	Price of long butterfly, consisting of options with strike $K = 90, 100, 110$ and $T = 0.5$ . . . . .	64
3.8	Delta of European put option priced under Bates' model with parameters: Strike $K = 100$ , time to expiry $T = 0.5$ . . . . .	66

3.9	Convergence of $l_2$ -error of Delta of a European put option priced under Bates' model with parameters: Strike $K = 100$ , time to expiry $T = 0.5$ . . .	67
3.10	Convergence of $l_\infty$ -error of Delta of a European put option priced under Bates' model with parameters: Strike $K = 100$ , time to expiry $T = 0.5$ . . .	68
3.11	Vega of European put option priced under Bates' model with parameters: Strike $K = 100$ , time to expiry $T = 0.5$ . . . . .	70
3.12	Convergence of $l_2$ -error of the vega of a European put option priced under Bates' model with parameters: Strike $K = 100$ , time to expiry $T = 0.5$ . . .	70
3.13	Convergence of $l_\infty$ -error of the vega of a European put option priced under Bates' model with parameters: Strike $K = 100$ , time to expiry $T = 0.5$ . . .	71
3.14	Payoff for ratio vertical put spread, examples include a 1:2 spread, where the trader writes two put options then goes long one put option with a higher strike price. . . . .	72
3.15	Gamma of European put option priced under Bates model' with parameters: Strike $K = 100$ , time to expiry $T = 0.5$ . . . . .	73
3.16	Convergence of $l_2$ -error of gamma of a European put option priced under Bates' model with parameters: Strike $K = 100$ , time to expiry $T = 0.5$ . . .	74
3.17	Convergence of $l_\infty$ -error of gamma of a European put option priced under Bates' model with parameters: Strike $K = 100$ , time to expiry $T = 0.5$ . . .	74
4.1	$l_2$ error in European put option price under the SVCJ model taken at mesh-sizes $h = 0.4, 0.2, 0.1, 0.05$ . . . . .	86
4.2	$l_\infty$ error in European put option price under the SVCJ model taken at mesh-sizes $h = 0.4, 0.2, 0.1, 0.05$ . . . . .	87
4.3	Computational efficiency comparison taken at mesh-sizes $h = 0.4, 0.2, 0.1, 0.05$ .	89
4.4	Contour plot of the $l_2$ -error for the HOC scheme for the SVCJ model. . . .	90
4.5	Contour plot of the $l_2$ -error for second-order scheme for the SVCJ model. .	90
4.6	Time series of implied volatility as measured by the VIX index from 1987-2003, <i>Cboe</i> . . . . .	92
4.7	Time series of implied volatility as measured by the VIX index from 2003-2019, <i>Cboe</i> . . . . .	94

# Chapter 1

## Introduction

This thesis focusses on the derivation and implementation of high-order compact (HOC) finite difference schemes to price a variety of options under various stochastic volatility and jump models, with the inclusion of further studies relating to the derivatives of options and the practice of hedging. In this introduction we give a brief historical background into the derivatives markets, the use of options, pricing methods in the pre Black-Scholes era and the impact of modern option pricing theory through to the creation of the sophisticated pricing methods that form the basis of our research.

### 1.1 The history of options

Records of forward contracts date back as far as 1750 B.C, with clay tablets from Mesopotamia. Modern derivative markets featured in the 16th century onwards, with examples, in Europe connecting Antwerp via Amsterdam to London, and in America, in the cities of Chicago and New York [40, 45]. With the introduction of the transatlantic cable connecting Europe and America in 1866, the practice of international arbitrage of securities became possible [45]. An option arbitrageur, S.A. Nelson, describes an active intercontinental arbitrage market, with trading on both options and securities [65]. At this time up 500 messages per hour crossed the Atlantic between the London and New York markets via cable companies. With messages displaying at their destination in less than a minute.

Late 19th century Europe had many active option exchanges [48]. The different option exchanges in Europe at the time were named by H. Deutsch [24, 45]. The London Stock Exchange, the Continental Bourse, the Berlin Bourse, and the Paris Bourse are all mentioned and the potential for trading arbitrage options between these exchanges is discussed [45].

Technological advances over the 20th century have led to expansion of the global options markets and granted access to the average investor. Despite the majority of options transactions being executed electronically, there still remains an options presence in trading pits, with the CBOE in Chicago being at the centre of the options universe. Advances are still occurring, in 2014 trading in options on VIX futures expanded to 24 hours a day [64] and most major countries now have options markets and exchanges on products including; commodities, weather and stocks.

## 1.2 Financial Background and Terminology

Options are a type of financial derivative which allow market participants to take a sophisticated view on the market dynamics affecting the future price of a single, or group of, assets. There are numerous types of options traded on today's financial markets, including but not limited to; European options, American options, Asian options and similar exotic options. We now introduce the general definition of a financial option.

**Definition 1.1** (*European Call/Put*):

A **European Call/Put** represents a contract between the **writer** (party which sells the option) and the **holder** (party which buys the option). The contract offers the buyer the **right**, but not the obligation, to buy (**Call**) or sell (**Put**) an underlying asset  $S$  (e.g. a commodity or a stock) at an agreed fixed strike price  $K > 0$  on a specific date  $T > 0$ . The pay-off at time  $T$  of the European Call/Put is thus

$$C(S, T) = \max(S - K, 0) \quad \text{for a Call} \quad \text{and} \quad P(S, T) = \max(K - S, 0) \quad \text{for a Put}$$

$$\text{where } S \in \Omega := [0, \infty[$$

It is clear from this definition that an option price cannot be negative, as the holder has only the obligation, but not the right, to buy the underlying asset. It also alludes to the versatility of options as a tool for market participants to take a view on the direction and size of movements, whether this be for speculative or hedging purposes. To express this usefulness we give an example of each scenario

**Example 1.1** (*Speculation on a stock*):

An investor predicts, based on new balance sheet information, that the price of a specific stock  $S$  will fall. He chooses to buy a European Put on the stock at strike price  $K$ , which

is above the price the investor expects the stock to be at, once this news has been factored in and at expiry time  $T$ . The option is purchased for a price, denoted by  $P_0$ . The payoff for a European Put is  $P(S, T) = \max(K - S, 0)$ , giving the investor a profit equal to  $\max(K - S, 0) - P_0$  and a maximum loss of  $P_0$ , regardless of how the stock is valued at expiry time,  $T$ . Alternatively and based on the same information, the investor may have chosen to sell the stock directly, with the stock valued at price  $K$ . In both scenarios it is possible, through miscalculation or market drivers outside the scope of the investors model, that the stock price rises, in the second scenario the investors has loss equal to  $S_T - K$ . By selling the stock directly, it is highly likely the investor will suffer a much greater loss, as the options on a stock have a much lower price than the stock itself. In the investors expected scenario, the stock price has fallen and is below strike price  $K$  and the difference between using the stock directly and the options strategy equals  $P_0$ . As noted, with the value of stocks being higher than options in absolute terms, the difference between the profit of both strategies declines, whereas in the alternative case the investor is exposed to an unlimited potential loss when the stock is sold directly. Herein lies the security that options provide, and one reason for their popularity among speculators.

In the above example is is worthwhile to note, that if the speculator is willing to use the balance of a margin account for the designated trade and depending on the dynamics of the particular stock, they may be able to purchase numerous options to leverage their capital investment. Still with a fixed maximum loss, leveraging offers speculators another advantage associated with options as opposed to directly buying or selling the stock.

**Example 1.2** (*Hedging for profit forecasting*):

*At the upcoming shareholders annual general meeting a publicly listed airline is due to offer profit guidance over a 3 year time horizon. A major component in this calculation is the price of jet fuel. While it is possible for the CFO to base calculations on projected forward prices, to assure shareholders the airline decides to minimise exposure to the oil market and use current high oil production to its advantage by purchasing a number of European calls to cover a large proportion of the expected required quantity of jet fuel. In this scenario, in the event of drops in production leading to sudden price spikes within the oil markets, the airline is able to use its right to purchase jet fuel at the agreed upon strike price  $K$ , and hence is assured that one potential risk to profitability is mitigated. The cost associated with insuring against this risk is given by the value of the European call options and is classed as an initial investment. If the jet fuel price does not increase above  $K$ , the airline is able to decline the right to use the options and may purchase jet fuel at lower*

prices, foregoing the initial cost of the options. It is clear that in this instance maintaining a fair price for the options is of importance and the company must be able to value the options accurately.

Efficient hedging of risk using options is used in many industries, with other possible applications including, currency exchange risk and crop or commodity producers. A further application of hedging with mathematical grounding involves using the ‘so called’ Greeks, which denotes the derivatives of the option with respect to parameters affecting the stock price. Here an option trader may mitigate exposure to certain characteristics of financial markets by forming a portfolio of different options and or stock positions. The calculations involved in forming and maintaining these portfolios often require achieving an accurate value of the option price at the tails, far from the current asset price. This search for accuracy provides a topic of research interest for both academics and market participants.

To allow further flexibility as a market instrument, the properties of options are not limited to the European variety. One such example is the American option.

**Definition 1.2** (*American Call/Put*):

An **American Call/Put** represents a contract between the **writer** (party which sells the option) and the **holder** (party which buys the option). The contract offers the buyer the **right**, but not the obligation, to buy (**Call**) or sell (**Put**) an underlying asset  $S$  (e.g. a commodity or a stock) at an agreed fixed strike price  $K > 0$  at any time  $t$ , such that  $0 < t < T$ . The pay-off at time  $t$  of the American Call/Put is thus

$$C(S, t) = \max(S_t - K, 0) \quad \text{for a Call} \quad \text{and} \quad P(S, t) = \max(K - S_t, 0) \quad \text{for a Put}$$

$$\text{where } S \in \Omega := [0, \infty[, 0 \leq t < T$$

An American style option allows investors the possibility to exercise the option during the whole life of the option, so at any point *up to* the expiration date instead of just *at* the expiration date. This change has distinct advantages for speculators who are now able to capture profit as soon as the asset price moves favourably. With the ability to gain instantaneous profits, option markets feature participants, who neither speculate or hedge but simply trade and profit from the options themselves.

**Example 1.3** (*Options trading*):

*A proprietary trading firm employs options traders, focussing on the power markets. The traders look to profit from day trading the global options markets, meaning they only enter positions with the intention of closing them by the end of that day's trading. The firm's weather forecasting model suggests a localised storm pattern is due to affect energy production that day. The traders use this information to buy short-dated American call options on the power markets, with value  $C_0$ . If the forecasting model is correct and energy supply is reduced it is likely the options price will increase and the traders will be able to profit from the intraday move. In the outcome where the model is incorrect and the desired shortfall in energy does not occur, the trader exits the option at current market price. The resulting profit or loss of this trade will be  $C_T - C_0$ .*

When options trading over a short term horizon, the trader must account for the inclusion of exchange commissions or broker fees. This is the fee associated with maintaining the marketplace or facilitating the trade between the holder and writer of the option, these fees can be a significant factor when options are used for speculation as often positions will be entered and exited over short horizons.

Having defined European and American options, we omit definitions for the multitude of other options which are traded in financial markets across the globe as they are outside of the scope of this thesis. We do, however, give a notable mention to fixed-strike Asian options, which share the qualities of a European option. However, where the final price of the asset  $S$  is substituted for an average price taken over the duration of the option. This leads to the pay-off at time fixed time  $T$ , where  $C(S, T) = \max(A(0, T) - K, 0)$  for a Call and  $P(S, T) = \max(K - A(0, T), 0)$  for a Put, at fixed strike  $K$  and with  $A(0, T)$  defined as,

$$A(0, T) = \frac{1}{T} \int_0^T S(t) dt.$$

The price of an Asian option is path-dependent, which leads to a volatile marketplace as different investors hold different views over the outlook of the underlying asset. Asian options are one example of the complicated pricing problems associated with financial derivatives. They offer an insight into the many types of options, all with differing qualities suited to particular types of investor.

For the purpose of this thesis, we will study European options. As many index options are European style they are an important research topic, where improvements in pricing will offer potential benefits to a large proportion of financial market participants.

### 1.3 Early mathematical modelling of options

The price of an option represents a profile of the behaviour of the underlying asset. Having defined options economically and described the importance of options within the financial world, we now discuss the methods mathematicians have used to effectively model the price of options. In the previous definitions, the price of an option is only defined at expiration date  $T > 0$ . However, in order to effectively perform hedging trades with options it is critical to know the current fair price, a pursuit which has inspired many option pricing formulas and models.

The fair price of an option is determined by stochastically modelling the price movement of the underlying asset. It can be seen when looking at the chart of a stock price that the value of an underlying asset drifts through periods of stability and instability. Price changes can occur suddenly as a result of factors including; balance sheet publications, related central bank policy or broad currency fluctuations. The impact of these factors can have both positive or negative implications on the asset price, with the direction and magnitude of movement determined by the factors affect on the expected future performance of the stock. Clearly the future price of the underlying is the subject of uncertainty, mathematical models of this uncertainty are typically achieved through the application of the Wiener process.

The concise definition of this stochastic process underlying Brownian motion was given by Wiener [83], and yields the so-called Wiener process.

**Definition 1.3** *Wiener process/Brownian motion/Bachelier Process*

*A stochastic process  $X(t)$ ,  $t \geq 0$  is said to be a Brownian motion process if*

- (i)  $X(0) = 0$ ;*
- (ii)  $\{X(t), t \geq 0\}$  has stationary and independent increments;*
- (iii) for every  $t > 0$ ,  $X(t)$  is normally distributed with mean 0 and variance  $\sigma^2 t$*

The first mathematical explanation of the phenomenon of Brownian motion was given by Bachelier [4] in a doctoral thesis discussing speculation on the Paris stock exchange. In this paper, Bachelier interprets Brownian motion as the limit of random walks. The concept of Brownian motion to display the movement of an underlying asset is often described within the confines of a stochastic differential equation.

**Definition 1.4** *Stochastic differential equation*

*A stochastic differential equation is an integral of the form*

$$X(t) - X(0) = \int_0^t \mu(X(s), s) ds + \int_0^t \sigma(X(s), s) dW(s), \quad (1.1)$$

where the second integral term denotes an Itô Integral and  $X$  is a vector of  $n \in \mathbb{N} + \geq 1$  random variables and  $W$  is a vector of  $n$  Wiener processes. The vector  $\mu(X(t), t) \in \mathbb{R}^{n \times 1}$  denotes the drift and  $\sigma(X(t), t) \in \mathbb{R}^{n \times n}$  the correlation matrix between the Wiener processes. A widely used alternative notation for (1.1) is

$$dX(t) = \mu(X(t), t)dt + \sigma(X(t), t)dW(t).$$

### 1.3.1 Bachelier's theory of speculation

In an early example of mathematicians interest in option pricing, Bachelier introduces a model where the price of the underlying is assumed to be normally distributed [4], and describes how using combinations of futures and options could alter the risk-reward profile. Bachelier's examples include modern hedges such as bull spreads and call-back spreads [45]. The fundamental principle of this work was an equilibrium consideration which mirrors the more recent concept of an efficient market hypothesis. The price on the underlying asset can be described by the following stochastic differential equation.

$$dS(t) = \sigma dW(t),$$

with the price of the underlying asset  $S$  and the volatility of the underlying asset  $\sigma$ ,  $W$  is a Wiener process. We see this equation does not feature a drift term, as in (1.1), this is a consequence of the omission of a parameter describing non-zero interest rates.

Bachelier, also introduced a formula, for the price of a European call option  $C$ , given by

$$C(S, T) = (S - K)\Phi(d_1) + \sigma\sqrt{T}\varphi(d_1),$$

where  $d_1 = \frac{S-K}{\sigma\sqrt{T}}$ , with the price of the underlying asset  $S$ , the strike price  $K$ , time to expiration in years  $T$ , the volatility of the underlying asset  $\sigma$ , the cumulative normal distribution function  $\Phi(x) = \frac{1}{\sqrt{2\pi}} \int_{-\infty}^x e^{-t^2/2} dt$  and the standard normal density function  $\varphi(x) = \frac{1}{\sqrt{2\pi}} e^{-\frac{1}{2}x^2}$ .

Bachelier's assumption of a normal distribution for the asset price is limiting, albeit easy to work with. However, the assumption of a normal distribution overlooks the small prospect of asset prices turning negative as a result of a significant negative move [70].

This is not suitable for assets with limited liability features, such as stocks, and thus is clearly not applicable.

Further, Bachelier’s assumption of constant variance dependent on the length of the time interval, disregards the fact that volatility itself appears to be volatile and therefore should not be proportional to the length of the time interval [70, 27, 75].

Despite these drawbacks, the Bachelier thesis remains an important piece of literature. It offered an introduction to mathematicians looking at the financial derivatives market and has led to many naming him “the founder of mathematical finance and the father of modern option pricing theory”, R. Cont, p.213, 2004 [20].

### 1.3.2 Sprenkle’s warrant prices and indicators of expectation

Featuring in a revision of another doctoral thesis, we now look to the work of Sprenkle, [79], who created a model based on the assumption that asset prices were log-normally distributed and where the drift and volatility of the asset price are constant over time but relative to the asset price and not in absolute terms, an example of geometric Brownian motion.

#### **Definition 1.5** *Geometric Brownian motion*

*Let  $W(t)$  be a Wiener Process, then the solution of*

$$dX(t) = \mu X(t)dt + \sigma X(t)dW(t) \quad \text{for } t > 0$$

*is a **geometric Brownian motion**  $X(t)$  with constant drift  $\mu \in \mathbb{R}$  and constant volatility  $\sigma \in \mathbb{R}$  for time  $t \in [0, T]$ .*

*We have  $\mathbb{E}[dX(t)] = \mu X(t)dt$  and  $\mathbb{V}[dX(t)] = \sigma^2 X(t)^2 dt$ , as the expected value and variance, respectively.*

Sprenkle modelled asset prices with the stochastic differential equation,

$$dS = \mu Sdt + \sigma SdW,$$

where  $\mu$  is the rate of return of the underlying asset,  $\sigma$  is the volatility of the rate of return and  $dW$  is a Wiener process.

This model ruled out the possibility of negative asset prices, consistent with limited liability. With the inclusion of positive drift in the underlying asset Sprenkle derived an option pricing formula, where  $C$  is the value of a European call option

$$C(S, T) = Se^{\mu T} N(d_1) - (1 - A)KN(d_2),$$

where  $d_1 = \frac{\ln(S/K) + (\rho + \sigma^2/2)T}{\sigma\sqrt{T}}$ ,  $d_2 = d_1 - \sigma\sqrt{T}$  and  $A$  is the adjustment for the degree of market-risk aversion.

This formula requires the estimation of numerous parameters, including the the degree of risk aversion,  $A$ , and the average growth of return,  $\rho$ , for which a clear process is not defined and market derived parameter information is not readily available.

## 1.4 Modern mathematical modelling of options

Using the concept of geometric Brownian motion to model the behaviour of the underlying asset, a major breakthrough was achieved through the realisation that the option price was explicitly connected to that of the underlying asset through a hedging strategy. The derivation of this model requires a number of mathematical frameworks to be discussed. We begin by defining an Itô process [55].

### Definition 1.6 Itô Process

*An Itô Process is a generalised Wiener Process with expected value  $a(x, t)$  and standard deviation  $b(x, t)$ . It has the form*

$$dX(t) = a(X(t), t)dt + b(X(t), t)dW(t).$$

*The drift and variance of the process are functions of  $(X, t)$  and can change over time.*

We now state the Lemma of Itô, which is useful in obtaining partial differential equations from stochastic differential equations.

### Lemma 1.1 One-dimensional Lemma of Itô

*Let  $V : \mathbb{R} \times \mathbb{R}_+ \rightarrow \mathbb{R}$  be a function, where  $V$  is twice continuously differentiable in the first variable and continuously differentiable in the second variable. Furthermore let  $S(t)$  be an Itô process with drift  $f(S(t), t)$  and standard deviation  $g(S(t), t)$ ,*

$$dS(t) = f(S(t), t)dt + g(S(t), t)dW(t).$$

*Then*

$$dV(S(t), t) = \left( \frac{\partial V(S(t), t)}{\partial S} + \frac{\partial V(S(t), t)}{\partial t} + \frac{1}{2} \frac{\partial^2 V(S(t), t)}{\partial S^2} g^2(S(t), t) \right) dt + \frac{\partial V(S(t), t)}{\partial S} g(S(t), t) dW(t)$$

holds. This means that  $V(S(t), t)$  is again an Itô process with drift

$$\frac{\partial V(S(t), t)}{\partial S} f(S(t), t) + \frac{\partial V(S(t), t)}{\partial t} + \frac{1}{2} \frac{\partial^2 V(S(t), t)}{\partial S^2} g^2(S(t), t)$$

and standard deviation

$$\frac{\partial V(S(t), t)}{\partial S} g(S(t), t).$$

We now state the definition of a partial differential equation (PDE), which is an equation involving two or more independent variables, an unknown function and partial derivatives of the unknown function with respect to the independent variables. In this thesis we study a particular family of PDEs, namely parabolic PDEs, these are often used to describe time-dependent phenomena, including heat conduction, particle diffusion, and in our case the pricing of financial derivatives.

**Definition 1.7** *Linear second-order parabolic PDE*

A linear second-order parabolic PDE is an equation of the form

$$f \frac{\partial u}{\partial \tau} + a \frac{\partial^2 u}{\partial x^2} + b \frac{\partial^2 u}{\partial y^2} + c \frac{\partial u^2}{\partial x \partial y} + d \frac{\partial u}{\partial x} + e \frac{\partial u}{\partial y} = g \quad \text{in } \Omega \times \Omega_\tau$$

with initial condition  $u_0 = u(x, y, 0)$ , where  $\Omega \subset \mathbb{R}$  and  $\tau > 0$ , the equation is subject to suitable boundary conditions. The coefficients  $a, b, c, d, e, f$  and  $g$  are functions of  $(x, y, \tau) \in \Omega \times \Omega_\tau$  and subject to the condition  $a(x, y, \tau), b(x, y, \tau), c(x, y, \tau), d(x, y, \tau), e(x, y, \tau) \in C^2(\Omega)$  for any  $\tau \in \Omega_\tau$ .

### 1.4.1 The Black-Scholes Equation

It was Black, Scholes [11] and independently Merton [62] who realised that the expected return of the option price should be the risk free rate and that by holding a certain amount of stock, referred to as the Delta, the option position could be dynamically completely hedged allowing for an equation which omitted the expected rate of return.

The Black-Scholes model describes the motion of an underlying asset  $S$  with a geometric Brownian motion at time  $t > 0$ . In the method pioneered by Sprenkle, we have the stochastic differential equation,

$$dS(t) = \mu S(t)dt + \sigma S(t)dW(t),$$

where  $\mu$  is the constant drift,  $\sigma$  is the constant volatility of the asset  $S$  and  $dW$  is a Wiener process.

However, it was the use of Lemma 1.1, in combination with standard arbitrage arguments which allowed for the derivation a PDE and led to success of the Black-Scholes paper. This derivation can for example be found in [84] and is shown in Appendix A.

The resulting Black-Scholes equation, in the case of no-dividends, is written as

$$\frac{\partial V}{\partial t} + \frac{\sigma^2 S^2}{2} \frac{\partial^2 V}{\partial S^2} + rS \frac{\partial V}{\partial S} - rV = 0 \quad (1.2)$$

where, the variable  $S \in \mathbb{R}_{\geq 0}$  denotes the asset price, which is assumed to have constant volatility  $\sigma > 0$  over time. The risk-less interest rate is given by  $r \geq 0$ . To complete this problem, suitable final and boundary conditions are applied and a computational domain is chosen. The selection of lower bound is trivial, where  $S = 0$ . However, the upper bound must be artificially chosen, such that  $S_{\max} > 0$  is sufficiently large to model the asset price, resulting in spatial domain  $\Omega = [0, S_{\max}]$ .

The final condition for a European Call option, with strike price  $K > 0$ , is

$$V(S, T) = \max(S - K, 0).$$

This model may be applied to the variety of different options discussed in Section 1.2, simply by altering the final condition. In the special case of European options, (A) has a closed-form solution. For the price of a call option,  $C$ , the formula is

$$C(S, T) = S_0 \Phi \left( \frac{rT + \frac{\sigma^2 T}{2} + \ln \frac{S_0}{K}}{\sigma \sqrt{T}} \right) - K e^{-rT} \Phi \left( \frac{rT - \frac{\sigma^2 T}{2} + \ln \frac{S_0}{K}}{\sigma \sqrt{T}} \right),$$

where  $S_0$  is the initial price of the asset,  $\Phi(x)$  represents the cumulative distribution function of a standard normal variable and  $T$  is the amount of time until the option expires.

The success of the Black-Scholes formula is widely known, earning both Fischer Black and Myron Scholes Nobel prizes for their contributions. In the period following their publication, research in the area of option pricing intensified and as practitioners began to use the model to compute option prices, situations arose where the calculated prices did not match the financial market reality. Black-Scholes formula is only valid in circumstances where the asset price dynamics are described by a continuous-time diffusion process, with the sample path being continuous and of probability equal to 1 [63]. This indicates that if the asset price dynamics are not to able to be represented by a stochastic process with a continuous sample path, solutions from the Black-Scholes equation are not valid. In circumstances where the price processes feature large jumps, continuous-time models fail

to explain the reason for the jumps occurrence, in these instances better suited models are those featuring jump-diffusion [82].

### 1.4.2 Jump-diffusion models

Merton [63] pioneered the field of jump-diffusion models in the context of financial instruments, by allowing the underlying dynamics to have random jumps, which in turn reproduced more realistic tails behaviour for related log-returns. The approach first suggested by Merton was the catalyst for the development of what has become to be known as jump-diffusion type models. In these models, the idea of sudden and unexpected events are inbuilt because of the inclusion of random noise defined by a Poisson process [42].

**Definition 1.8** *Poisson Process*

Let  $\{\tau_i\}_{i \geq 1}$  be a sequence of exponential random variables with rate  $\lambda$ . Let  $T_n = \sum_{i=1}^n \tau_i$ . Then the Poisson process  $\{N_t\}_{t \geq 0}$  is defined as

$$N_t = \sum_{n \geq 1} 1_{t \geq T_n},$$

where the intensity  $\lambda$  is the expected number of jumps per unit time.

**Definition 1.9** *Compound Poisson Process*

Let  $\{Q_i\}_{i \geq 1}$  be a sequence of independent or identically distributed random variables exponential random variables and  $\{N_t\}_{t \geq 0}$  be a Poisson process with intensity parameter  $\lambda$ . Then the compound Poisson process  $\{Y_t\}_{t \geq 0}$  is defined by

$$Y_t = \sum_{i=1}^{N_t} Q_i,$$

with jump intensity  $\lambda$ , If  $N_t = 0$ , then  $Y_t$  is defined as  $Y_t = \sum_{i=1}^0 Q_i = 0$ .

### Merton's Jump model

Merton models the behaviour on the underlying asset using the following stochastic differential equation

$$\begin{cases} S|_{t=0} = S_0 > 0, \\ dS_t = (\mu - \lambda k)S_t dt + \sigma S_t dW_t + S_t dQ_t, \quad 0 < t \leq T, \end{cases} \quad (1.3)$$

where  $\{W_t\}_{0 \leq t \leq T}$  is a Brownian motion and  $\{Q_t\}_{0 \leq t \leq T}$  is a compound Poisson process, which takes the form

$$Q_t = \sum_{i=1}^{N_t} (Y_i - 1).$$

$$Y_i = \frac{S_{T_i}}{S_{T_{i-1}}} > 0, i \in N,$$

is the ratio of the price linked to the  $i$ -th jump on the time path of the asset price, which occurs at the random time  $T_i > 0$ . Merton assumes that the random variables  $\{Y_i\}_{i \in N}$  are i.i.d and additionally independent of both  $W_t$  and  $N_t$ , with  $N_t$  being a Poisson process of intensity  $\lambda > 0$ . Furthermore, it is assumed that,

$$V_i = \log Y_i \sim N(m, \delta^2)$$

with probability density

$$f_V(y) = \frac{1}{\delta\sqrt{2\pi}} e^{-\frac{(y-m)^2}{2\delta^2}}, \quad y \in \mathbb{R}.$$

Following pricing arguments it follows that,

$$\mathbb{E}[Q_t] = \lambda kt, 0 \leq t \leq T,$$

$$k = \mathbb{E}[Y_i - 1] = e^{m + \frac{\delta^2}{2}} - 1.$$

In (1.3), we defined a compensated variant of  $Q_t$ , which is a martingale. Therefore, the asset price can be modelled using the equation,

$$S_t = S_0 \exp\left\{\sigma W_t + \left(\mu - \lambda k - \frac{1}{2}\sigma^2\right)t\right\} \prod_{i=1}^{N_t} Y_i, \quad 0 \leq t \leq T.$$

Before describing any further properties of the Merton model, it is important to remember that such jump-diffusion models are not complete. In this Merton model, it is clear that there are multiple potential choices which can be used to define a martingale measure, for example the measure  $Q - P$ , leads to the discounted price  $e^{-rt} S_t$ , which is a martingale. Using this martingale, Merton describes the dynamics of the asset price under  $Q$  as,

$$S_t = S_0 \exp\left\{\sigma W_t^Q + \left(r - \lambda k - \frac{1}{2}\sigma^2\right)t\right\} \prod_{i=1}^{N_t} Y_i, \quad 0 \leq t \leq T.$$

This leads to a closed form solution, limited to jumps of Gaussian type and only valid in the specific case of European options. The price of a European call option can be written as, where  $C_{BS}$  is the Black-Scholes price of a European call option,

$$C_M(\tau, x) = \sum_{j=0}^{\infty} \exp^{-\lambda\tau} \frac{(\lambda\tau)^j}{j!} C_{BS}(\tau, x_j, \sigma_j), \quad (1.4)$$

where  $\sigma_j^2 = \sigma^2 + \frac{j\delta^2}{\tau}$  and  $x_j = x \exp\{jm + \frac{j\delta^2}{\tau} - \lambda\tau e^{m + \frac{\delta^2}{2}} + \lambda\tau\}$ . If  $\lambda = 0$  in (1.4) then  $C_M(\tau, x) = C_{BS}(\tau, x)$ .

Merton's jump model allows for the existence of sudden and unpredictable events present in financial markets. These are often caused by financial data releases, global conflicts, political tensions and natural disasters. These types of events cannot be taken into account by models based only on a Brownian type of noise, where behaviour is characterised using continuous trajectories.

Additionally, allowing the underlying dynamics to have random jumps reproduced the observed behaviour in the tails for related log-returns. Further research on this topic has led to a range of complex models, using jump processes to model the dynamics of asset prices [12, 58, 25, 21].

### 1.4.3 Stochastic volatility models

Focussing back on the Black-Scholes model, despite its clear successes, it features limitations which in reality do not match the observed price movements of assets. Firstly, the assumption of constant volatility and drift is only suited to short time periods, meaning the formula is inaccurate when looking at longer dated maturities. Secondly, the assumption that asset prices increase gradually over time does not allow for the possibility of extended bear markets. These factors may be overcome by using an Itô process.

The inclusion of time dependent deterministic drift and volatility allows for a more realistic model, where the value of options with longer dated maturities may be calculated more accurately. The Black-Scholes model's assumption of constant volatility has led to another notable measure, the Black-Scholes implied volatility. In financial markets it is noted, that when comparing the value of options on the same underlying asset, across different maturities and strike prices, the calculated volatilities of the options using the Black-Scholes model form a smile or skew pattern [23]. This feature has become a gauge used by many practitioners to predict future volatility in the financial markets.

These considerations have led to further adaptations and mathematical models which better fit the financial markets, including stochastic volatility models.

**Definition 1.10** *Stochastic volatility model*

There are a range of stochastic volatility models with varying methods of explaining the evolution of the volatility from  $t > 0$ , with a given initial volatility  $\sigma(0) > 0$ . These models are based on a two-dimensional stochastic diffusion process with two Brownian motions, correlated by  $\rho$ , i.e.

$$dW^{(1)}(t)dW^{(2)}(t) = \rho dt$$

with stochastic volatility  $\sigma(t)$ , we have

$$\begin{aligned} dS(t) &= \mu S(t)dt + \sqrt{\sigma(t)}S(t)dW^{(1)}(t), \\ d\sigma(t) &= a(\sigma(t))dt + b(\sigma(t))dW^{(2)}(t), \end{aligned}$$

where  $\mu$  is the drift of the asset,  $a(\sigma(t))$  and  $b(\sigma(t))$  denote the drift and diffusion coefficient of the stochastic volatility.

Stochastic volatility models have a two-dimensional stochastic process. In order to derive PDEs in this situation we must use the two-dimensional Lemma of Itô.

**Lemma 1.2** *Two-dimensional Lemma of Itô*

Let  $X(t)$  be a two-dimensional Itô process, i.e.

$$dX(t) = a(X(t), t)dt + b(X(t), t)dW(t)$$

with  $X(t) = (X^{(1)}(t), X^{(2)}(t))^{\top}$ ,  $W(t) = (W^{(1)}(t), W^{(2)}(t))^{\top}$ ,  
 $a(X(t), t) = (a_1(X(t), t), a_2(X(t), t))^{\top}$  and  $b(X(t), t) = (b_1(X(t), t), b_2(X(t), t))$ .

Further we have  $g : \mathbb{R}^n \times [0, \infty) \rightarrow \mathbb{R}^p$  with  $g \in C^2(\mathbb{R}^n \times [0, \infty))$ . Then  $Y(t) = g(X(t), t)$  is again an Itô process and for  $k = 1, \dots, p$  we have

$$\begin{aligned} dY(t)^{(k)} &= \frac{\partial g_k}{\partial t}(X(t), t)dt + \frac{\partial g_k}{\partial x_1}(X(t), t)dX(t)^{(1)} + \frac{\partial g_k}{\partial x_2}(X(t), t)dX(t)^{(2)} \\ &\quad + \frac{1}{2} \sum_{i,j=1}^2 \frac{\partial^2 g_k}{\partial x_i \partial x_j}(X(t), t)dX(t)^{(i)}dX(t)^{(j)}, \end{aligned}$$

where  $dW(t)^{(1)}dW(t)^{(2)} = \langle dW(t)^{(1)}, dW(t)^{(2)} \rangle dt$  with  $\langle dW(t)^{(1)}, dW(t)^{(2)} \rangle$  being the correlation between  $dW(t)^{(1)}$  and  $dW(t)^{(2)}$ . Therefore  $dt dt = 0$ ,  $dW(t)^{(1)}dt = 0$  as well as  $dt dW(t)^{(1)} = 0$  holds.

Scott, Hull and White [51, 52] generalised the model to allow stochastic volatility, this adaptation was shown to better explain the prices of currency options [61]. These papers did not offer closed form solutions to their models and require extensive use of numerical techniques to solve two-dimensional PDEs [53].

### Heston's closed-form solution for options with stochastic volatility

Heston [47] offered a model of stochastic volatility which moves away from those based on the Black-Scholes formula. Heston's model provides a closed-form solution for the price of a European call option, where the asset is correlated to the volatility and is capable of adaptations to incorporate stochastic interest rates, which makes it more suited to bond options and currency options.

Using the definition of a stochastic volatility model, the Heston model has variance following the square root process used by Cox, Ingersoll, and Ross (1985) [21].

$$d\sigma(t) = \kappa\sigma(t)(\theta - \sigma(t))dt + v\sigma(t)dW^{(2)}(t),$$

where  $\mu$  is the drift of the asset,  $\kappa$  denotes the mean reversion speed,  $v$  the volatility of the volatility and  $\theta$  the long run mean of  $\sigma$ .

Applying the two-dimensional lemma of Itô, Lemma 1.2 yields a second order parabolic PDE that has to be solved for the asset price  $S$ , the volatility  $\sigma$ , the time  $0 \leq t \leq T$  with  $T > 0$  and subject to final and boundary conditions dependent on the particular option being priced. The derivation of the PDE from the stochastic equation above can be found in Appendix B.

The Heston PDE is

$$\frac{\partial V}{\partial t} + \frac{1}{2}\sigma S^2 \frac{\partial^2 V}{\partial S^2} + \rho v \sigma S \frac{\partial^2 V}{\partial S \partial \sigma} + \frac{1}{2}v^2 \sigma \frac{\partial^2 V}{\partial \sigma^2} + rS \frac{\partial V}{\partial S} + \kappa(\theta - \sigma) \frac{\partial V}{\partial \sigma} - rV = 0,$$

with  $r > 0$  is the riskless interest rate and  $\kappa = \kappa^* + \lambda_0$ , with  $\lambda(S, \sigma, t) = \lambda_0 \sigma$  the market price of volatility risk and  $\theta = \frac{\kappa^* \theta^*}{\kappa^* + \lambda_0}$  as the long run mean of  $\sigma$ .

The Heston PDE holds where  $S \in [0, S_{\max}]$  with designated  $S_{\max} > 0$ ,  $\sigma \in [\sigma_{\min}, \sigma_{\max}]$  with  $0 \leq \sigma_{\min} < \sigma_{\max}$  and  $t \in [0, T[$  with  $T > 0$ , after imposing artificial boundary conditions for  $S$  and  $\sigma$  in a classical manner.

In the special case related to risk-neutral pricing of European options a closed-form solution is given. This is achieved by first converting the problem into characteristic functions, then using the Fourier inversion formula for probability distribution functions to find a more numerically robust form.

The characteristic function solution, subject to the terminal condition  $f_f(x, v, T; \phi) = e^{i\phi x}$ , is given by

$$f_f(x, v, t; \phi) = e^{C(T-t; \phi) + D(T-t; \phi)v + i\phi x},$$

where

$$\begin{aligned} C(\tau; \phi) &= r\phi i\tau + \frac{\kappa\theta}{\sigma^2} \left\{ (\kappa + \lambda - \rho\sigma\phi i + d)\tau - 2 \ln \left[ \frac{1 - ge^{d\tau}}{1 - g} \right] \right\}, \\ D(\tau; \phi) &= \frac{\kappa + \lambda - \rho\sigma\phi i + d}{\sigma^2} \left[ \frac{1 - e^{d\tau}}{1 - ge^{d\tau}} \right], \\ g &= \frac{\kappa + \lambda - \rho\sigma\phi i + d}{\kappa + \lambda - \rho\sigma\phi i - d}, \\ d &= \sqrt{(\rho\sigma\phi i - \kappa + \lambda)^2 - \sigma^2 \left( 2 \pm \frac{\phi i}{2} - \phi^2 \right)}. \end{aligned}$$

The inclusion of a closed form formula is particularly useful for practitioners looking to calibrate the model to market prices, as during the calibration process the repricing of many options is usually required in order to find the optimal parameters.

Stochastic volatility models account for the markets observed long term implied volatility smile or volatility skew [69]. The shape of this “smile” is dependent on the correlation,  $\rho$ , between the Weiner process affecting  $\sigma_t$  and  $dW_t$ , When  $\rho = 0$ , i.e.  $(\sigma_t)_{t \geq 0}$  and  $(W_t)_{t \geq 0}$  are independent, the implied volatility pattern forms a “smile”. Whereas if  $\rho < 0$  or  $\rho > 0$  the implied volatility curve forms a downward or upward volatility skew, respectively.

Stochastic volatility models pronounced implied volatility profile, however, does not feature for short-term maturities, as the effect of stochastic volatility becomes apparent in longer time scales. For short-term maturities the performance of stochastic volatility models is similar to that of the Black-Scholes model [60].

Furthermore, the positiveness of  $\sigma_t$  requires the use of a square root, Cox, Ingersoll and Ross, process. The CIR process, as in the case of Ornstein-Uhlenbeck processes, is mean reverting and yields nonlinear diffusion. Given these properties it is clear that a successful combination of the qualities of jump-diffusion models, introduced in Section 1.4.2 and stochastic volatility models would yield a model capable of a more accurate market representation [3].

#### 1.4.4 Stochastic volatility models with jumps

There are two ways to add jumps to stochastic volatility models, the first being to introduce jumps into the volatility process. One can use a positive Lèvy process to drive the volatility

$\sigma_t$  this allows for positive, mean-reverting volatility processes featuring realistic dynamics, whilst avoiding non-linear models, i.e. Ornstein-Uhlenbeck processes [37]. An example using this method is the model of Barndorff-Nielsen and Shephard [6].

The second method is to add jumps into the returns and in the evolution of volatility. By adding an independent jump component to the returns of a diffusion-based stochastic volatility model, we can improve the short-maturity behaviour of implied volatility without having an adverse impact on long-term smiles. This combination is famously achieved in Bates' model.

### **Bates' stochastic volatility with jumps model**

The stochastic volatility with jump-diffusion, SVJ, model introduced by Bates [7] inserts proportional log-normal jumps into the Heston stochastic volatility model. The model is formed by coupled stochastic differential equations describing the behaviour of the asset value,  $S$ , and its variance,  $\sigma$ , given by

$$\begin{aligned} dS(t) &= \mu_B S(t)dt + \sqrt{\sigma(t)}S(t)dW_1(t) + S(t)dJ, \\ d\sigma(t) &= \kappa(\theta - \sigma(t))dt + v\sqrt{\sigma(t)}dW_2(t), \end{aligned}$$

for  $0 \leq t \leq T$  and with  $S(0), \sigma(0) > 0$ . Here,  $\mu_B = r - \lambda\xi_B$  is the drift rate, where  $r \geq 0$  is the risk-free interest rate. The jump process  $J$  is a compound Poisson process with intensity  $\lambda \geq 0$  and  $J+1$  has a log-normal distribution  $p(\tilde{y})$  with the mean in  $\log(\tilde{y})$  being  $\gamma$  and the variance in  $\log(\tilde{y})$  being  $v^2$ , i.e. the probability density function is given by

$$p(\tilde{y}) = \frac{1}{\sqrt{2\pi\tilde{y}v}} e^{-\frac{(\log \tilde{y} - \gamma)^2}{2v^2}}.$$

The parameter  $\xi_B$  is defined by  $\xi_B = e^{\gamma + \frac{v^2}{2}} - 1$ . The variance has mean level  $\theta$ ,  $\kappa$  is the rate of reversion back to mean level of  $\sigma$  and  $v$  is the volatility of the variance  $\sigma$ . The two Wiener processes  $W_1$  and  $W_2$  have correlation  $\rho$ .

In Bates' model the shape of the volatility skew is determined on short-term intervals by the introduction of asymmetric jumps and in long-term intervals by the introduction of negative correlation between returns and volatility movements. The separation of these patterns allows practitioners to calibrate the model to fit both short maturities, through adjustment of the jump parameters, and longer maturities through the remaining parameters.

The inclusion of jump terms in the model means that rather than obtaining a PDE for the solution of the option price, we yield a partial integro-differential equation (PIDE). A

PIDE is a functional equation involving an unknown function  $f(x_1, x_2, \dots)$ , depending on independent variables  $x_1, x_2, \dots$ , together with both differential and integral operations on  $f$ . Specifically In the case of Bates' model we have a linear second-order parabolic PIDE. For details of the derivation of the PIDE from Bates' model, we refer to Appendix C.

**Definition 1.11** *Linear second-order parabolic PIDE*

A linear second-order parabolic PIDE is an equation of the form

$$f \frac{\partial u}{\partial \tau} + a \frac{\partial^2 u}{\partial x^2} + b \frac{\partial^2 u}{\partial y^2} + c \frac{\partial u^2}{\partial x \partial y} + d \frac{\partial u}{\partial x} + e \frac{\partial u}{\partial y} + \int_0^\tau k(x, y, \tau, z, u(x, y, \tau)) dz = g \quad \text{in } \Omega \times \Omega_\tau$$

with initial condition  $u_0 = u(x, y, 0)$ , where  $\Omega \in \mathbb{R}$  and  $\tau > 0$ , the equation is subject to suitable boundary conditions. The coefficients  $a, b, c, d, e, f$  and  $g$  are functions of  $(x, y, \tau) \in \Omega \times \Omega_\tau$  and subject to the condition  $a(x, y, \tau), b(x, y, \tau), c(x, y, \tau), d(x, y, \tau), e(x, y, \tau) \in C^2(\Omega)$  for any  $\tau$  in  $\Omega_\tau$ .

By standard derivative pricing arguments for the Bates model, we obtain the PIDE

$$\begin{aligned} \frac{\partial V}{\partial t} + \frac{1}{2} S^2 \sigma \frac{\partial^2 V}{\partial S^2} + \rho v \sigma S \frac{\partial^2 V}{\partial S \partial \sigma} + \frac{1}{2} v^2 \sigma \frac{\partial^2 V}{\partial \sigma^2} + (r - \lambda \xi_B) S \frac{\partial V}{\partial S} + \kappa(\theta - \sigma) \frac{\partial V}{\partial \sigma} - (r + \lambda) V \\ + \lambda \int_0^{+\infty} V(S\tilde{y}, v, t) p(\tilde{y}) d\tilde{y} = 0, \quad (1.5) \end{aligned}$$

which has to be solved for  $S, \sigma > 0$ ,  $0 \leq t < T$  and subject to a suitable final condition, e.g.  $V(S, \sigma, T) = \max(K - S, 0)$ , in the case of a European put option, with  $K$  denoting the strike price.

Under additional restrictions, closed form solutions to (1.5) can be obtained by Fourier methods (e.g. [20]). In general, however, one has to rely on numerical methods for option pricing under the Bates model. Moreover, in the case of American options, which feature an additional early exercise right. One has to solve a free boundary problem, consisting of a PIDE and an early exercise constraint for the option price. In this instance, numerical approximations are well suited to solving the problem.

**Duffie, Pan and Singleton's SVCJ model**

Studies of the volatility smiles implied by S&P 500 index options have shown that, while offering an improvement on solely jump or stochastic volatility models, stochastic-volatility models with jumps in returns are not fully able to produce the "smirk" seen in historical option prices [8, 5].

In an effort to overcome these shortcomings Duffie, Pan and Singleton proposed models which featured jumps in both returns and volatility [25]. These models allow jumps to be simultaneous, or have correlated stochastic arrival intensities and are named the SVCJ and SVJJ models, respectively.

The SVCJ model particularly can be seen as an extension of Bates' model and describes the behaviour of the asset value,  $S$ , and its variance,  $\sigma$ , by the coupled stochastic differential equations,

$$\begin{aligned} dS(t) &= \mu_S S(t)dt + \sqrt{\sigma(t)}S(t)dW_1(t) + S(t)dJ^S, \\ d\sigma(t) &= \kappa(\theta - \sigma(t)) + v\sqrt{\sigma(t)}dW_2(t) + dJ^\sigma, \end{aligned}$$

for  $0 \leq t \leq T$  and with  $S(0), \sigma(0) > 0$ . Here,  $\mu_S = r - \lambda\xi_S$  is the drift rate, where  $r \geq 0$  is the risk-free interest rate. The two-dimensional jump process  $(J^S, J^\sigma)$  is a compound Poisson process with intensity  $\lambda \geq 0$ . The distribution of the jump size in variance is assumed to be exponential with mean  $v$ . In respect to jump size  $z^\sigma$  in the variance process,  $J + 1$  has a log-normal distribution  $p(z^S, z^\sigma)$  with the mean in  $\log z^s$  being  $\gamma + \rho_J z^\sigma$ , i.e. the probability density function is given by

$$p(z^S, z^\sigma) = \frac{1}{\sqrt{2\pi}z^S\delta v} e^{-\frac{z^\sigma}{v} - \frac{(\log z^S - \gamma - \rho_J z^\sigma)^2}{2\delta^2}}.$$

The parameter  $\xi_s$  is defined by  $\xi_s = e^{\gamma + \frac{\delta^2}{2}}(1 - v\rho_J)^{-1} - 1$ , where  $\rho_J$  defines the correlation between jumps in returns and variance,  $\gamma$  is the jump size log-mean and  $\delta^2$  is the jump size log-variance. The variance has mean level  $\theta$ ,  $\kappa$  is the rate of reversion back to mean level of  $\sigma$  and  $v$  is the volatility of the variance  $\sigma$ . The two Wiener processes  $W_1$  and  $W_2$  have constant correlation  $\rho$ .

By standard derivative pricing arguments for the SVCJ model, we obtain the PIDE

$$\begin{aligned} \frac{\partial V}{\partial t} + \frac{1}{2}S^2\sigma \frac{\partial^2 V}{\partial S^2} + \rho v\sigma S \frac{\partial^2 V}{\partial S \partial \sigma} + \frac{1}{2}v^2\sigma \frac{\partial^2 V}{\partial \sigma^2} + (r - \lambda\xi_s)S \frac{\partial V}{\partial S} + \kappa(\theta - \sigma) \frac{\partial V}{\partial \sigma} \\ - (r + \lambda)V + \lambda \int_0^{+\infty} \int_0^{+\infty} V(S.z^S, \sigma + z^\sigma, t)p(z^S, z^\sigma) dz^\sigma dz^S = 0, \end{aligned}$$

which has to be solved for  $S, \sigma > 0$ ,  $0 \leq t < T$  and subject to a suitable final condition, e.g.  $V(S, \sigma, T) = \max(K - S, 0)$ , in the case of a European put option, with  $K$  denoting the strike price.

The addition of jumps to the volatility process in the SVCJ model allows for a degree of volatility of volatility sufficient to produce the implied volatility smiles observed in the previous studies [26]. However, as a result of the inclusion of jumps in the volatility process, a far higher analytical and computational cost is required than that of Bates' model.

We have seen, that for some option pricing models closed-form solutions are available for vanilla payoffs (see e.g. [25]) or at least approximate analytic expressions, see e.g. [9] and the literature cited therein. In general, however, one has to rely on numerical methods for pricing options.

## 1.5 Numerical Methods

For approximating the PDEs or PIDEs arising from option pricing, we can employ at least four different classes of numerical methods [1]. These include; finite difference methods, finite volume methods, spectral methods and finite element methods.

Finite difference methods are a popular choice, mainly for their simplicity. However, in cases where mesh adaptivity is important it can be difficult to control and minimise the numerical error (see e.g. [81] and the references therein).

Finite volume methods are more suited to hyperbolic PDEs, however, can be applied for Asian options when, as the option approaches maturity, the PDE becomes close to hyperbolic [86].

Spectral methods are Galerkin methods using Fourier series with high degree polynomials. They are best suited to problems with constant coefficients of the PDE, examples of their use can be seen in [50].

Finite element methods are complex, however, they are very flexible with regards to mesh adaptivity. In cases where key difficulties with implementation can be overcome they offer a powerful tool for financial problems [86].

We employ both finite element and finite difference methods and now introduce these methods in further detail.

### 1.5.1 Finite element method

The finite element method is a numerical technique, which performs finite element analysis of a physical phenomenon as described by a PDE [56]. The PDE is often referred to as the strong form, while the integral form is referred to as the weak form. The weak form of the problem is obtained by Green's Theorem.

**Definition 1.12** *Green's Theorem*

*Green's first formula states that*

$$\int_{\Omega} (\Delta u)v + \int_{\Omega} \nabla u \cdot \nabla v = \int_{\Gamma} (\partial_n u)v,$$

where  $\Omega$  is the domain in  $\mathbb{R}^2$  and  $\Gamma$  is boundary of the domain, where suitable boundary conditions are defined, with  $\Gamma_D$  denoting a Dirichlet boundary and  $\Gamma_N$  denoting a Neumann boundary.

To explain we consider a widely used two-dimensional elliptic PDE, the Laplace equation.

$$\Delta U = \nabla^2 U = \frac{\partial^2 U}{\partial x^2} + \frac{\partial^2 U}{\partial y^2} = 0, \quad \text{defined on } \Omega \in \mathbb{R}^2 \quad (1.6)$$

We set the domain  $\Omega = (0, 1)^2$  and choose only homogeneous Dirichlet boundary conditions, with  $U(\partial\Omega) = 0$  and  $\partial\Omega = \{(x, y) \mid x = 0, 1 \text{ or } y = 0, 1\}$ . This is the strong formulation. We now apply Green's theorem, where (1.6) is multiplied by a trial function,  $v(x, y)$ .

$$v\Delta U = v\nabla^2 U = 0$$

Integrating over the domain  $\Omega$  and using integration by parts, gives

$$\int_{\Omega} v\nabla^2 U = \int_{\Omega} \nabla(v\nabla U) - \int_{\Omega} \nabla v \cdot \nabla U. \quad (1.7)$$

Using Gauss' theorem on  $\nabla(v\nabla U)$ , we get

$$\int_{\Omega} \nabla(v\nabla U) = \int_{\partial\Omega} \underbrace{v}_{v|_{\partial\Omega}=0} \nabla U \cdot \hat{n} \, dS = 0,$$

where  $dS$  refers to an infinitesimal line segment. (1.7) now reduces to

$$\int_{\Omega} v\nabla^2 U = - \int_{\Omega} \nabla U \cdot \nabla v$$

hence, giving the final weak formulation as,

$$- \int_{\Omega} \nabla U \cdot \nabla v = 0$$

This process enables the order of continuity, which is required for the unknown function  $U(x, y)$  to be reduced by one. In the previous differential equation, we required  $U(x, y)$  to be differentiable at least twice, however in the integral equation  $U(x, y)$  is only required to be once differentiable. This holds for higher multi-dimensional functions, where the derivatives are replaced by gradients and/or divergence [56].

The weak form is discretised, with the domain being split into small pieces which are called *elements*. The corner point of each element is called a *node*, see Figure 1.1. The unknown functional  $U(x, y)$  is computed at the nodal points while interpolation functions must be defined for the purpose of interpolating the values inside the element, using

nodal values. These interpolation functions,  $\phi(x, y)$ , are also commonly known as *ansatz* functions. We are now able to reduce the unknown functional  $U(x, y)$  to

$$\hat{U}(x, y) = \sum_{i=1}^{nen} \hat{U}_i \phi_i(x, y),$$

with nodal basis

$$\hat{U}(x_j, y_j) = \sum_{i=1}^{nen} \hat{U}_i \phi_i(x_j, y_j) = \hat{U}_j,$$

where  $nen$  is the number of nodes in the element and  $\phi_i$  and  $U_i$  are the interpolation functions and the unknowns related to node ( $i$ ), respectively. We now define our approximation  $\hat{U}$ , trial function  $v$  and rewrite the weak form as

$$\hat{U}(x, y) = \sum_{i=1}^{nen} \hat{U}_i \phi_i(x, y), \quad v(x, y) = \sum_{j=1}^{nen} v_j \phi_j(x, y) \quad \text{and} \quad a(U, v) = \int_{\Omega} \nabla U \cdot \nabla v$$

Combining these expressions into  $a(U, v)$  and further manipulation yields,

$$a \left( \sum_{j=1}^{nen} v_j \phi_j, \sum_{i=1}^{nen} \hat{U}_i \phi_i \right) = \sum_{j=1}^{nen} \sum_{i=1}^{nen} a(v_j \phi_j, \hat{U}_i \phi_i) = \sum_{j=1}^{nen} v_j \sum_{i=1}^{nen} a(\phi_j, \phi_i) \hat{U}_i = 0$$

To solve this equation, it is written in compact form  $v^T A \hat{U} = 0$  with  $v = [v_1 \ v_3 \ \dots \ v_{nen}]^T$ ,  $\hat{U} = [\hat{U}_1 \ \hat{U}_3 \ \dots \ \hat{U}_{nen}]^T$  and

$$A = \begin{bmatrix} a(\phi_1, \phi_1) & a(\phi_1, \phi_2) & \cdots & a(\phi_1, \phi_{nen}) \\ a(\phi_2, \phi_1) & a(\phi_2, \phi_2) & \cdots & a(\phi_2, \phi_{nen}) \\ \vdots & \vdots & \ddots & \vdots \\ a(\phi_{nen}, \phi_1) & a(\phi_{nen}, \phi_2) & \cdots & a(\phi_{nen}, \phi_{nen}) \end{bmatrix}.$$

Boundary conditions are now applied, with  $\hat{U} = 0$  at the boundary and the linear system is solved through methods such as the Conjugate gradient method.

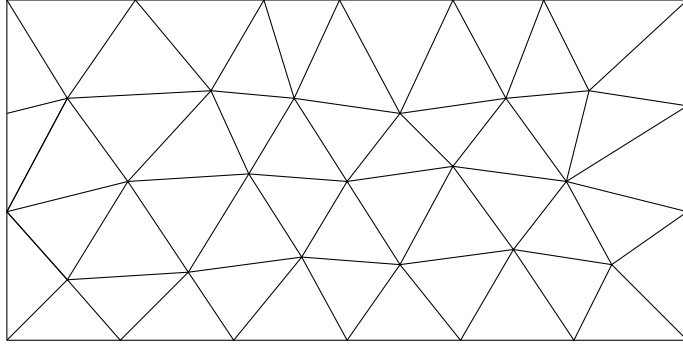


Figure 1.1: Typical finite element discretisation, a triangular grid of a rectangle

The order of the finite element method, is dependent on the interpolation functions chosen. Typical examples are linear, polynomial or cubic Lagrangian polynomials, giving order 1, 2 and 3, respectively. The choice of desired order is important as when the order of method is increased the number of unknowns in the numerical model increases. This leads to a greater computational time and can be prohibitive for financial applications where speed is important.

### 1.5.2 Finite difference method

The finite difference approximations for derivatives are one of the simplest and oldest methods to solve differential equations. The finite difference method works by supplanting the region that the independent variables in the PDE are defined on by a finite grid (mesh) of points at which the dependent variable is approximated [17]. The partial derivatives in the PDE are approximated at each grid point using neighbouring values obtained by Taylor's theorem.

**Theorem 1.13** *Taylor's Theorem*

Let  $U(x)$  have  $n$  continuous derivatives over the interval  $(a, b)$ . Then for  $a < x_0, x_0 + h < b$ ,

$$U(x_0 + h) = U(x_0) + h \frac{\partial U(x_0)}{\partial x} + \frac{h^2}{2!} \frac{\partial^2 U(x_0)}{\partial x^2} + \dots + \frac{h^{n-1}}{(n-1)!} \frac{\partial^{n-1} U(x_0)}{\partial x^{n-1}} + \mathcal{O}(h^n).$$

The conventional interpretation of Taylor's theorem is that if the value of  $U$  is known, and we know the values of its derivatives at point  $x_0$  then it is possible to find its value at the (nearby) point  $x_0 + h$ . If we discard the term  $\mathcal{O}(h^n)$ , we obtain an approximation to  $U(x_0 + h)$ , with error  $\mathcal{O}(h^n)$ .

To explain further we again refer to the Laplace equation (1.6), where

$$\frac{\partial^2 U}{\partial x^2} + \frac{\partial^2 U}{\partial y^2} = 0, \quad \text{defined on } \Omega \in \mathbb{R}^2$$

The computational domain,  $\Omega$ , is discretised by implementing constant grid spacings,  $\Delta x$  and  $\Delta y$ , in the  $x$  and  $y$  directions respectively. We then index grid points by  $(i, j)$  in the normal manner and denote the approximate value of  $U$  at grid point  $(i, j)$  as  $u_{(i,j)}$ . Figure 1.2 displays a uniform rectangular grid in the  $x$  and  $y$  directions, with  $\Delta x = \Delta y = h$  defined. The value of  $u$  is known at the boundary points, we are required to find  $u$  at the interior grid points.

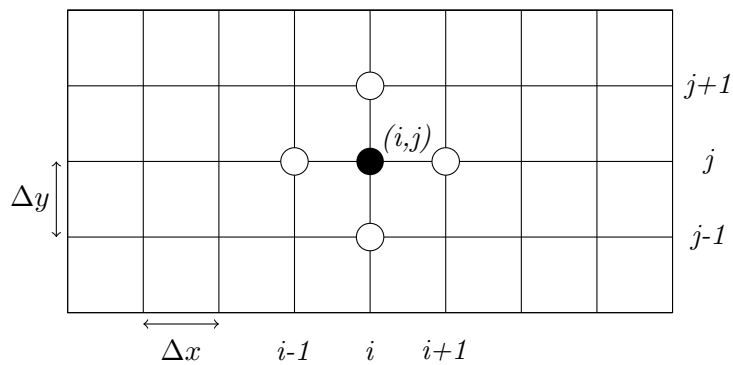


Figure 1.2: Typical finite difference discretisation

Each partial derivative in (1.6) is replaced by a central FD approximation, leaving,

$$\frac{u_{i+1,j} - 2u_{i,j} + u_{i-1,j}}{\Delta x^2} + \frac{u_{i,j+1} - 2u_{i,j} + u_{i,j-1}}{\Delta y^2} = 0,$$

which can be rearranged to give,

$$u_{i,j} = \frac{u_{i+1,j} + u_{i-1,j} + u_{i,j+1} + u_{i,j-1}}{4}.$$

with leading truncation error  $\tau_{i,j} = \frac{h^2}{6}(u_{xxxx} + u_{yyyy}) + \mathcal{O}(h^4)$ .

For higher-dimension systems, or systems with mixed derivative terms Taylor's theorem is applied in a similar manner. To increase the order of the system a larger stencil must be used, this leads to a high computational cost and adds the additional complication of ghost points, (points which are required in the stencil but are located outside of the domain).

### 1.5.3 High-order compact finite difference method

In recent years, high-order accurate compact finite difference methods have been increasingly used for numerically solving PDEs [43, 44, 77, 78, 57, 10]. These schemes exploit the

smoothness of solutions to elliptic and parabolic PDE problems in order to achieve high-order numerical convergence rates, typically larger than two in the spatial discretisation, while generally having good stability properties. This class of methods is also attractive since they offer a means to obtain high accuracy solutions with less computational costs. The computational stencil for HOC methods is composed of the desired point and its eight neighbouring points, see Figure 1.3.

We consider (1.5.2), on a square domain  $\Omega = (0, 1) \times (0, 1)$  with  $\Delta x = \Delta y$ . The domain  $\Omega$  is divided uniformly with lines  $\{(x_i, y_j) : x_i = ih, y_j = jh, i, j = 0, 1, \dots, J\}$ , where  $h$  is the spacial mesh-size. Using the notation  $\delta_x^2, \delta_y^2$  to denote the second-order central difference with respect to  $x, y$ , respectively:

$$\delta_x^2 u_{i,j} = \frac{u_{i-1,j} - 2u_{i,j} + u_{i+1,j}}{h^2}, \quad \delta_y^2 u_{i,j} = \frac{u_{i,j-1} - 2u_{i,j} + u_{i,j+1}}{h^2}.$$

By the Taylor series expansion, omitting the subscripts  $i, j$ , we get for every sufficiently smooth  $u$ ,

$$\delta_x^2 = \frac{\partial^2 u}{\partial x^2} + \frac{h^2}{12} \frac{\partial^4 u}{\partial x^4} + \frac{h^4}{360} \frac{\partial^6 u}{\partial x^6} + \mathcal{O}(h^6),$$

and (1.5.2) becomes,

$$\frac{\partial^2 u}{\partial x^2} + \frac{\partial^2 u}{\partial y^2} = (\delta_x^2 + \delta_y^2) u - \frac{h^2}{12} \left( \frac{\partial^4 u}{\partial x^4} + \frac{\partial^4 u}{\partial y^4} \right) - \frac{h^4}{360} \left( \frac{\partial^6 u}{\partial x^6} + \frac{\partial^6 u}{\partial y^6} \right) + \mathcal{O}(h^6).$$

Mixed derivatives are computed in a similar manner with the application of Taylor's theorem, this process is continued until the desired order is achieved.

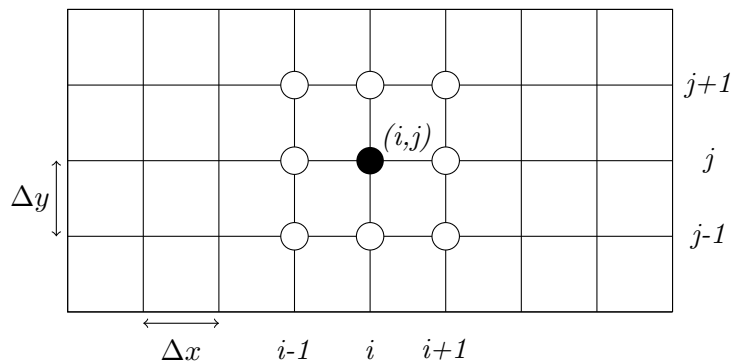


Figure 1.3: Nine-point compact stencil

#### 1.5.4 Time-stepping scheme

Having introduced the different discretisation techniques we now introduce the time-stepping scheme. For the discretisation in time there are numerous possibilities. Popular

one-step methods include the Explicit or Implicit Euler time discretisation or the Crank-Nicolson type time discretisation, while two-step methods include the alternating direction implicit method (ADI). Focussing on one-step methods, the Implicit and Explicit Euler methods are both first-order in time, while the Crank-Nicolson type time discretisation has been shown to converge with order two [84], allowing for high-order convergence to be achieved without loss of computation speed, often prohibitive to financial type problems.

To introduce these schemes, we consider the two-dimensional heat equation, which can be spatially discretised using either finite elements or finite differences, on both simple and compact stencils. For the case of this introduction we will focus on a standard finite difference approach.

The two-dimensional heat equation is a second order parabolic PDE which refers to the solution regarding the temperature  $U(x, y, t)$  in a thin plate as a function of time and position, with initial temperature and the boundary conditions of the plate given. We have

$$\frac{\partial U}{\partial t} = \beta \left( \frac{\partial^2 U}{\partial x^2} + \frac{\partial^2 U}{\partial y^2} \right), \quad 0 \leq t < T \quad (1.8)$$

with  $0 \leq x \leq 1$  and  $0 \leq y \leq 1$ , and with  $U(x, 0, t)$ ,  $U(x, 1, t)$ ,  $U(0, y, t)$ ,  $U(1, y, t)$  and  $U(x, y, 0)$  given.

### Explicit Euler

First looking at the Explicit, forward, Euler method, we discretise the LHS of (1.8) in time with time step  $\Delta t = T/m = k$ , leaving the first order finite difference approximation, given by

$$\frac{\partial U(x_i, y_j, t_k)}{\partial t} = \frac{u_{i,j}^{k+1} - u_{i,j}^k}{\Delta t} + \mathcal{O}(\Delta t).$$

Discretising the RHS of (1.8) using a second order central finite difference approximation, with  $\Delta x$  and  $\Delta y$  indicating the node spacing in both spatial directions, we have

$$\frac{u_{i,j}^{k+1} - u_{i,j}^k}{\Delta t} = \beta \left( \frac{U_{i,j+1}^k - 2U_{i,j}^k + U_{i,j-1}^k}{(\Delta x)^2} + \frac{U_{i+1,j}^k - 2U_{i,j}^k + U_{i-1,j}^k}{(\Delta y)^2} \right).$$

Rearranging, and setting  $s_x = \frac{\beta \Delta t}{\Delta x^2}$ ,  $s_y = \frac{\beta \Delta t}{\Delta y^2}$ , gives

$$U_{i,j}^{k+1} = U_{i,j}^k + s_x \left( U_{i,j+1}^k - 2U_{i,j}^k + U_{i,j-1}^k \right) + s_y \left( U_{i+1,j}^k - 2U_{i,j}^k + U_{i-1,j}^k \right).$$

The implementation of the Explicit Euler is simple, as each time-step is computed using known values. However, the disadvantage of this scheme is, that it is only stable if  $\frac{2\beta\Delta t}{\min((\Delta x)^2, (\Delta y)^2)} \leq 1$ , which imposes a restriction on the step-size needed to ensure convergence.

### Implicit Euler

The Implicit, backward, Euler method, is similar but has the benefit of being unconditionally stable. To develop this scheme we refer again to (1.8). We discretise the LHS in time with time step  $\Delta t = T/m = k$ , leaving the first order finite difference approximation, given by

$$\frac{\partial U(x_i, y_j, t_{k+1})}{\partial t} = \frac{u_{i,j}^{k+1} - u_{i,j}^k}{\Delta t} + \mathcal{O}(\Delta t)$$

Then discretising the RHS of (1.8) using a second order central finite difference approximation, with  $\Delta x$  and  $\Delta y$  indicating the node spacing in both spatial directions, we have

$$\frac{u_{i,j}^{k+1} - u_{i,j}^k}{\Delta t} = \beta \left( \frac{U_{i,j+1}^{k+1} - 2U_{i,j}^{k+1} + U_{i,j-1}^{k+1}}{(\Delta x)^2} + \frac{U_{i+1,j}^{k+1} - 2U_{i,j}^{k+1} + U_{i-1,j}^{k+1}}{(\Delta y)^2} \right).$$

Rearranging gives,

$$-s_y U_{i+1,j}^{k+1} - s_x U_{i,j+1}^{k+1} + (1 + 2s_x + 2s_y) U_{i,j}^{k+1} - s_y U_{i-1,j}^{k+1} - s_x U_{i,j-1}^{k+1} = U_{i,j}^k.$$

Which has to be solved through an equation of the form  $Ax = b$ , where  $b$  is a linearised list of the known solution at time-step  $k$ ,  $x$  is the unknown solution at time-step  $k+1$  and  $A$  is the stiffness matrix holding the equations. To solve for the unknown  $x$  the inverse of  $A$  must be computed, which requires the use of further numerical methods.

### Crank-Nicolson

The Crank-Nicolson scheme is the average of the Explicit and Implicit Euler schemes and is unconditionally stable, hence allowing large time steps to be taken while retaining stability. To develop this scheme we refer again to (1.8). We discretise the LHS in time with time step  $\Delta t = T/m = k$ , leaving the first order finite difference approximation, given by

$$\frac{\partial U(x_i, y_j, t_{k+\Delta t/2})}{\partial t} = \frac{u_{i,j}^{k+1} - u_{i,j}^k}{\Delta t} + \mathcal{O}(\Delta t)$$

Then discretising the RHS of (1.8) using a second order central finite difference approximation, with  $\Delta x$  and  $\Delta y$  indicating the node spacing in both spatial directions, we have

$$\begin{aligned} \frac{u_{i,j}^{k+1} - u_{i,j}^k}{\Delta t} = & \frac{\beta}{2} \left( \frac{U_{i,j+1}^{k+1} - 2U_{i,j}^{k+1} + U_{i,j-1}^{k+1}}{(\Delta x)^2} + \frac{U_{i+1,j}^{k+1} - 2U_{i,j}^{k+1} + U_{i-1,j}^{k+1}}{(\Delta y)^2} \right) + \\ & \frac{\beta}{2} \left( \frac{U_{i,j+1}^k - 2U_{i,j}^k + U_{i,j-1}^k}{(\Delta x)^2} + \frac{U_{i+1,j}^k - 2U_{i,j}^k + U_{i-1,j}^k}{(\Delta y)^2} \right), \end{aligned}$$

which is equivalent to,

$$\begin{aligned} u_{i,j}^{k+1} - \frac{s_x}{2} \left( U_{i,j+1}^{k+1} - 2U_{i,j}^{k+1} + U_{i,j-1}^{k+1} \right) - \frac{s_y}{2} \left( U_{i+1,j}^{k+1} - 2U_{i,j}^{k+1} + U_{i-1,j}^{k+1} \right) \\ = u_{i,j}^k + \frac{s_x}{2} \left( U_{i,j+1}^k - 2U_{i,j}^k + U_{i,j-1}^k \right) + \frac{s_y}{2} \left( U_{i+1,j}^k - 2U_{i,j}^k + U_{i-1,j}^k \right). \end{aligned}$$

As in the case of the fully implicit method, we again are required to solve through an equation of the form  $Ax = b$ . Where typically  $A$  is an  $(n-1)^2 \times (n-1)^2$  block-tridiagonal matrix, with blocks that are  $(n-1) \times (n-1)$ . The structure of the matrix  $A$ , allows for this calculation to be achieved with reduced computational costs. Widely applicable methods include a form of LU factorisation, where through Gaussian elimination a square matrix  $A$  is separated into a lower triangular matrix  $L$  and an upper triangular matrix  $U$ . This multiplication may also include a permutation matrix  $P$ , which may be left-multiplied by  $A$  in order to rearrange the rows of  $A$ . LUP factorisation can be achieved for all square matrices and is numerically stable [67].

To solve  $Ax = b$ , one first factorises  $A$  using LUP factorisation to give  $PA = LU$ , hence  $LUx = Pb$ . The solution is then computed in two stages, first, we must solve the equation  $Ly = Pb$  for  $y$  and second, we must solve the equation  $Ux = y$  for  $x$ . Both of these steps can be completed directly due to the triangular structure of  $L$  and  $U$  by forward and backward substitution. The above procedure can be repeatedly applied at each time-step and as the matrix  $A$  is not dependent on  $t$ , we only require a single LU decomposition of  $A$ .

## 1.6 Overview of the thesis

In this section we give an overview of the current literature regarding numerical methods for option pricing, before laying out the structure of the thesis, with a summary of each chapter and the contributions to knowledge. In each instance we state specifically the

roles of the author in the published works, which are the basis of each chapter and this thesis.

### 1.6.1 Numerical methods for option pricing

In the introduction we have given an overview of the classical models for pricing financial options, from the model of Bachelier [4], through to the model of Black and Scholes [11] and the more recent models which have been proposed to alleviate the shortcomings of their predecessors. Each model considers an underlying asset following a form of Brownian motion, while some models incorporate a second Brownian motion process for the volatility of the underlying asset.

We have shown that for some option pricing models closed-form solutions are available. In general, however, one has to rely on numerical methods for pricing options. The mathematical literature for pricing options using numerical methods is vast, however, much of this is focussed on option pricing models with a single risk factor, leading to partial differential equations in one spatial dimension, e.g. variants of the the Black-Scholes model. In many of these cases authors rely on standard finite difference methods to solve the pricing problem [81, 76]. For one-dimensional models with jump-diffusion we refer to [20, 26, 13, 72, 73].

Once we focus on option pricing models with more than one risk factor, e.g. in stochastic volatility models, which involve solving partial differential equations in two or more spatial dimensions, there are fewer works, e.g. [54] where different efficient methods for solving the American option pricing problem for the Heston model are proposed. Other approaches include finite element-finite volume [86], multigrid [19], sparse wavelet [50], FFT-based [71], spectral [85], hybrid tree-finite difference [14] methods and operator splitting techniques [49, 30, 33, 46, 31].

For problems which additionally include jumps in the underlying's process, and require the solution of PIDE in two or more spatial dimensions, there are even fewer works. We mention [74, 80] who propose an implicit-explicit time discretisation in combination with a standard, second-order finite difference discretisation in space for option prices under both the SVCJ and Bates models, [38] discusses and analyses an explicit discretisation for options priced with the Bates model. A method of lines algorithm for pricing American options under the Bates model is presented in [18]. An alternative approach is discussed in [15], where the authors combine tree methods and finite differences in a hybrid scheme for the Bates model with stochastic interest rates.

More recently, high-order finite difference schemes (fourth order in space) have been proposed for solving partial differential equations arising from stochastic volatility models. In [28] a high-order compact finite difference scheme for option pricing in the Heston model is derived. This approach is extended to non-uniform grids in [29], and to multiple space dimensions in [32].

We propose to further the literature by applying HOC finite differences to the Bates and SVCJ models. With current literature limited to standard second order schemes, we see an opportunity for significant improvements in computational efficiency, in a model which is highly regarded and frequently used in industry.

From an industry perspective, we anticipate traders will utilise our high-order scheme to enhance pricing models, through more accurate pricing on coarser grids. For example, this will better enable rapid computation of an option’s Delta for strategies which require frequent re-hedging.

The challenge of this proposal includes the algebraically demanding derivation of HOC schemes, which is often why these schemes are tailored to rather specific problems. In the literature they were originally proposed for the numerical approximation of problems, such as the Poisson or the heat equation and it is only gradually over the last two decades that progress has been made to extend this approach to more complex, and multi-dimensional or nonlinear, problems.

### 1.6.2 Thesis structure and contributions to knowledge

Chapter 2 is based on the article ‘High-order compact finite difference scheme for option pricing in stochastic volatility jump models’ published in the Journal of Computational and Applied Mathematics, is the collaborative work of Bertram Düring, and Alexander Pitkin [35]. While Düring proposed the study of this model and provided guidance and valuable advice for the work on this manuscript, the paper is primarily the original work of Alexander Pitkin and nearly all the results, including ideas, analysis and simulations, were obtained by Alexander Pitkin.

The originality of the work presented in this chapter consists in proposing a new *implicit-explicit high-order compact finite difference scheme* for option pricing in Bates model. To the best of this author’s knowledge it presents the first high-order scheme for this highly popular option pricing model. It combines a —suitably adapted— version of the high-order compact scheme from [28] with an explicit treatment of the integral term which matches the high-order, inspired by the work of Salmi *et al.* [74]. The new compact

scheme is fourth order accurate in space and second order accurate in time. We validate the stability of the scheme numerically and compare its performance to both standard finite difference methods and finite element approaches. The new scheme outperforms a standard discretisation based on a second-order central finite difference approximation. Compared to the finite element approach, it is very parsimonious in terms of memory requirements and computational effort, since it achieves high-order convergence without requiring additional unknowns —unlike finite element methods with higher polynomial order. At the same time, the new HOC scheme is very efficient, requiring only one initial  $LU$ -factorisation of a sparse matrix to perform the option price valuation. It can also be useful to upgrade existing implementations based on standard finite differences in a straightforward manner to obtain a highly efficient option pricing code.

Chapter 3 is based on the article ‘Efficient hedging in Bates model using high-order compact finite differences’ published in *Recent Advances in Mathematical and Statistical Methods for Scientific and Engineering Applications*, is the collaborative work of Bertram Düring, and Alexander Pitkin [34]. While Düring provided guidance and valuable advice for the work on this manuscript, the paper is primarily the original work of Alexander Pitkin and nearly all the results, including ideas, analysis and simulations, were obtained by Alexander Pitkin.

The originality of the work presented in this chapter consists of the evaluation of the hedging performance of the numerical option pricing scheme derived in Chapter 2. Through a series of experiments we compare the scheme’s hedging performance to standard finite difference methods. Furthermore we present examples of hedging strategies, involving combinations of options and their underlying assets. Throughout the results it is shown that the new scheme outperforms a standard discretisation, based on a second-order central finite difference approximation.

Chapter 4 is based on the article ‘High-order compact finite difference scheme for option pricing in stochastic volatility with contemporaneous jump models’ published in *Progress in Industrial Mathematics at ECMI 2018*, is the collaborative work of Bertram Düring, and Alexander Pitkin [36]. While Düring proposed the study of this model and provided guidance and valuable advice for the work on this manuscript, the paper is primarily the original work of Alexander Pitkin and nearly all the results, including ideas, analysis and simulations, were obtained by Alexander Pitkin.

The originality of the work presented in this chapter consists in proposing a new *implicit-explicit high-order compact finite difference scheme* for option pricing in the SVCJ

model, derived by Duffie, Pan and Singleton [25]. To the best of this author's knowledge it presents the first high-order scheme for this complex option pricing model. It involves a suitably adapted version of the high-order compact scheme introduced in Chapter 2 with an explicit treatment of the double integral term which matches the high-order. The new compact scheme is fourth order accurate in space and second order accurate in time. We validate the stability of the scheme numerically and compare its performance to a standard finite difference approach. The new scheme outperforms a standard discretisation based on a second-order central finite difference approximation in terms of convergence.

## Chapter 2

# High-order compact finite difference scheme for option pricing in stochastic volatility jump models

The evolution in option pricing models has been motivated by the desire to achieve a model with enough calibration flexibility to produce the observed market prices, which across the broad variety of financial assets is a vast challenge.

The publication of the widely successful Black-Scholes model [11] led to a period of intense research into pricing financial derivatives. Of the numerous research papers published since, many have helped to alleviate the shortcomings of this model and to produce an ever more accurate representation of observed option prices.

Two key advances were brought about with by the jump diffusion model of Merton [63] and models including stochastic volatility, notably by Heston [47]. These two models individually compensate for many of the market observed option price characteristics, such as jumps in the price of the underlying asset and observed volatility smiles featured across stock and currency market option prices, however, it was thought a combination of both models had potential to yield the desired model with vast calibration offerings.

Bates' model [7] adds jumps into the returns and in the evolution of volatility. It is a quasi market standard for option pricing and as closed form solutions are only available under certain assumptions, a prime candidate for the application of efficient numerical methods. In this chapter we shall apply numerical methods to Bates' model with the

intention of deriving a pricing algorithm which offers high-order convergence, through application of the HOC finite difference stencils, introduced in Section 1.5.3.

This chapter is organised as follows. In the next section we recall Bates' model for option pricing and the related PIDE. Section 2.2 is devoted to a variable transformation for the problem. The new scheme is derived in Section 2.3. The smoothing of the initial condition and the discretisation of the boundary conditions are discussed in Section 2.4. In Section 2.5 we state the finite element formulation which we use for the numerical comparison experiments. In Section 2.6 we present numerical convergence and stability results and investigate and compare the efficiency of the scheme to other methods. Section 2.7 summarises this chapter.

## 2.1 Bates' model

Bates' model introduced in Section 1.4.4 is a stochastic volatility model which allows for jumps in returns [7]. Within this model the behaviour of the asset value,  $S$ , and its variance,  $\sigma$ , is described by the coupled stochastic differential equations,

$$\begin{aligned} dS(t) &= \mu_B S(t)dt + \sqrt{\sigma(t)}S(t)dW_1(t) + S(t)dJ, \\ d\sigma(t) &= \kappa(\theta - \sigma(t))dt + v\sqrt{\sigma(t)}dW_2(t), \end{aligned}$$

for  $0 \leq t \leq T$  and with  $S(0), \sigma(0) > 0$ . Here,  $\mu_B = r - \lambda\xi_B$  is the drift rate, where  $r \geq 0$  is the risk-free interest rate. The jump process  $J$  is a compound Poisson process with intensity  $\lambda \geq 0$  and  $J+1$  has a log-normal distribution  $p(\tilde{y})$  with the mean in  $\log(\tilde{y})$  being  $\gamma$  and the variance in  $\log(\tilde{y})$  being  $v^2$ , i.e. the probability density function is given by

$$p(\tilde{y}) = \frac{1}{\sqrt{2\pi\tilde{y}v}} e^{-\frac{(\log \tilde{y} - \gamma)^2}{2v^2}}.$$

The parameter  $\xi_B$  is defined by  $\xi_B = e^{\gamma + \frac{v^2}{2}} - 1$ . The variance has mean level  $\theta$ ,  $\kappa$  is the rate of reversion back to mean level of  $\sigma$  and  $v$  is the volatility of the variance  $\sigma$ . The two Wiener processes  $W_1$  and  $W_2$  have correlation  $\rho$ .

By standard derivative pricing arguments for the Bates model, we obtain the PIDE

$$\begin{aligned} \frac{\partial V}{\partial t} + \frac{1}{2}S^2\sigma \frac{\partial^2 V}{\partial S^2} + \rho v\sigma S \frac{\partial^2 V}{\partial S \partial \sigma} + \frac{1}{2}v^2\sigma \frac{\partial^2 V}{\partial \sigma^2} + (r - \lambda\xi_B)S \frac{\partial V}{\partial S} + \kappa(\theta - \sigma) \frac{\partial V}{\partial \sigma} - (r + \lambda)V \\ + \lambda \int_0^{+\infty} V(S\tilde{y}, v, t)p(\tilde{y}) d\tilde{y} = L_D V + L_I V = 0, \end{aligned} \quad (2.1)$$

which has to be solved for  $S, \sigma > 0$ ,  $0 \leq t < T$  and subject to a suitable final condition, e.g.  $V(S, \sigma, T) = \max(K - S, 0)$ , in the case of a European put option, with  $K$  denoting

the strike price. For clarity the operators  $L_D V$  and  $L_I V$  are defined as the differential part (including the term  $-(r + \lambda)V$ ) and the integral part, respectively.

## 2.2 Transformation of the equation

Using the transformation of variables

$$x = \log S, \quad \tau = T - t, \quad y = \frac{\sigma}{v} \quad \text{and} \quad u = \exp(r + \lambda)V,$$

we obtain

$$u_\tau = \frac{1}{2}vy \left( \frac{\partial^2 u}{\partial x^2} + \frac{\partial^2 u}{\partial y^2} \right) + \rho v y \frac{\partial^2 u}{\partial x \partial y} - \left( \frac{1}{2}vy - r + \lambda \xi_B \right) \frac{\partial u}{\partial x} + \kappa \frac{(\theta - vy)}{v} \frac{\partial u}{\partial y} + \exp(r + \lambda)L_I V, \quad (2.2)$$

which is now posed on  $\mathbb{R} \times \mathbb{R}^+ \times (0, T)$ , with

$$L_I V = \lambda \int_0^\infty V(S\tilde{y}, v, t)p(\tilde{y}) d\tilde{y}.$$

Applying the same transformation to the intergral term,  $L_I$ ,

$$\exp(r + \lambda)L_I V = \lambda \int_0^{+\infty} u(x\tilde{y}, y, \tau)p(\tilde{y}) d\tilde{y}.$$

Now by setting  $z = \log \tilde{y}$ ,  $\tilde{u}(z, y, \tau) = u(e^z, y, \tau)$  and  $\tilde{p}(z) = e^z p(e^z)$  we have

$$\exp(r + \lambda)L_I V = \lambda \int_0^{+\infty} u(x\tilde{y}, y, \tau)p(\tilde{y}) d\tilde{y} = \lambda \int_{-\infty}^{+\infty} \tilde{u}(x + z, y, \tau)\tilde{p}(z) dz.$$

The problem is completed by the following initial and boundary conditions:

$$u(x, y, 0) = \max(1 - \exp(x), 0), \quad x \in \mathbb{R}, \quad y > 0,$$

$$u(x, y, t) \rightarrow 1, \quad x \rightarrow -\infty, \quad y > 0, \quad t > 0,$$

$$u(x, y, t) \rightarrow 0, \quad x \rightarrow +\infty, \quad y > 0, \quad t > 0,$$

$$u_y(x, y, t) \rightarrow 0, \quad x \in \mathbb{R}, \quad y \rightarrow \infty, \quad t > 0,$$

$$u_y(x, y, t) \rightarrow 0, \quad x \in \mathbb{R}, \quad y \rightarrow 0, \quad t > 0.$$

## 2.3 Implicit-explicit (IMEX) scheme

Following the idea employed by Salmi, Toivanen and von Sydow in [74, 80], we accomplish the implicit-explicit discretisation in time by means of the IMEX-CN method. This method is an adaptation of the Crank-Nicholson method, whereby an explicit treatment is added for the integral operator. To achieve high-order convergence we adapt the HOC finite difference scheme developed in [28] to implicitly approximate the differential operator, while we evaluate the integral explicitly using the Simpson's rule to match the high-order accuracy of the high-order compact scheme.

### 2.3.1 High-order compact scheme for the differential operator

Following the discretisation employed in [28], we replace  $\mathbb{R}$  by  $[-R_1, R_1]$  and  $\mathbb{R}^+$  by  $[L_2, R_2]$  with  $R_1, R_2 > L_2 > 0$ . We consider a uniform grid  $Z = \{x_i \in [-R_1, R_1] : x_i = ih_1, i = -N, \dots, N\} \times \{y_j \in [L_2, R_2] : y_j = L_2 + jh_2, j = 0, \dots, M\}$  consisting of  $(2N + 1) \times (M + 1)$  grid points with  $R_1 = Nh_1$ ,  $R_2 = L_2 + Mh_2$  and with space steps  $h_1, h_2$  and time step  $k$ . Let  $u_{i,j}^n$  denote the approximate solution of (2.2) in  $(x_i, y_j)$  at the time  $t_n = nk$  and let  $u^n = (u_{i,j}^n)$ .

#### Convection-Diffusion problem

We introduce the HOC discretisation for the convection-diffusion problem with Laplacian operator,

$$-\frac{1}{2}vy \left( \frac{\partial^2 u}{\partial x^2} + \frac{\partial^2 u}{\partial y^2} \right) - y\rho v \frac{\partial^2 u}{\partial x \partial y} - \left( r - \frac{1}{2}vy - \lambda\xi_B \right) \frac{\partial u}{\partial x} - \kappa \frac{(\theta - vy)}{v} \frac{\partial u}{\partial y} = f(x, y). \quad (2.3)$$

We construct a fourth-order compact finite difference scheme with a nine-point computational stencil using the eight nearest neighbouring points around a reference grid point  $(i, j)$ , following the approach in [28]. The idea behind the derivation of the HOC scheme is to operate on the differential equations as an auxiliary relation to obtain finite difference approximations for high-order derivatives in the truncation error. Inclusion of these expressions in a central difference approximation increases the order of accuracy while retaining a compact computational stencil.

Introducing a uniform grid with mesh spacing  $h = h_1 = h_2$  in both the  $x$ - and  $y$ -directions, the standard central difference approximation to equation (2.3) at grid point  $(i, j)$  is

$$-\frac{1}{2}vy_j (\delta_x^2 u_{i,j} + \delta_y^2 u_{i,j}) - \rho v y_j \delta_x \delta_y u_{i,j} + \left( \frac{1}{2}v y_j - r + \lambda\xi_B \right) \delta_x u_{i,j} - \kappa \frac{(\theta - v y_j)}{v} \delta_y u_{i,j} - \tau_{i,j} = f(i, j), \quad (2.4)$$

where  $\delta_x$  and  $\delta_x^2$  ( $\delta_y$  and  $\delta_y^2$ , respectively) denote the first and second order central difference approximations with respect to  $x$  (with respect to  $y$ ). The associated truncation error is given by

$$\tau_{i,j} = \frac{1}{24}vyh^2 (u_{xxxx} + u_{yyyy}) + \frac{1}{6}\rho v y h^2 (u_{xyyy} + u_{xxyy}) + \frac{1}{12}(2r - vy - 2\lambda\xi_B) h^2 u_{xxx} + \frac{1}{6} \frac{\kappa(\theta - vy)}{v} h^2 u_{yyy} + \mathcal{O}(h^4). \quad (2.5)$$

For the sake of clarity the subindices  $j$  and  $(i, j)$  on  $y_j$  and  $u_{i,j}$  (and its derivatives) are omitted from here. Differentiating (2.3) with respect to  $x$  and  $y$ , respectively, yields,

$$u_{xxx} = -u_{xyy} - 2\rho u_{xxy} + \frac{2\lambda\xi_B + vy - 2r}{vy}u_{xx} - \frac{2\kappa(-vy + \theta)}{yv^2}u_{xy} - \frac{2}{vy}f_x, \quad (2.6)$$

$$u_{yyy} = -u_{yxx} - 2\rho u_{yyx} - \frac{1}{y}u_{xx} + \frac{2\lambda\xi_B - 2\rho v + vy - 2r}{vy}u_{yx} - \frac{-2\kappa vy + 2\kappa\theta + v^2}{v^2y}u_{yy} + \frac{1}{y}u_x + \frac{2\kappa}{vy}u_y - \frac{2}{vy}f_y. \quad (2.7)$$

Differentiating equations (2.6) and (2.7) with respect to  $y$  and  $x$ , respectively, and adding the two expressions we obtain

$$u_{xyyy} + u_{xxxy} = -2\rho u_{xxyy} - \frac{u_{xxx}}{2y} + \frac{(2\lambda\xi_B - \rho v + vy - 2r)u_{xxy}}{vy} - \frac{(-4\kappa vy + 4\kappa\theta + v^2)u_{xyy}}{2yv^2} - \frac{(2\lambda\xi_B - vy - 2r)u_{xx}}{2vy^2} + \frac{\kappa(vy + \theta)u_{xy}}{y^2v^2} + \frac{f_x}{vy^2}. \quad (2.8)$$

By differentiating equation (2.3) twice with respect to  $x$  and twice with respect to  $y$  and adding the two expressions, we obtain

$$u_{xxxx} + u_{yyyy} = -2\rho u_{xxx} - 2\rho u_{yyy} - 2u_{xxyy} + 2\frac{(\kappa vy - v^2 - \kappa\theta)}{v^2y}u_{xxy} - \frac{(2r - vy - 2\lambda\xi_B)}{vy}u_{xxx} + 2\frac{(\kappa vy - v^2 - \kappa\theta)}{v^2y}u_{yyy} - \frac{(-vy + 4\rho v - 2\lambda\xi_B + 2r)}{vy}u_{xyy} + 4\frac{\kappa}{vy}u_{yy} + \frac{2}{y}u_{xy} - \frac{2}{vy}(f_{xx} + f_{yy}). \quad (2.9)$$

We now substitute equations (2.6)–(2.9) into (2.5) to yield a new expression of the error term  $\tau_{i,j}$  that only consists of terms which are either  $\mathcal{O}(h^4)$  or  $\mathcal{O}(h^2)$  multiplied by derivatives of  $u$  which can be approximated to  $\mathcal{O}(h^2)$  within the compact stencil.

$$\begin{aligned} \tau_{i,j} = & \frac{1}{24vy} \left( 2h^2v^2 - 4h^2\lambda\rho v\xi - 4h^2\lambda v\xi y + 8h^2\lambda r\xi - 4h^2\lambda^2\xi^2 + 2h^2\kappa vy \right. \\ & \left. + 4h^2r\rho v + 4h^2rvy - 2h^2\kappa\theta - h^2v^2y^2 - 4h^2r^2 \right) \delta_x^2 \\ & + \frac{1}{12v^3y} \left( h^2v^4 + 4\kappa^2\theta vy - 2h^2\kappa^2v^2y^2 + h^2\kappa v^3y + h^2\kappa\theta v^2 - 2h^2\kappa^2\theta^2 \right) \delta_y^2 \\ & - \frac{1}{6v^2y} \left( 4h^2\kappa^2vy - 4h^2\kappa^2\theta + 4h^2\kappa v^2 \right) \delta_y - \frac{1}{12} \left( vyh^2 + 2h^2\rho^2vy \right) \delta_x^2 \delta_y^2 \\ & - \frac{1}{12vy} \left( h^2v^2 + h^2\kappa v^2y + h^2\kappa\theta v - 12\lambda v^2\xi y \right) \delta_x \\ & - \frac{1}{6v} \left( 2h^2r\rho v + h^2\kappa\theta - h^2\rho v^2y - h^2\kappa vy - 2h^2\lambda\rho v\xi \right) \delta_x^2 \delta_y \\ & + \frac{1}{12v} \left( 4h^2\kappa\rho vy + 2h^2\lambda v\xi - 2h^2rv - 4h^2\kappa\rho\theta + h^2v^2 \right) \delta_x \delta_y^2 \\ & + \frac{1}{6v^2y} \left( h^2\kappa\rho v^2y + 2h^2\kapparvy + h^2\kappa\theta vy - 2h^2\kappa r\theta - h^2\kappa v^2y^2 \right. \\ & \left. - h^2\lambda v^2\xi - 2h^2\kappa\lambda v\xi y + 2h^2\kappa\lambda\theta\xi + h^2\rho v^3 + h^2rv^2 \right) \delta_x \delta_y \end{aligned} \quad (2.10)$$

Inserting (2.10) in (2.4) we obtain the following  $\mathcal{O}(h^4)$  approximation to the partial differential equation (2.3),

$$\begin{aligned}
& -\frac{1}{24} \frac{4h^2\lambda\xi_B(\lambda\xi_B + \rho v - 2) + vy_j(vy_j - 2\kappa - 2r) - 2(r\rho v + \kappa\theta + 2r^2 - v^2) + 12v^2y_j^2}{vy_j} \delta_x^2 u_{i,j} \\
& -\frac{1}{12} \frac{2h^2\kappa^2v^2y_j^2 - 4h^2\kappa^2\theta vy_j - h^2\kappa v^3y_j + 2h^2\kappa^2\theta^2 - h^2\kappa\theta v^2 - h^2v^4 + 6v^4y_j^2}{v^3y_j} \delta_y^2 u_{i,j} \\
& -\frac{1}{12} vy_j h^2 (2\rho^2 + 1) \delta_x^2 \delta_y^2 u_{i,j} - \frac{1}{6} \frac{(-2v\lambda\rho\xi_B - y_j\rho v^2 - \kappa vy_j + 2vr\rho + \kappa\theta) h^2}{v} \delta_x^2 \delta_y u_{i,j} \\
& \quad - \frac{1}{12} \frac{(-4\kappa\rho vy_j + 4\rho\kappa\theta - 2\lambda v\xi_B - y_jv^2 + 2rv) h^2}{v} \delta_x \delta_y^2 u_{i,j} \\
& + \frac{1}{6} \frac{h^2\kappa(\rho v^2y_j + v^2y_j^2 - 2rvy_j - \theta vy_j + 2vy_j\xi_B + 2r\theta - 2\theta\xi_B) - h^2v^2(\rho v - r + \xi_B)}{v^2y_j} \delta_x \delta_y u_{i,j} \\
& \quad + \frac{1}{12} \frac{-h^2\kappa y_j v + h^2\kappa\theta - h^2v^2 + 12vy_j\lambda\xi_B + 6y_j^2v^2 - 12vy_jr}{vy_j} \delta_x u_{i,j} \\
& \quad + \frac{1}{6} \frac{\kappa(-h^2\kappa y_j v + h^2\kappa\theta - h^2v^2 + 6y_j^2v^2 - 6\theta vy_j)}{v^2y_j} \delta_y u_{i,j} \\
& = f_{i,j} + \frac{h^2}{6} \frac{\rho}{v} \delta_x \delta_y f_{i,j} - \frac{h^2}{6} \frac{(v^2 + \kappa(vy_j - \theta))}{v^2y_j} \delta_y f_{i,j} - \frac{h^2}{12} \frac{(2\lambda\xi_B + 2\rho v + vy_j - 2r)}{vy_j} \delta_x f_{i,j} \\
& \quad + \frac{h^2}{12} \delta_x^2 f_{i,j} + \frac{h^2}{12} \delta_y^2 f_{i,j}. \quad (2.11)
\end{aligned}$$

The fourth-order compact scheme (2.11) considered at mesh point  $(i, j)$  involves the nearest eight neighbouring meshpoints. Associated to the shape of the computational stencil, we introduce indexes for each node from zero to eight,

$$\begin{pmatrix} u_{i-1,j+1} = u_6 & u_{i,j+1} = u_2 & u_{i+1,j+1} = u_5 \\ u_{i-1,j} = u_3 & u_{i,j} = u_0 & u_{i+1,j} = u_1 \\ u_{i-1,j-1} = u_7 & u_{i,j-1} = u_4 & u_{i+1,j-1} = u_8 \end{pmatrix}.$$

With this indexing the scheme (2.11) is defined by

$$\sum_{l=0}^8 \alpha_l u_l = \sum_{l=0}^8 \gamma_l f_l,$$

with the coefficients  $\alpha_l$  and  $\gamma_l$  given by

$$\begin{aligned}
\alpha_0 &= \left( \frac{4\kappa^2 + v^2}{12v} - \frac{v(2\rho^2 - 5)}{3h^2} \right) y - \frac{2\kappa^2\theta + \kappa v^2 + rv^2 - v^2\xi_B}{3v^2} \\
& \quad + \frac{-r\rho v^3 + \rho v^3\xi_B + \kappa^2\theta^2 + r^2v^2 - 2rv^2\xi_B - v^4 + v^2\xi_B^2}{3v^3y}, \\
\alpha_{1,3} &= \left( -\frac{v}{24} + \frac{2\kappa\rho \pm v}{6h} + \frac{v(\rho - 1)(\rho + 1)}{3h^2} \right) y \mp \frac{1}{24} \kappa h + \frac{\kappa}{12} + \frac{r}{6} - \frac{\xi_B}{6} \pm \frac{\kappa\rho\theta - rv + v\xi_B}{3vh} \\
& \quad + \frac{1}{y} \left( \pm \frac{(\kappa\theta - v^2)h}{24v} - \frac{-2r\rho v + 2\rho v\xi_B + \kappa\theta + 2r^2 - 4r\xi_B - v^2 + 2\xi_B^2}{12v} \right),
\end{aligned}$$

$$\begin{aligned}
\alpha_{2,4} &= \left( \frac{\kappa^2}{6v} + \frac{\mp \rho v \pm 2\kappa}{6h} + \frac{v(\rho-1)(\rho+1)}{3h^2} \right) y \mp \frac{\kappa^2 h}{12v} + \frac{\kappa(4\kappa\theta + v^2)}{12v^2} - \frac{-r\rho v + \rho v \xi_B + \kappa\theta}{3vh} \\
&\quad + \frac{1}{y} \left( \frac{\kappa(\kappa\theta - v^2)h}{12v^2} - \frac{(2\kappa\theta + v^2)(\kappa\theta - v^2)}{12v^3} \right), \\
\alpha_{5,7} &= \left( -\frac{\kappa}{24} \pm \frac{(2\rho+1)(2\kappa+v)}{24h} - \frac{v(\rho+1)(2\rho+1)}{12h^2} \right) y + \frac{\kappa(\rho v + 2r + \theta - 2\xi_B)}{24v} \\
&\quad \mp \frac{(2\rho+1)(\kappa\theta + rv - v\xi_B)}{12vh} - \frac{-\rho v^3 + 2\kappa r\theta - 2\kappa\theta\xi_B - rv^2 + v^2\xi_B}{24v^2y}, \\
\alpha_{6,8} &= \left( \frac{\kappa}{24} \mp \frac{(2\rho-1)(2\kappa-v)}{24h} - \frac{v(2\rho-1)(\rho-1)}{12h^2} \right) y - \frac{\kappa(\rho v + 2r + \theta - 2\xi_B)}{24v} \\
&\quad \pm \frac{(2\rho-1)(\kappa\theta - rv + v\xi_B)}{12vh} + \frac{-\rho v^3 + 2\kappa r\theta - 2\kappa\theta\xi_B - rv^2 + v^2\xi_B}{24v^2y},
\end{aligned}$$

and

$$\begin{aligned}
\gamma_0 &= 2/3, \quad \gamma_{1,3} = \frac{1}{12} \mp \frac{h}{24} \pm \frac{(-\rho v + r - \xi_B)h}{12vy}, \quad \gamma_{2,4} = \frac{1}{12} \mp \frac{\kappa h}{12v} \pm \frac{(\kappa\theta - v^2)h}{12v^2y}, \\
\gamma_5 &= \gamma_7 = \frac{\rho}{24}, \quad \gamma_6 = \gamma_8 = -\frac{\rho}{24}.
\end{aligned}$$

When multiple indexes are used with  $\pm$  and  $\mp$  signs, the first index corresponds to the upper sign.

### Extension to the parabolic problem

To extend the above approach to the parabolic problem we replace  $f(x, y)$  in (2.3) by the time derivative. We consider the class of two time step methods. By differencing at  $t_\mu = (1 - \mu)t_n + \mu t_{n+1}$ , where  $0 \leq \mu \leq 1$  and the superscript  $n$  denotes the time level, we yield a set of integrators including the forward and backward Euler scheme, for  $\mu = 0$  and  $\mu = 1$ , respectively, and the Crank-Nicolson scheme ( $\mu = 1/2$ ). By defining  $\delta_t^+ u^n = \frac{u^{n+1} - u^n}{k}$ , the resulting fully discrete difference scheme of node  $(i, j)$  at the time level  $n$  becomes

$$\sum_{l=0}^8 \mu \alpha_l u_l^{n+1} + (1 - \mu) \alpha u_l^n = \sum_{l=0}^8 \gamma_l \delta_t^+ u_l^n,$$

which can be written as

$$\sum_{l=0}^8 \beta_l u_l^{n+1} = \sum_{l=0}^8 \zeta_l u_l^n,$$

with the coefficients  $\beta_l$  and  $\zeta_l$  given by

$$\begin{aligned}
\beta_0 &= (((2y_j^2 - 8)v^4 + ((-8\kappa - 8r + 8\xi_B)y_j - (8r + 8\xi_B)\rho)v^3 + (8\kappa^2 y_j^2 + 8r^2 - 16r\xi_B + 8\xi_B)v^2 \\
&\quad - 16\kappa^2 \theta v y_j + 8\kappa^2 \theta^2) \mu k + 16v^3 y_j) h^2 + (16\rho^2 + 40) y_j^2 v^4 \mu k, \\
\beta_{1,3} &= \pm ((\kappa\theta v^2 - v^4 - \kappa y_j v^3) \mu k - (y_j + 2\rho)v^3 + 2v^2 r - 2v^2 \xi_B) h^3 + (((-y_j^2 + 2)v^4 \\
&\quad + ((4r - 4\xi_B + 2\kappa)y_j + 4\rho r - 4\rho \xi_B)v^3 - (2\kappa\theta + 4r^2 - 4xi_B^2 + 8r\xi_B)v^2) \mu k + 2v^3 y_j) h^2
\end{aligned}$$

$$\begin{aligned}
& \pm (4v^4y_j^2 + (-8y_j^2\kappa\rho - 8y_jr + 8y_j\xi_B)v^3 + 8y_j\kappa\theta\rho v^2)\mu kh + (8\rho^2 - 8)y_j^2v^4\mu k, \\
\beta_{2,4} = & \pm ((2\kappa^2\theta v - 2\kappa^2v^2y_j - 2v^3\kappa)\mu k - 2v^2y_j\kappa + 2v\kappa\theta - 2v^3)h^3 + ((2v^4 + 2\kappa y_jv^3 \\
& + (-4\kappa^2y_j^2 + 2\kappa\theta)v^2 + 8\kappa^2vy_j - 4\kappa^2\theta^2)\mu k + 2v^3y_j)h^2 \pm ((8y_j^2\kappa + 8y_j\rho r - 8y_j\rho\xi_B)v^3 \\
& - 4v^4y_j^2\rho - 8v^2y_j\kappa\theta)\mu kh + (8\rho^2 - 8)y_j^2v^4\mu k, \\
\beta_{5,7} = & ((v^4\rho + (-y^2\kappa + \kappa y_j\rho + r - \xi_B)v^3 + (\theta + 2r - 2\xi_B)\kappa y_jv^2 - 2r\kappa\theta v + 2\xi_B\kappa\theta v)\mu k + v^3\rho y_j)h^2 \\
& \pm ((2\rho + 1)y_j^2v^4 + ((2 + 4\rho)\kappa y_j^2 + (-2r + 2\xi_B - 4\rho r + 4\rho\xi_B)y_j)v^3 + (-4\theta\rho - 2\theta)\kappa y_jv^2)\mu kh \\
& + (-4\rho^2 - 6\rho - 2)y_j^2v^4\mu k, \\
\beta_{6,8} = & ((-v^4\rho + (y^2\kappa - \kappa y_j\rho - r + \xi_B)v^3 + (-\theta - 2r + 2\xi_B)\kappa y_jv^2 + 2r\kappa\theta v - 2\xi_B\kappa\theta v)\mu k - v^3\rho y_j)h^2 \\
& \pm ((2\rho - 1)y_j^2v^4 + ((2 - 4\rho)\kappa y_j^2 + (2r - 2\xi_B - 4\rho r + 4\rho\xi_B)y_j)v^3 + (4\theta\rho - 2\theta)\kappa y_jv^2)\mu kh \\
& + (-4\rho^2 + 6\rho - 2)y_j^2v^4\mu k,
\end{aligned}$$

and

$$\begin{aligned}
\zeta_0 = & 16v^3y_jh^2 + (1 - \mu)k(((8 - 2y_j^2)v^4 + ((8\kappa + 8r - 8\xi_B)y_j + 8\rho r - 8\rho\xi_B)v^3 \\
& + (-8r^2 - 8\xi_B^2 + 16r\xi_B - 8\kappa^2y_j^2)v^2 + 16\kappa^2\theta vy_j - 8\kappa^2\theta^2)h^2 + (-40 + 16\rho^2)y_j^2v^4), \\
\zeta_{1,3} = & \pm (2r - 2\xi_B - (y_j + 2\rho)v)v^2h^3 + 2v^3y_jh^2 + (1 - \mu)k(\pm(v\kappa y_j + v^2 - \kappa\theta)v^2h^3 \\
& + (v^2y_j^2 - (4r + 4\xi_B + 2\kappa)vy_j + 4r^2 + 4\xi_B^2 + 2\kappa\theta + 2vy_j - 4\rho vr + 4\rho v\xi_B)v^2h^2 \\
& \pm ((-4v + 8\kappa\rho)v^3y_j^2 + (-8\kappa\theta\rho + 8vr - 8v\xi_B)v^2y_j)h + (8v^2 - 8v^2\rho^2)v^2y_j^2), \\
\zeta_{2,4} = & \pm (2v\kappa\theta - 2v^2y_j\kappa - 2v^3)h^3 + 2v^3y_jh^2 + (1 - \mu)k(\pm(v\kappa y_j + v^2 - \kappa\theta)v^2h^3 \\
& + (v^2y_j^2 - (4r + 2\kappa)vy_j + 2\kappa\theta(2\kappa\theta - v^2) - 2v^4)h^2 \pm ((-8v^3\kappa + 4v^4\rho)y_j^2 \\
& + (8\kappa\theta v^2 - 8v^3\rho r)y_j)h + (-8v^4\rho^2 + 8v^4)y_j^2), \\
\zeta_{5,7} = & v^3\rho y_jh^2 + (1 - \mu)k((v^3y_j^2\kappa - v(v\kappa\theta + 2r\kappa v - 2\xi_B\kappa v + \kappa v^2\rho)y_j) \\
& - v(v^2r - 2v^2\xi_B - 2r\kappa\theta + 2\xi_B\kappa\theta + v^3\rho))h^2 \pm (-v(2v^3\rho + v^3 + 4\kappa v^2\rho + 2v^2\kappa)y_j^2 \\
& + v(2v\kappa\theta + 4v\kappa\theta\rho + 4v^2\rho r + 4v^2\rho\xi_B + 2v^2r + 2v^2\xi_B)y_j)h + v(2v^3 + 6v^3\rho + 4v^3\rho^2)y_j^2), \\
\zeta_{6,8} = & -v^3\rho y_jh^2 + (1 - \mu)k((-v^3y_j^2\kappa + v(v\kappa\theta + 2r\kappa v - 2\xi_B\kappa v + \kappa v^2\rho)y_j \\
& + v(v^2r - v^2\xi_B - 2r\kappa\theta + 2\xi_B\kappa\theta + v^3\rho)) \pm (v(-2v^3\rho + v^3 + 4\kappa v^2\rho - 2v^2\kappa)y_j^2 \\
& + v(2v\kappa\theta - 4v\kappa\theta\rho + 4v^2\rho r - 4v^2\rho\xi_B - 2v^2r - 2v^2\xi_B)y_j)h + v(2v^3 - 6v^3\rho + 4v^3\rho^2)y_j^2).
\end{aligned}$$

Where multiple indexes are used with  $\pm$  and  $\mp$  signs, the first index corresponds to the upper sign. The Crank-Nicolson scheme is used by setting  $\mu = 1/2$ , yielding a scheme which is second-order accurate in time and fourth-order accurate in space.

### 2.3.2 Integral operator

After the initial transformation of variables we have the integral operator in the following form,

$$\tilde{L}_I = \lambda \int_{-\infty}^{+\infty} \tilde{u}(x+z, y, \tau) \tilde{p}(z) dz,$$

where the probability density function,  $\tilde{p}(z)$  is given by

$$\tilde{p}(z) = \frac{1}{\sqrt{2\pi}zv} e^{-\frac{(\log(z)-\gamma)^2}{2v^2}}.$$

We make a final change of variables  $\zeta = x+z$  with the intention of studying the value of the integral at the point  $x_i$ ,

$$\begin{aligned} I_i = \int_{-\infty}^{+\infty} \tilde{u}(\zeta, y, \tau) \tilde{p}(\zeta - x_i) d\zeta &= \int_{x_{min}}^{x_{max}} \tilde{u}(\zeta, y, \tau) \tilde{p}(\zeta - x_i) d\zeta + \int_{x_{max}}^{\infty} \tilde{u}(\zeta, y, \tau) \tilde{p}(\zeta - x_i) d\zeta \\ &+ \int_{-\infty}^{x_{min}} \tilde{u}(\zeta, y, \tau) \tilde{p}(\zeta - x_i) d\zeta. \end{aligned} \quad (2.12)$$

#### Simpson's rule

To estimate the integral we require a numerical integration method of high order to match our finite difference scheme, we choose to use the composite Simpson's rule, defined as

$$\int_a^b f(x) dx \approx \frac{h}{3} \left[ f(x_0) + 2 \sum_{j=1}^{n/2-1} f(x_{2j}) + 4 \sum_{j=1}^{n/2} f(x_{2j-1}) + f(x_n) \right].$$

The error committed by the composite Simpson's rule is bounded by

$$\frac{h^4}{180} (b-a) \max_{\xi \in [a,b]} |f^{(4)}(\xi)|.$$

Through the choice of the interval  $(x_{min}, x_{max})$  we can assure that the integrals outside this range are of negligible value. Allowing the integral to be evaluated using Simpsons rule on a equidistant grid in  $x$  with spacing  $\Delta x$  and  $m_x$  grid-points in  $(x_{min}, x_{max})$ , where each interval has length mesh-size  $h/2$ . Equation (2.12) can now be written as,

$$\begin{aligned} I_i &\approx \int_{x_{min}}^{x_{max}} \tilde{u}(\zeta, y, \tau) \tilde{p}(\zeta - x_i) d\zeta \\ &\approx \frac{\Delta x}{3} \sum_{j=1}^{\frac{m_x}{2}} [\tilde{u}(\zeta_{2j-2}, y, \tau) \tilde{p}(\zeta_{2j-2} - x_i) + 4\tilde{u}(\zeta_{2j-1}, y, \tau) \tilde{p}(\zeta_{2j-1} - x_i) \\ &\quad + \tilde{u}(\zeta_{2j}, y, \tau) \tilde{p}(\zeta_{2j} - x_i)] = \tilde{I}_i. \end{aligned}$$

This computation is calculated explicitly at each time-step by the matrix-vector equation,

$\tilde{I} = W_{m_x} \tilde{u}$ , defined as follows,

$$\tilde{I} = \begin{pmatrix} \tilde{I}_1 & \tilde{I}_3 & \dots & \tilde{I}_{m_x-1/2} & \tilde{I}_{m_x/2} \end{pmatrix}^\top, \quad \tilde{u} = \begin{pmatrix} \tilde{u}_1 & \tilde{u}_3 & \dots & \tilde{u}_{m_x-1/2} & \tilde{u}_{m_x/2} \end{pmatrix}^\top,$$

$$W_{m_x} = \begin{bmatrix} \tilde{p}(\zeta_0 - x_0) & 4\tilde{p}(\zeta_1 - x_0) & 2\tilde{p}(\zeta_2 - x_0) & \dots & \tilde{p}(\zeta_{m_x} - x_0) \\ \tilde{p}(\zeta_0 - x_1) & 4\tilde{p}(\zeta_1 - x_1) & 2\tilde{p}(\zeta_2 - x_1) & \dots & \tilde{p}(\zeta_{m_x} - x_1) \\ \vdots & \vdots & \vdots & \ddots & \vdots \\ \tilde{p}(\zeta_0 - x_{m_x}) & 4\tilde{p}(\zeta_1 - x_{m_x}) & 2\tilde{p}(\zeta_2 - x_{m_x}) & \dots & \tilde{p}(\zeta_{m_x} - x_{m_x}) \end{bmatrix}.$$

The integral operator  $L_I$  is estimated over  $(x_{min}, x_{max})$  using Simpson's rule. The tails could be discarded as they are assumed to be of negligible value for sufficiently small (large) choice of  $x_{min}$  ( $x_{max}$ ). A direct result of this approach would be the necessity to compute the option price over a wider domain than practically relevant. To alleviate this issue we assume that the option price follows the payoff function outside of the range  $(x_{min}, x_{max})$ , and approximate the tails by the following integrals

$$\int_{x_{max}}^{\infty} \tilde{u}(\zeta, y, \tau) \tilde{p}(\zeta) d\zeta \approx \int_{x_{max}}^{\infty} \max(1 - \exp(\zeta), 0) \tilde{p}(\zeta) d\zeta,$$

$$\int_{-\infty}^{x_{min}} \tilde{u}(\zeta, y, \tau) \tilde{p}(\zeta) d\zeta \approx \int_{-\infty}^{x_{min}} \max(1 - \exp(\zeta), 0) \tilde{p}(\zeta) d\zeta.$$

The value of the first of these integrals is trivial as the payoff function for the Put option is zero in the region  $(x_{max}, +\infty)$ . We estimate the second integral using Simpson's rule on an equal-sized adjacent equidistant grid to our original grid.

### 2.3.3 Time discretisation for IMEX method

Having set the framework for the discretisation of the operators  $L_D$  and  $L_I$ , we now introduce the implicit-explicit method,

$$\sum_{l=0}^8 \beta_l u^{n+1} = \sum_{l=0}^8 \zeta_l \left( 1 + \frac{3\Delta\tau}{2} \tilde{L}_I \right) u^n - \sum_{l=0}^8 \zeta_l \left( \frac{\Delta\tau}{2} \tilde{L}_I \right) u^{n-1}.$$

## 2.4 Initial condition and boundary conditions

### 2.4.1 Initial condition

The initial condition is given by the transformed payoff function of the Put option,

$$u(x, \sigma, 0) = \max(1 - \exp(x), 0), \quad x \in \mathbb{R}, \sigma > 0.$$

To maintain the order of the scheme we smooth this function around zero, this follows from [59] which states that we cannot expect to achieve fourth order convergence if the initial condition is not sufficiently smooth. In [59] suitable smoothing operators are defined in

the Fourier space. Since the order of convergence of our HOC scheme is four we follow [32] and select the smoothing operator  $\phi_4$ , given by its Fourier transform

$$\phi_4(\omega) = \left( \frac{\sin(\omega/2)}{\omega/2} \right)^4 \left[ 1 + \frac{2}{3} \sin^2(\omega/2) \right].$$

This leads to the smoothed initial condition

$$\tilde{u}_0(x_1) = \frac{1}{h} \int_{-3h}^{3h} \phi_4\left(\frac{x}{h}\right) u_0(x_1 - x) dx.$$

As  $h \rightarrow 0$ , this smoothed initial condition converges to the original initial condition. The results in [59] prove high-order convergence of the approximation to the smoothed problem to the true solution of (2.2).

Note that in [28] a Rannacher style smoothing start-up [68] is used with four fully implicit quarter time steps. In our experiments with the HOC scheme we notice no benefit by employing such a start-up, and use the Crank-Nicolson time stepping throughout. Since the coefficients in (2.2) do not depend on time, we are required to build up the discretisation matrices for the new scheme only once. They can then be  $LU$ -factorised once, and the factorisation can be used in each time step, leading to a highly efficient scheme.

### 2.4.2 Boundary conditions

We impose artificial boundary conditions as follows. Due to the compactness of the scheme, the Dirichlet boundary conditions are considered without introduction of numerical error by imposing

$$u_{-N,j}^n = 1 - e^{rt_n - Nh}, \quad u_{+N,j}^n = 0, \quad j = 0, \dots, M.$$

At the other boundaries we impose homogeneous Neumann boundary conditions, these require more attention as no value is prescribed, therefore, they must be set by extrapolation from values in the interior. Here the introduction of numerical error must be negated by choice of an extrapolation formulae of order high enough not to affect the overall order of accuracy. We choose the following extrapolation formulae:

$$\begin{aligned} u_{i,0}^n &= 4u_{i,1}^n - 6u_{i,2}^n + 4u_{i,3}^n - u_{i,4}^n + \mathcal{O}(h^4), \quad i = -N + 1, \dots, N - 1, \\ u_{i,M}^n &= 4u_{i,M-1}^n - 6u_{i,M-2}^n + 4u_{i,M-3}^n - u_{i,M-4}^n + \mathcal{O}(h^4), \quad i = -N + 1, \dots, N - 1. \end{aligned}$$

## 2.5 A finite element method for comparison

In addition to standard, second-order finite difference methods we will compare our new scheme to different finite element methods. In this short section we briefly state the variational formulation of the PIDE problem.

We can rewrite the equation for the differential operator  $L_D$  in divergence form,

$$u_\tau - \operatorname{div}(A\nabla u) + b \cdot \nabla u = 0,$$

where the coefficients  $A$  and  $b$  are given by

$$A = \frac{1}{2}vy \begin{bmatrix} 1 & \rho \\ \rho & 1 \end{bmatrix}, \quad b = \begin{bmatrix} \frac{1}{2}vy - r + \lambda\xi_B - \frac{v\rho}{2} \\ -\kappa\frac{(\theta-vy)}{v} - \frac{v}{2} \end{bmatrix}.$$

To solve this problem using finite elements we produce a variational formulation, which requires multiplying by suitable test functions  $\phi$  and integrating over the domain  $\Omega$ .

Mirroring the approach defined in Section 2.3, we employ an IMEX discretisation with the integral operator,  $L_I$ , being computed using the Simpson's rule. We have the following Crank-Nicholson scheme,

$$\left( \int_{\Omega} u^{n+1} \phi \, dx dy + \left[ \int_{\Omega} A \nabla u^{n+1} \cdot \nabla \phi \, dx dy + \int_{\Omega} b \cdot \nabla u^{n+1} \phi \, dx dy \right] \frac{\Delta\tau}{2} \right) = \left( \int_{\Omega} u^n \phi \, dx dy + \left[ \frac{1}{2} \int_{\Omega} A \nabla u^n \cdot \nabla \phi \, dx dy + \frac{1}{2} \int_{\Omega} b \cdot \nabla u^n \phi \, dx dy + \frac{3}{2} \tilde{L}_I u^n - \frac{1}{2} \tilde{L}_I u^{n-1} \right] \Delta\tau \right).$$

## 2.6 Numerical experiments

In our numerical experiments we compare the performance of two finite difference schemes, a standard, second-order central difference scheme and the new HOC scheme, against two variants of the finite element approach presented in the previous section, using Lagrange elements with linear ( $p = 1$ ) and quadratic ( $p = 2$ ) polynomial basis functions on quadrilateral meshes. While a finite element method with cubic basis functions ( $p = 3$ ) would be expected to give a similar numerical convergence order as the HOC scheme, the number of degrees of freedom would increase substantially, and make this approach less viable, see also comments below in Section 2.6.1.

Both finite difference schemes are implemented in C++. For our numerical experiments with finite elements we use the FEniCS FEM solver. FEniCS is a popular open-source platform which allows users quickly to obtain efficient FEM code for solving partial differential equations. The code is written in Python 3.5 and utilises the inbuilt packages of NumPy and SciPy to improve efficiency.

We measure the convergence, computational time, number of unknowns and the memory usage for each method. As a separate study we compare the stability of the new HOC finite difference scheme against a standard, second-order central difference scheme.

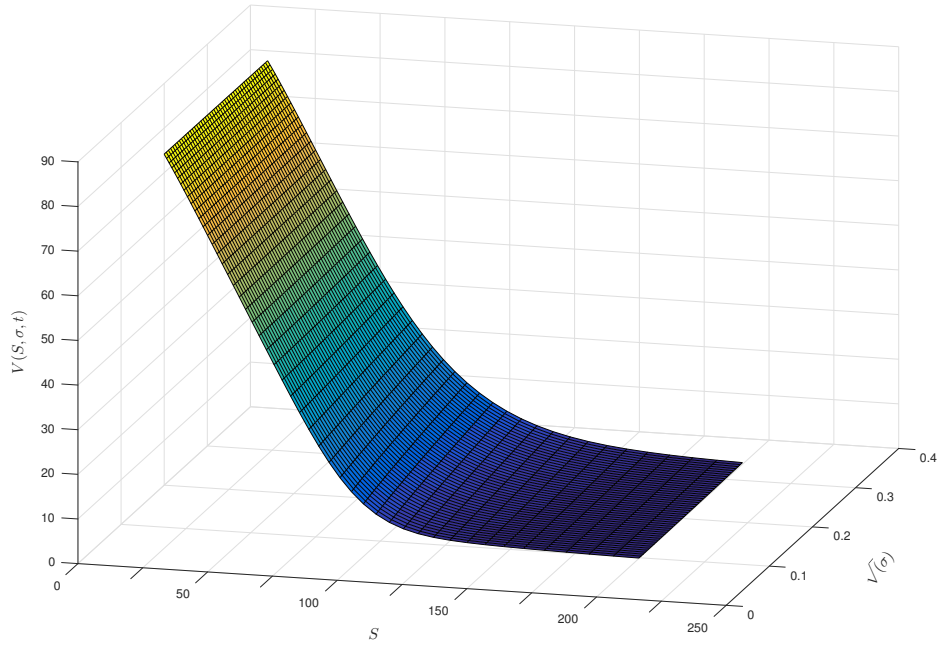


Figure 2.1: Price of a European put option under Bates' model.

Figure 2.1 shows the price of a European put option plotted against the volatility  $\sqrt{\sigma}$  and the asset price  $S$ . The default parameters used for the numerical experiments are given in Table 2.1.

Parameter	Value
Strike Price	$K = 100$
Time to maturity	$T = 0.5$
Interest rate	$r = 0.05$
Volatility of volatility	$v = 0.1$
Mean reversion speed	$\kappa = 2$
Long-run mean of $\sigma$	$\theta = 0.01$
Correlation	$\rho = -0.5$
Jump Intensity	$\lambda = 0.2$

Table 2.1: Default parameters for numerical simulations associated with Bates' model.

### 2.6.1 Numerical convergence

We perform a numerical study to evaluate the rate of convergence of the schemes. We refer to both the  $l_2$ -error  $\epsilon_2$  and the  $l_\infty$ -error  $\epsilon_\infty$  with respect to a numerical reference solution on a fine grid with  $h_{\text{ref}} = 0.025$ , which is experimentally chosen by the limits of computer memory. With the parabolic mesh ratio  $k/h^2$  fixed to a constant value we expect these errors to converge as  $\epsilon = Ch^m$  for some  $m$  and  $C$  which represent constants. From this we generate a double-logarithmic plot  $\epsilon$  against  $h$  which should be asymptotic to a straight line with slope  $m$ , thereby giving a method for experimentally determining the order of the scheme.

We compare the new HOC scheme to the finite element approach from Section 2.5 (with polynomial orders  $p = 1, 2$ ) and a standard, second-order central finite difference scheme. The second-order finite difference scheme requires a Rannacher style start-up [68] which involves starting by four quarter fully implicit Euler steps to combat stability issues [41].

These numerical convergence results are included in Figure 2.2 for the  $l_2$ -error  $\epsilon_2$  and Figure 2.3 for the  $l_\infty$ -error  $\epsilon_\infty$ . The numerical convergence orders are estimated from the slope of a least squares fitted line.

We observe that the numerical convergence orders are consistent with the theoretical order of the schemes. We note that the finite element approach with  $p = 2$  achieves a rate close to three whereas the new HOC scheme has convergence rates close to four. With a finite element method with cubic basis functions ( $p = 3$ ) one would be able to match the fourth order of the HOC scheme, but only at the expense of solving a much larger system, due to the much larger number of degrees of freedom for  $p = 3$ . For example, on a mesh with  $h = 0.05$  the cubic finite element method would employ 58081 degrees of freedom, almost ten times more than the HOC scheme on the same mesh.

### 2.6.2 Computational efficiency comparison

We conduct an efficiency comparison between the new high-order scheme, a standard second-order discretisation and the finite element method with polynomial basis order  $p = 1$  and  $p = 2$ . The finite element methods employ quadrilateral meshes to allow for better comparison with the finite difference methods.

We compare the computational time to obtain a given accuracy, taking into account matrix setups, factorisation and boundary condition evaluation. The timings depend obviously on technical details of the computer as well as on specifics of the implementation.

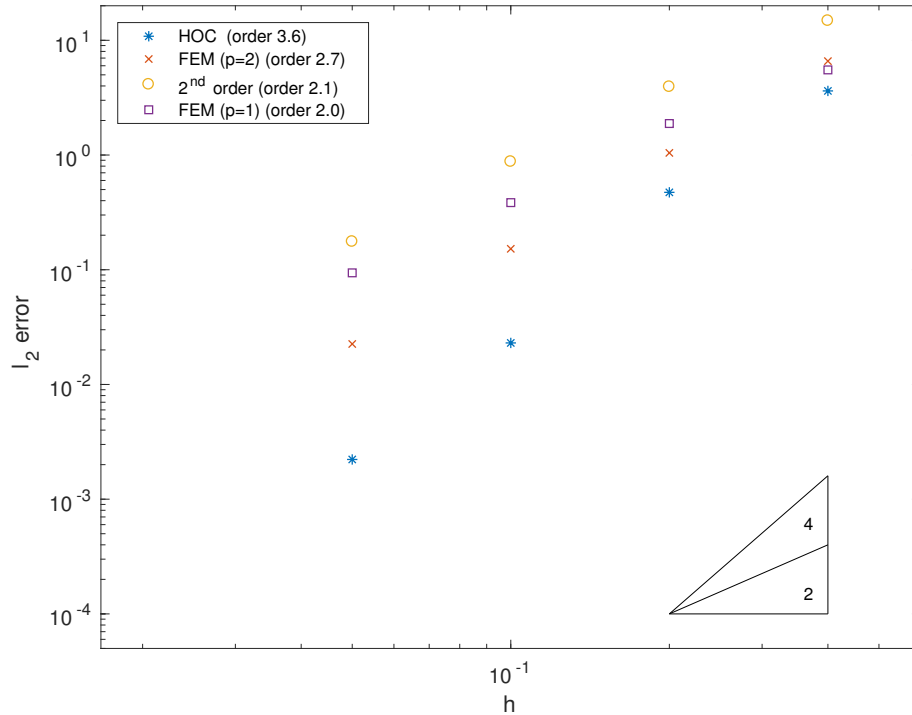


Figure 2.2:  $l_2$ -error in European put option price under Bates’ model taken at mesh-sizes  $h = 0.4, 0.2, 0.1, 0.05$ .

Care was taken to implement both finite difference schemes in an efficient and consistent manner, using standard libraries where possible, to avoid unnecessary bias in the results. Direct comparison of computational times with the Python based FEM schemes are difficult, but still give an indication what can be achieved with a standard ‘black-box’ solver. All results were computed on the same laptop computer (2015 MacBook Air 11”).

Since the coefficients in (2.2) do not depend on time, we are required to build up the discretisation matrices for the new scheme only once (twice for the second-order scheme with Rannacher start-up). The new scheme requires only one initial  $LU$ -factorisation of a sparse matrix. This factorisation is then employed in each time step, leading to a highly efficient scheme. Further efficiency gains are obtainable by parallelisation or GPU computing.

The results are shown below in Figure 2.4. The mesh-sizes used for this comparison are  $h = 0.4$ ,  $h = 0.2$ ,  $h = 0.1$  and  $h = 0.05$ , with the reference mesh-size used being  $h_{\text{ref}} = 0.025$ . From this comparison it is clear to note that the HOC scheme achieves higher accuracy with less computational time at all mesh-sizes. The improvement in computational time over the second-order finite difference scheme can be partly attributed

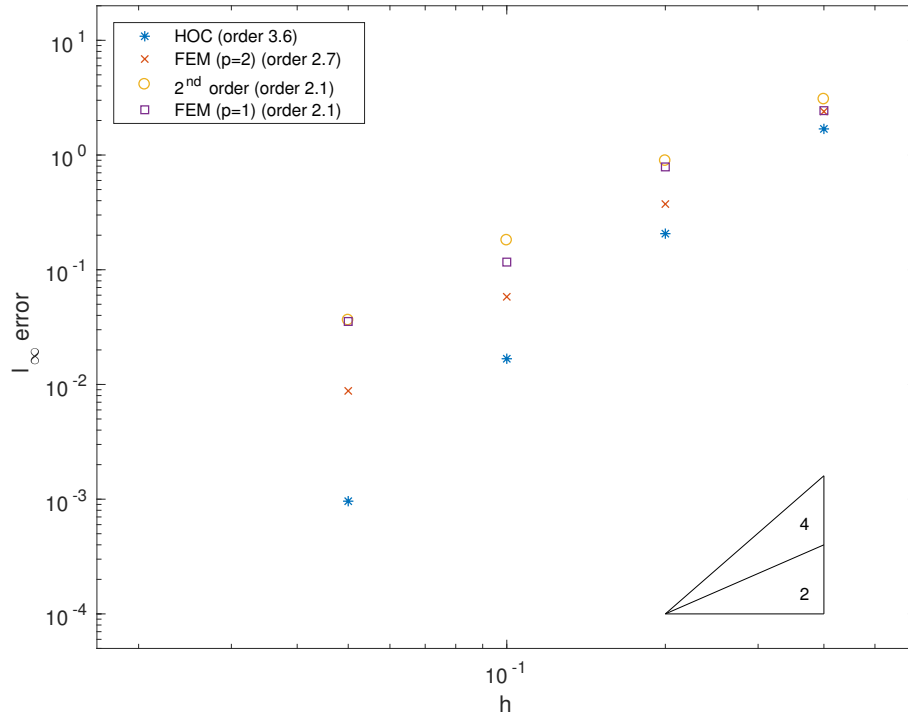


Figure 2.3:  $l_\infty$ -error in European put option price under Bates' model taken at mesh-sizes  $h = 0.4, 0.2, 0.1, 0.05$ .

to the absence of the Rannacher start-up which requires the additional construction and factorisation of a sparse matrix populated with coefficients for the implicit Euler steps.

The finite element method with  $p = 1$  has comparable results for both computational time and  $l_2$ -error to the second-order finite difference scheme, however, for  $p = 2$  the computational time for the finite element method increases substantially with the size of the linear system to be solved.

Table 2.2 summarises more detailed results of the numerical comparison. The number of degrees of freedom for all schemes are shown in the third column. The standard finite difference scheme and the linear FEM use the same number of unknowns. It is noticeable that the HOC scheme, unlike the high-order FEM approach with  $p = 2$ , achieves high-order convergence without requiring additional unknowns. As a result the HOC scheme is very parsimonious in terms of computational effort and memory requirements.

The memory requirements are an important factor in numerical computations. Direct comparisons of memory usage between the C++ implementations of the finite difference schemes and the 'black box' FEniCS FEM approaches are not viable. Moreover, FEniCS allocates already a rather large amount of memory at the coarsest mesh with  $h = 0.4$ .

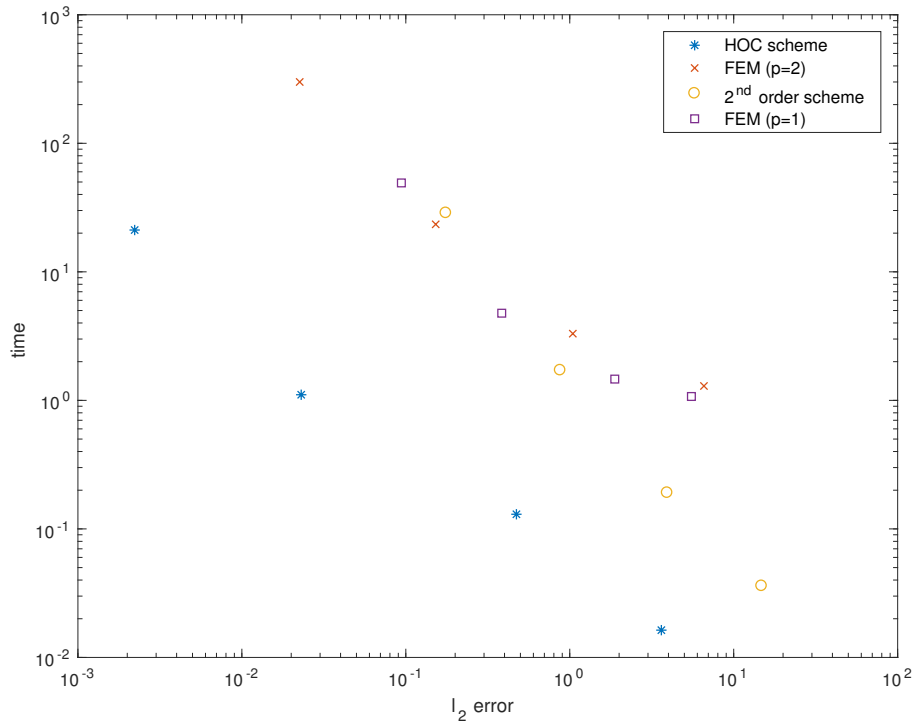


Figure 2.4: Computational speed comparison for pricing algorithms for Bates' model taken at mesh-sizes  $h = 0.4, 0.2, 0.1, 0.05$ .

Hence, rather than looking at total memory used, we report the memory usage at each subsequent refinement as the extra memory required to the base mesh size  $h = 0.4$ . The results demonstrate both the improvements of the HOC scheme over the second-order alternative and also the greater memory required to achieve comparable convergence with the finite element methods.

### 2.6.3 Numerical stability analysis

To assess the stability of the scheme we present a numerical stability analysis. We propose to test to what extent the parabolic mesh ratio  $k/h^2$  impacts the convergence of the scheme. If the effect is minimal this will allow numerically regular solutions to be obtained without restriction on the time step-size. We proceed to compute numerical solutions for varying values of the parabolic mesh ratio  $k/h^2$  and the mesh width  $h$ , then plot these against the associated  $l_2$ -errors to detect stability restrictions depending on  $k/h^2$ . This numerical test

<sup>1</sup>Rather than total memory usage, increases in memory usage at each subsequent refinement from the base mesh size  $h = 0.4$  are given for each scheme.

Scheme	$h$	DOF	$l_2$ -error	$l_\infty$ -error	time (s)	memory (kB)
HOC	0.4	121	3.6201	1.6891	0.016	6916
	0.2	441	0.4728	0.2063	0.130	+1060
	0.1	1681	0.0230	0.0168	1.106	+5536
	0.05	6561	0.0022	0.0009	21.145	+18284
FEM ( $p = 2$ )	0.4	441	6.5837	2.3944	1.294	123128
	0.2	1681	1.0438	0.3737	3.304	+1780
	0.1	6561	0.1522	0.0581	23.426	+8268
	0.05	25921	0.0225	0.0088	300.019	+40828
FD	0.4	121	14.8087	3.0653	0.036	6948
	0.2	441	3.9321	0.8913	0.191	+1772
	0.1	1681	0.8751	0.1806	1.715	+8384
	0.05	6561	0.1758	0.0364	28.706	+23064
FEM ( $p = 1$ )	0.4	121	5.5209	2.4373	1.072	123276
	0.2	441	1.8816	0.7876	1.462	+192
	0.1	1681	0.3846	0.1166	4.727	+2052
	0.05	6561	0.0940	0.0354	49.171	+8176

Table 2.2: Performance results for the HOC, second-order FD and FEM ( $p = 1, 2$ ) schemes for Bates' model. Comparison for computational time and memory usage between the finite difference schemes (HOC and second-order) and the FEM schemes ( $p = 1, 2$ ) are only indicative since implementations are different<sup>1</sup>.

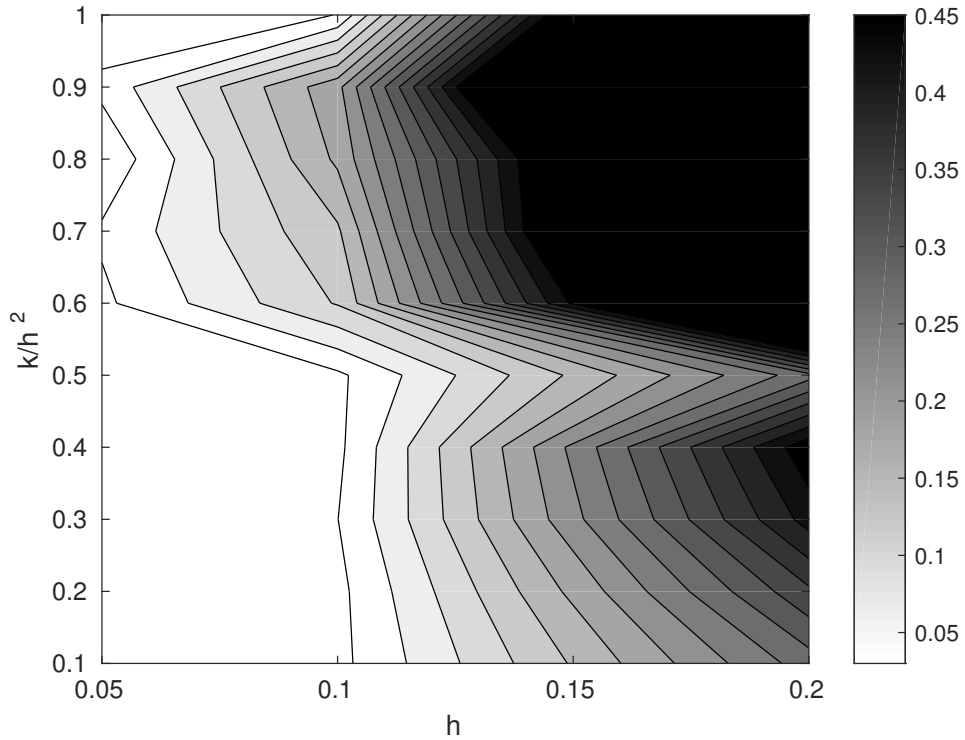


Figure 2.5: Contour plot of the  $l_2$ -error for the HOC scheme for Bates' model.

is performed for both the high-order and the second-order schemes, with the results shown in Figure 2.5 and Figure 2.6 respectively. We use default parameters from Table 2.1, and vary the parabolic mesh size from 0.1 to 1 in increments of 0.1. Note the difference in the error scales between the two schemes.

For both schemes the error increases gradually as the parabolic mesh ratio and  $h$  are increased. We note that for the second-order scheme the contour plot of the error may indicate some mild condition on the time stepping, the effect being stronger for larger mesh size  $h$ . The high-order scheme also features a mild dependence on the parabolic mesh ratio. Although there is no apparent stability restriction, it appears that values of the parabolic mesh ratio below and close to 0.5 are most useful. We attribute this dependence of the scheme to the parabolic mesh ratio as a consequence of the implicit-explicit nature of the scheme. For the present option pricing problem, the restriction on the time stepping for the new scheme is not severe, since the discretisation matrices do not change in time (the coefficients in the partial integro-differential equation (2.2) do not depend on time). Hence, the sparse matrix factorisation is performed only once, and additional time steps do not require additional factorisations to solve the problem.

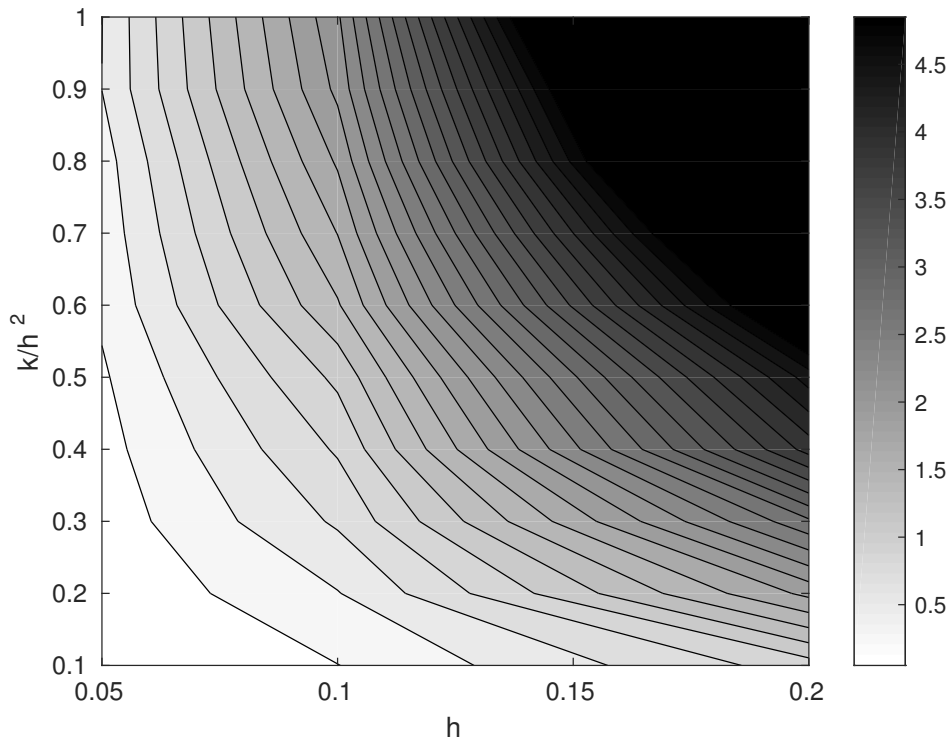


Figure 2.6: Contour plot of the  $l_2$ -error for second-order scheme for Bates' model.

#### 2.6.4 Feller Condition

To further test the robustness of the new HOC scheme, we examine the convergence rates achieved when the Feller condition,  $2\kappa\theta \geq v^2$ , is not satisfied for the Cox-Ingersol-Ross (CIR) volatility process [21].

We use the default parameters defined in Table 2.1, with exceptions for long-run variance mean  $\theta$  and volatility of volatility  $v$ , which we alter to test the condition as shown in Table 2.3.

$\theta$	$v$	Condition
	0.7	$2\kappa\theta < v^2$
0.04	0.4	$2\kappa\theta = v^2$
	0.1	$2\kappa\theta > v^2$

Table 2.3: Parameters for different regimes of the Feller condition.

We study the  $l_2$  and  $l_\infty$  -error associated with each condition. The results are shown in Table 2.4, the  $l_2$ -error numerical convergence rates, obtained from a least squares fitted line as explained earlier, are 4.0, 3.9 and 3.9 for  $v = 0.7, 0.4$  and  $0.1$ , respectively. As a

consequence we can confirm the new HOC scheme performs well irrespective of the validity of the Feller condition.

Condition	$h$	$l_2$ -error	$l_\infty$ -error
$2\kappa\theta < v^2$	$h = 0.2$	2.3342	0.1930
	$h = 0.1$	0.0473	0.0057
	$h = 0.05$	0.0096	0.0011
$2\kappa\theta = v^2$	$h = 0.2$	1.3593	0.1429
	$h = 0.1$	0.0289	0.0052
	$h = 0.05$	0.0057	0.0010
$2\kappa\theta > v^2$	$h = 0.2$	0.9436	0.1906
	$h = 0.1$	0.0394	0.0123
	$h = 0.05$	0.0043	$9.05 \cdot 10^{-4}$

Table 2.4: Numerical convergence results for HOC scheme for Bates' model with varying Feller condition.

## 2.7 Summary of chapter

We have derived a new HOC finite difference method for option pricing in stochastic volatility jump models. Numerical experiments confirm high-order convergence in the option price without stability restrictions. The method is based on an implicit-explicit scheme in combination with HOC finite difference stencils for solving the partial integro-differential equation. It can be implemented in a highly efficient manner and can be used to upgrade existing finite difference codes. Compared to finite element methods, it is very parsimonious in terms of memory requirements and computational effort, since it achieves high-order convergence without requiring additional unknowns (unlike finite elements with higher polynomial order).

## Chapter 3

# Efficient hedging in Bates model using high-order compact finite differences

Market practitioners who trade derivatives will affirm that hedging is a crucially important aspect of pricing. If a contract is purchased but not hedged, it can be sold at any price, even the correct one, and still result in a loss. This means that the price of the contract is the cost of the hedge, plus any margin, and the profit/loss resulting from the trade will depend on the hedge being completely effective.

Hedging techniques typically involve the use of complicated financial instruments known as derivatives, of which the two most common are options and futures. With these instruments, it is possible to develop trading strategies which allow for a loss in one investment to be negated by a profit in a derivative.

In Chapter 2 we have derived and tested a HOC finite difference scheme for pricing options in stochastic and volatility jump models. We propose that the high-order convergence displayed in the option price will offer an improvement in the hedging properties required by market practitioners.

In this chapter we evaluate the hedging performance of the numerical option pricing scheme derived in Chapter 2 through a series of experiments. We will compare the scheme's hedging performance to standard finite difference methods. Furthermore we will present examples of hedging strategies, involving combinations of options and their underlying assets. Throughout the results it is shown that the new scheme outperforms a standard discretisation, based on a second-order central finite difference approximation.

This chapter is organised as follows. In the next section we recall the transformed

Bates PIDE, which was presented in Section 2.1 for the case of European put options. Here we introduce initial and boundary conditions suitable for a European call option and produce convergence results for this case using the new HOC scheme, and a comparative second-order discretisation. In Section 3.2, we give examples of popular option trading strategies, including straddles and spreads, which are created through a combination of long or short put and call options. Section 3.3 is devoted to the computation of the so-called *Greeks* and further evidence of the scheme's hedging performance is given through examples of hedged portfolios. Section 3.4 summarises this chapter.

### 3.1 The Bates PIDE for a European call option

By standard derivative pricing arguments for the Bates model, we obtain the PIDE

$$\begin{aligned} \frac{\partial V}{\partial t} + \frac{1}{2}S^2\sigma\frac{\partial^2 V}{\partial S^2} + \rho v\sigma S\frac{\partial^2 V}{\partial S\partial\sigma} + \frac{1}{2}v^2\sigma\frac{\partial^2 V}{\partial\sigma^2} + (r - \lambda\xi_B)S\frac{\partial V}{\partial S} + \kappa(\theta - \sigma)\frac{\partial V}{\partial\sigma} \\ - (r + \lambda)V + \lambda\int_0^{+\infty} V(S\tilde{y}, v, t)p(\tilde{y})\,d\tilde{y} = 0, \end{aligned}$$

which has to be solved for  $S, \sigma > 0$ ,  $0 \leq t < T$  and subject to a suitable final condition of  $V(S, \sigma, T) = \max(S - K, 0)$ , in the case of a European call option, with  $K$  denoting the strike price.

Through the following transformation of variables

$$x = \log S, \quad \tau = T - t, \quad y = \frac{\sigma}{v} \quad \text{and} \quad u = \exp(r + \lambda)V$$

we obtain

$$\begin{aligned} u_\tau = \frac{1}{2}vy\left(\frac{\partial^2 u}{\partial x^2} + \frac{\partial^2 u}{\partial y^2}\right) + \rho vy\frac{\partial^2 u}{\partial x\partial y} - \left(\frac{1}{2}vy - r + \lambda\xi_B\right)\frac{\partial u}{\partial x} \\ + \kappa\frac{(\theta - vy)}{v}\frac{\partial u}{\partial y} + \lambda\int_{-\infty}^{+\infty} \tilde{u}(x + z, y, \tau)\tilde{p}(z)\,dz, \quad (3.1) \end{aligned}$$

which is now posed on  $\mathbb{R} \times \mathbb{R}^+ \times (0, T)$ , with  $\tilde{u}(z, y, \tau) = u(e^z, y, \tau)$  and  $\tilde{p}(z) = e^z p(e^z)$ . The problem is completed by suitable initial and boundary conditions, which for a European call option are:

$$u(x, y, 0) = \max(\exp(x) - 1, 0), \quad x \in \mathbb{R}, \quad y > 0,$$

$$u(x, y, t) \rightarrow 0, \quad x \rightarrow -\infty, \quad y > 0, \quad t > 0,$$

$$u(x, y, t) \rightarrow 1, \quad x \rightarrow +\infty, \quad y > 0, \quad t > 0,$$

$$u_y(x, y, t) \rightarrow 0, \quad x \in \mathbb{R}, \quad y \rightarrow \infty, \quad t > 0,$$

$$u_y(x, y, t) \rightarrow 0, \quad x \in \mathbb{R}, \quad y \rightarrow 0, \quad t > 0.$$

### 3.1.1 Numerical approximation

We discretise (3.1) by replacing  $\mathbb{R}$  by  $[-R_1, R_1]$  and  $\mathbb{R}^+$  by  $[L_2, R_2]$  with  $R_1, R_2 > L_2 > 0$ . We consider a uniform grid  $Z = \{x_i \in [-R_1, R_1] : x_i = ih_1, i = -N, \dots, N\} \times \{y_j \in [L_2, R_2] : y_j = L_2 + jh_2, j = 0, \dots, M\}$  consisting of  $(2N + 1) \times (M + 1)$  grid points with  $R_1 = Nh_1$ ,  $R_2 = L_2 + Mh_2$  and with space step  $h := h_1 = h_2$  and time step  $k$ . Let  $u_{i,j}^n$  denote the approximate solution of (3.1) in  $(x_i, y_j)$  at the time  $t_n = nk$  and let  $u^n = (u_{i,j}^n)$ .

To compute the numerical solution of (3.1) we use the implicit-explicit HOC scheme presented in Chapter 2. Whereby, adjustments are made to fit the case of a European call option. In Section 2.3.2, we discretised the integral operator for a European put option by making assumptions based on the value of the payoff. For the case of a European call option, we assume that the option price follows the payoff function outside of the range  $(x_{min}, x_{max})$ , and approximate the tails by the following integrals

$$\int_{-\infty}^{x_{min}} \tilde{u}(\zeta, y, \tau) \tilde{p}(\zeta) d\zeta \approx \int_{-\infty}^{x_{min}} \max(\exp(\zeta) - 1, 0) \tilde{p}(\zeta) d\zeta.$$

$$\int_{x_{max}}^{\infty} \tilde{u}(\zeta, y, \tau) \tilde{p}(\zeta) d\zeta \approx \int_{x_{max}}^{\infty} \max(\exp(\zeta) - 1, 0) \tilde{p}(\zeta) d\zeta,$$

The value of the first of these integrals is trivial as the payoff function for the Call option is zero in the region  $(-\infty, x_{min})$ . We estimate the second integral using Simpson's rule on an equal-sized adjacent equidistant grid to our original grid.

Below we present Figure 3.1, which shows the price of a European call option plotted against the volatility  $\sqrt{\sigma}$  and the asset price  $S$ . The default parameters used for the numerical experiments are consistent with those used in Chapter 2 and displayed in Table 2.1.

### 3.1.2 Numerical convergence

We perform a numerical study to evaluate the rate of convergence of the HOC scheme against a second order standard finite difference discretisation. In an identical approach to that used in Chapter 2, we refer to both the  $l_2$ -error  $\epsilon_2$  and the  $l_\infty$ -error  $\epsilon_\infty$  with respect to a numerical reference solution on a fine grid with  $h_{ref} = 0.025$ . With the parabolic mesh ratio  $k/h^2$  fixed to a constant value we expect these errors to converge as  $\epsilon = Ch^m$  for some  $m$  and  $C$  which represent constants. From this we generate a double-logarithmic plot  $\epsilon$  against  $h$  which should be asymptotic to a straight line with slope  $m$ , thereby giving a method for experimentally determining the order of the scheme.

These numerical convergence results are included in Figure 3.2 for the  $l_2$ -error  $\epsilon_2$  and Figure 3.3 for the  $l_\infty$ -error  $\epsilon_\infty$ . The numerical convergence orders are estimated from the

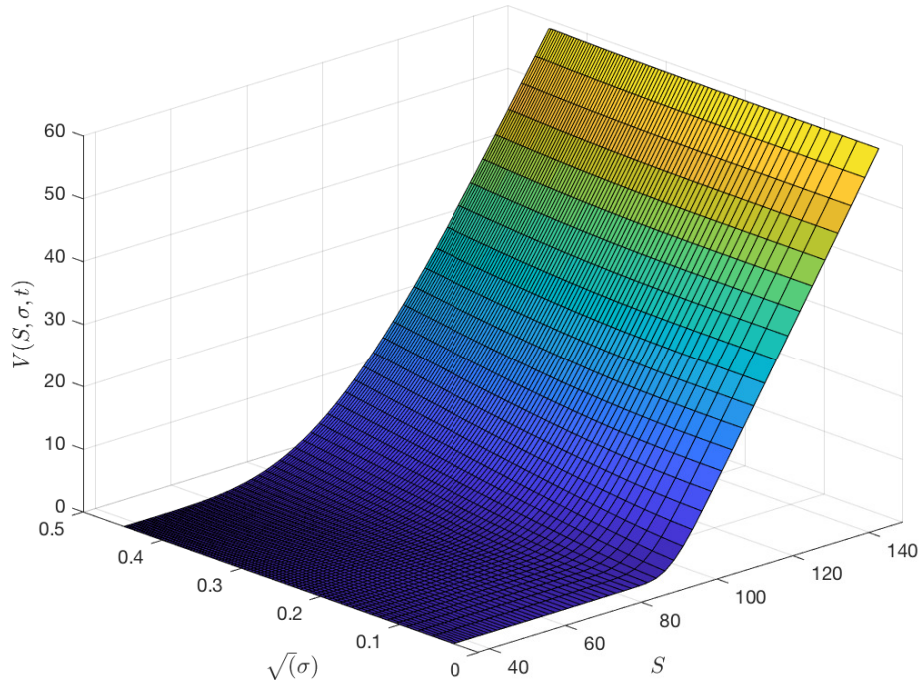


Figure 3.1: Price of a European call option under Bates' model.

slope of a least squares fitted line.

We observe that the numerical convergence orders are consistent with those achieved for the European put option, seen in Chapter 2, and match the theoretical order of the schemes, with the new HOC scheme achieving convergence rates close to four.

## 3.2 Option trading strategies

The main uses of options are speculation, arbitrage and hedging. Some trades can be considered as a means for speculation, some as hedging strategies and others as a means to exploit arbitrage opportunities in the markets. In this section we focus on two speculative strategies, which are composed on multiple options and offer traders a different market risk profile to that of a call or put option individually.

### 3.2.1 Straddles

Straddles are composed of two options, a put and a call, both with the same expiry date and both written on the same underlying asset. In the case of a regular straddles, the options are stuck *at-the-money*, i.e. with strike prices equal to the current market price of the underlying asset. It is possible to be long or short straddles by taking long positions

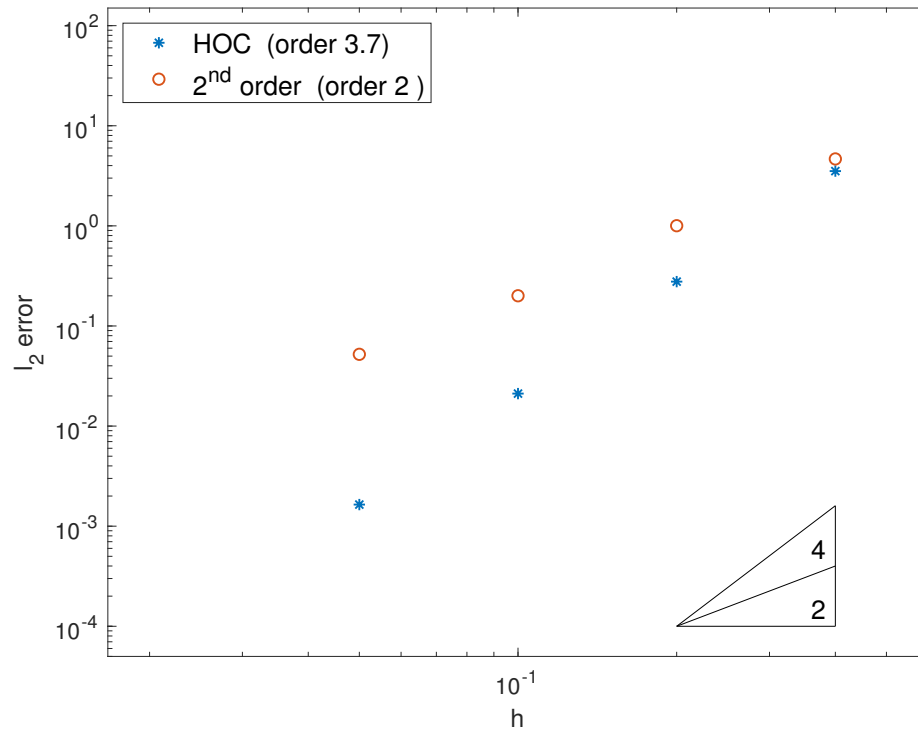


Figure 3.2:  $l_2$ -error in European call option price under Bates' model taken at mesh-sizes  $h = 0.4, 0.2, 0.1, 0.05$ .

in the call and put, or short positions in both the call and the put, respectively.

The position diagrams are shown in Figure 3.4, and from these it is clear to understand how straddles are useful, for one they are non-directional, meaning the payoff depends on the magnitude of the price change of the underlying, not whether it was up or down.

### Trading Example 1 — Long straddle

A publicly listed company XYZ is due to report quarterly earnings in two weeks time. An options trader anticipates increased volatility in the stock price in the build up the earnings announcement but is unable to predict whether the stock price will see a positive or negative movement.

The trader decides to enter a regular long straddle position, this involves putting on long positions in both put and call options with strike price equal to the current market price of XYZ. The trader will exit the position before the market closes on the day before the earning announcement. Importantly, as the trader is trading European options and intends to exit the position before maturity, they choose a liquid option contract, with time to maturity  $T = 0.5$ , this ensures there will be open interest in the contract when the

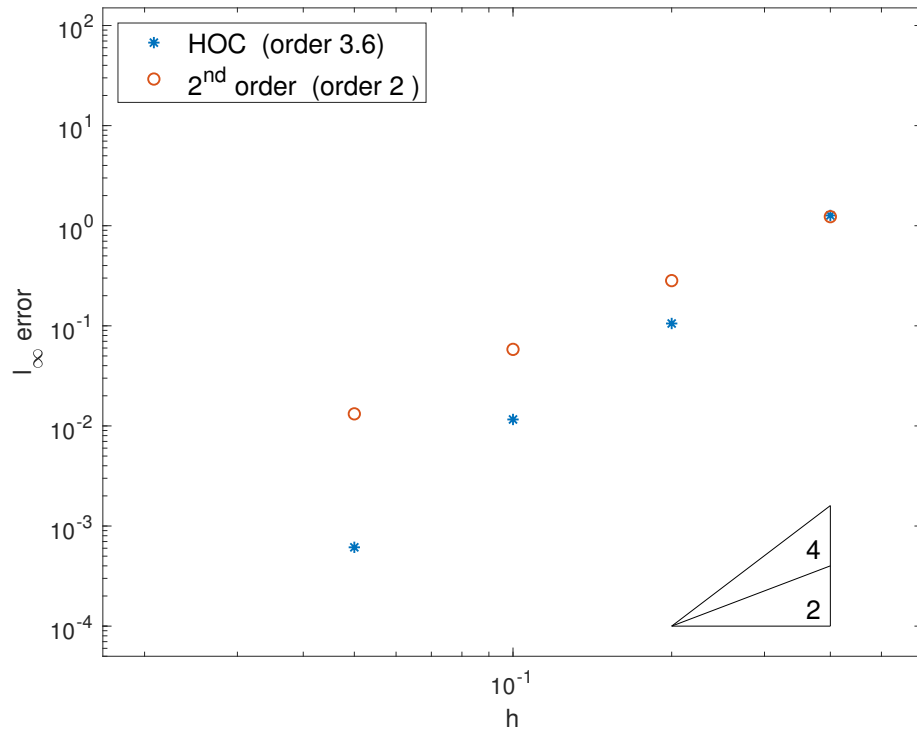


Figure 3.3:  $l_\infty$ -error in European call option price under Bates' model taken at mesh-sizes  $h = 0.4, 0.2, 0.1, 0.05$ .

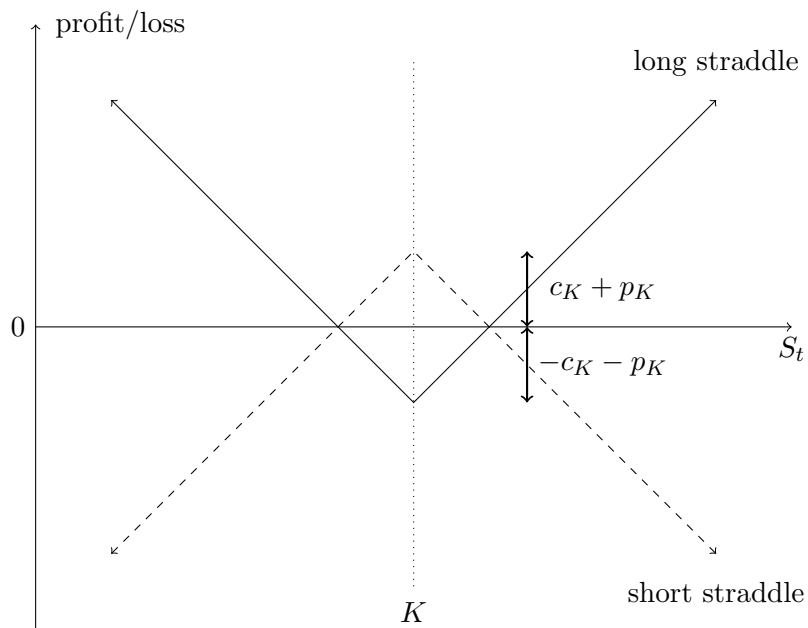


Figure 3.4: Payoff for long and short straddle strategies

trader decides to exit the position. The price of the straddle is 8.61, with current implied volatility relatively low at 10%.

The position has potential for positive payoff on a move in stock price, regardless of direction. The trader will make a profit if the value of the strategy is greater than the cost of the initial price of the options, plus commission. The potential profit in this instance is unlimited. Table 3.1 shows potential values of the straddle before the earning announcement with  $T = 0.47$ , at various prices in the underlying asset and levels of volatility. The trader will achieve a profit, before commissions, if the price of the underlying is outside the range 99.29 —101.71 at volatility 10% and be guaranteed a profit on the strategy at all prices if volatility is greater than 11%.

$\sigma = 0.1$		$\sigma = 0.2$		$\sigma = 0.3$	
Straddle	Price of XYZ	Straddle	Price of XYZ	Straddle	Price of XYZ
11.18	94	13.69	94	17.11	94
9.85	96	12.93	96	16.68	96
8.93	98	12.46	98	16.42	98
8.49	100	12.28	100	16.38	100
8.93	102	12.46	102	16.42	102
9.85	104	12.93	104	16.68	104
11.18	106	13.69	106	17.11	106

Table 3.1: Volatility, price of XYZ and respective straddle price with  $T = 0.47$ ,  $K = 100$ .

From the example above it is evident that the structure and variety of option contracts allow for market participants to trade not only the price, but specific characteristics of the underlying asset. The value of a straddle contract, as described above, is not dependent on the direction of movements in the price of the underlying asset, but rather on the magnitude. It is also positively correlated to increases in the volatility of the underlying asset, as can be seen in Figure 3.5, which further displays how changes in the volatility and the underlying will affect the payoff.

It is the decision of the trader to find a strategy or combination of strategies with a suitable risk profile. For example in the case of a short straddle strategy, the writer is exposed to unlimited losses either side of the strike price, even in a market with low volatility. However, a trader may limit the exposure to such losses a trader by entering a

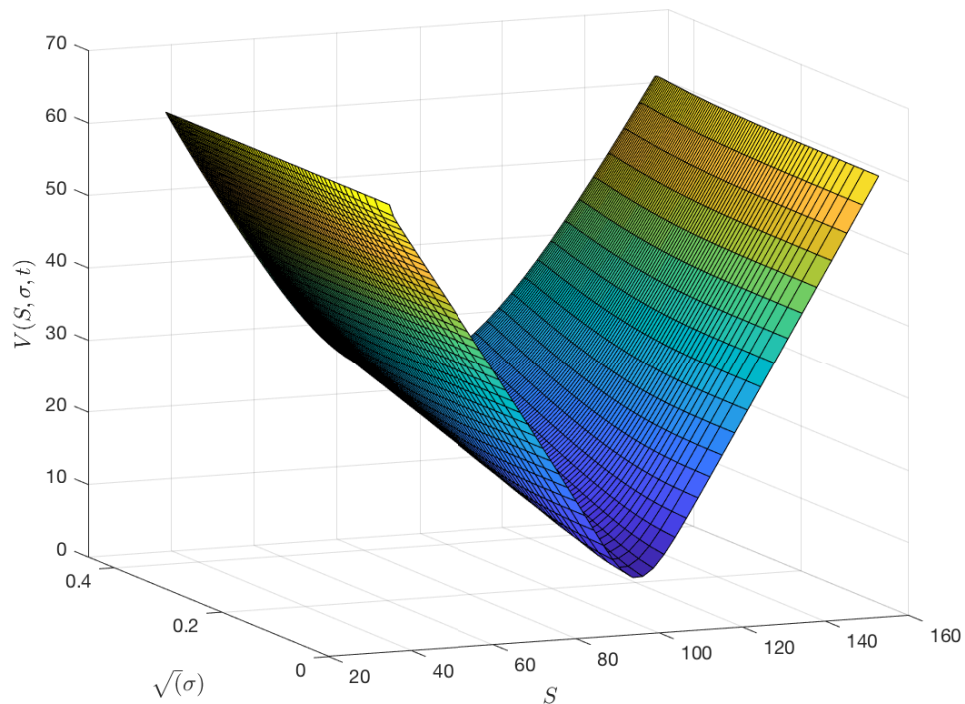


Figure 3.5: Price of long straddle with strike  $K = 100$ ,  $T = 0.5$

butterfly spread.

### 3.2.2 Butterfly Spread

A butterfly spread is an options strategy combining bull and bear spreads, with a fixed risk and capped profit, see the position diagram in Figure 3.6. Butterfly spreads use four option contracts with the same expiration but three different strike prices. An *out-the-money* strike price, an *at-the-money* strike price, and an *in-the-money* strike price. The *in* and *out-the-money* options, with the higher and lower strike prices are the same distance from the *at-the-money* options. If the *at-the-money*. Puts or calls can be used to form a butterfly spread and different combinations lead to different types of butterfly spread, each designed to profit from changes in volatility.

#### Trading Example 2 — Long Butterfly

An investor believes, based on fundamental analysis, that a publicly traded stock XYZ, which is currently trading at 100 with implied volatility of 20%, will not move significantly over the next several months. To benefit from this prediction they choose to implement a long call butterfly spread, which will profit if the price stays where it is. The investor

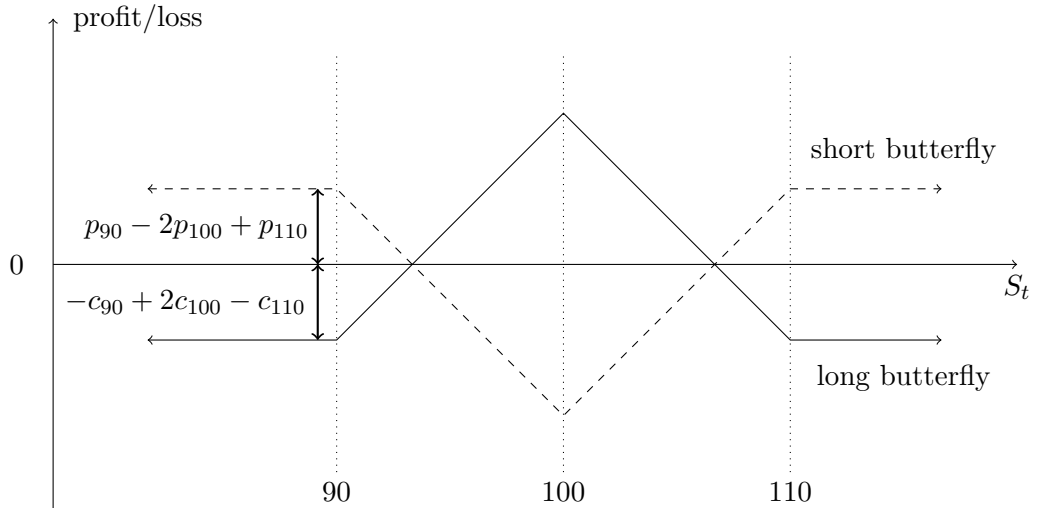


Figure 3.6: Payoff for long and short butterfly strategies, options strike  $K = 90, 100, 110$

writes two call options on XYZ at a strike price of 100, and also goes long two additional call options, one at 90 and the other at 110, all with the same maturity  $T = 0.5$ .

The investors realised profit will be dependent on the asset price at maturity and will of course take into account the combined premium paid for the butterfly position, which is 3.13. Figure 3.7 displays the price surface of the Butterfly, at different levels of volatility and for prices of XYZ. Table 3.2 gives a selection of potential profit outcomes when the position reaches maturity, we see the investor will be profitable, before commissions, within the range 93.131 — 106.869.

Price of XYZ	Profit
85	-3.13
90	-3.13
95	1.90
100	6.90
105	1.90
110	-3.13
115	-3.13

Table 3.2: Price of XYZ at expiry and associated profit of butterfly spread

As an alternative strategy the investor may decide to exit the butterfly before expiry by closing the open positions, this will be dependent on liquidity in the options market.

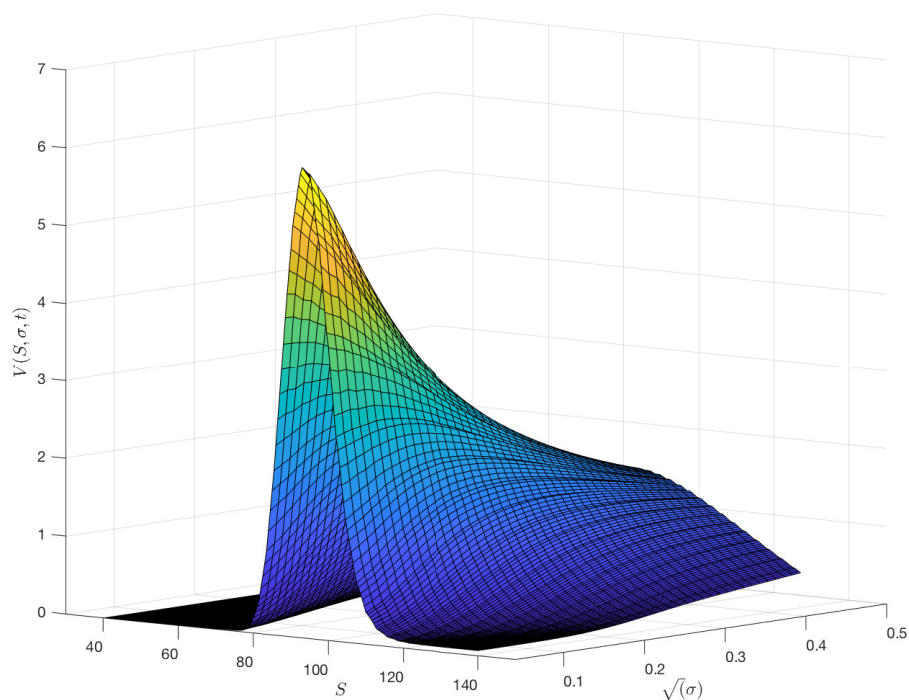


Figure 3.7: Price of long butterfly, consisting of options with strike  $K = 90, 100, 110$  and  $T = 0.5$

Taking the midpoint in time, with  $T = 0.25$ , Table 3.3 shows how the implied volatility of XYZ may influence this decision. If the implied volatility has dropped to 10% the strategy is profitable, before commissions, between 94.67 — 105.33. Likewise, if the implied volatility has remained at 20% the butterfly strategy is profitable between 95.30 — 104.70. In contrast if the implied volatility has risen to 30% the butterfly will be unprofitable for all values of XYZ.

A consequence of the early exit strategy is the lower potential maximum return the investor may receive compared to holding the position to expiry. This displays an interesting characteristic of the butterfly strategy, where profits grow with time at, and around, the strike and decay with time in the tails. The investor must make the decision to hold or exit based on their perception of market sentiment with regard to XYZ and whether the butterfly position still remains the optimum use of capital.

It is clear from this example that the premium paid to enter the position is key, and when purchasing multiple options market participants require an accurate pricing model that can be calibrated to fit across a wide array of strikes, volatility, maturities and payoff conditions. Furthermore, in OTC markets where liquidity is scarce, it is important for

$\sigma = 0.1$		$\sigma = 0.2$		$\sigma = 0.3$	
Price of XYZ	Profit	Price of XYZ	Profit	Price of XYZ	Profit
85	-2.8592	85	-2.1366	85	-1.7230
90	-2.3359	90	-1.4545	90	-1.3456
95	0.1643	95	-0.1041	95	-0.7166
100	2.7295	100	0.7728	100	-0.3389
105	0.1643	105	-0.1041	105	-0.7166
110	-2.3359	110	-1.4545	110	-1.3456
115	-2.8592	115	-2.1366	115	-1.7230

Table 3.3: Price of XYZ at  $T = 0.25$  and associated profit of butterfly spread for given volatility.

market participants to be able to price efficiently as many arbitrage algorithms exist, which will take the other side of mis-priced option orders.

During the process of trade selection a market participant will assess which conditions will lead to the position becoming profitable, we have seen in the examples above that certain strategies react differently to changes in volatility, require the underlying asset to remain near or move away from the strike price, or become more or less profitable as time elapses. The quantities driving these changes are measurable and can be evaluated by studying the option price surface, these quantities are known as the *Greeks*.

### 3.3 The Greeks

The so-called *Greeks* are the partial derivatives of the option price with respect to independent variables or parameters. These quantities represent the market sensitivities of options. Practitioners use these quantities to gain an insight into the effects of different market conditions on an options price and furthermore to develop hedging strategies against unfavourable changes in a portfolio of assets.

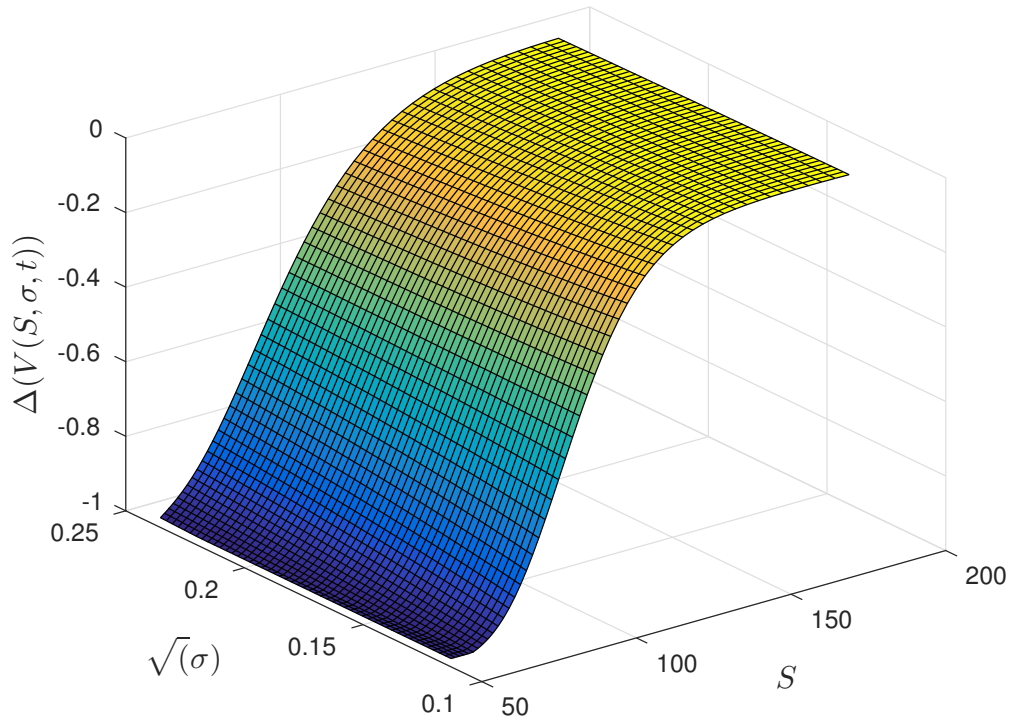


Figure 3.8: Delta of European put option priced under Bates' model with parameters: Strike  $K = 100$ , time to expiry  $T = 0.5$ .

### 3.3.1 Delta

Delta measures the sensitivity of the option price with respect to the price the underlying asset, i.e.

$$\Delta = \frac{\partial V}{\partial S}.$$

Delta hedging is a common strategy employed by options traders, an options strategy that aims to hedge the risk associated with price movements in the underlying asset, by offsetting long and short positions. This strategy allows a trader to profit from potential shifts in volatility or the option duration, however to be fully hedged a trader must adapt their portfolio by managing the position in the underlying. In this instance the higher order convergence of our scheme may be of use to traders.

We propose that the higher-order convergence achieved in the option price will also be represented in the Delta of the option, and as a consequence we will achieve a better hedge.

We calculate the Delta from the option price  $V_{i,j}^n \approx V(S_i, \sigma_j, t_n)$ . To maintain the order of the scheme we use the following fourth-order approximation formula with the

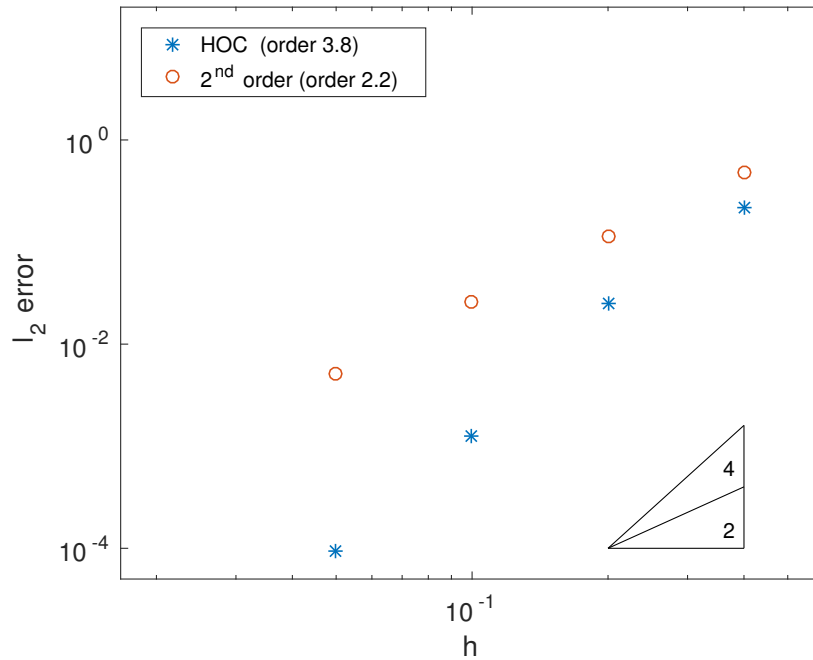


Figure 3.9: Convergence of  $l_2$ -error of Delta of a European put option priced under Bates' model with parameters: Strike  $K = 100$ , time to expiry  $T = 0.5$ .

boundaries trimmed to remove the need for extrapolation,

$$\Delta_{i,j}^n = \frac{1}{S_i} \frac{V_{i,j-2}^n - 8V_{i,j-1}^n + 8V_{i,j+1}^n - V_{i,j+2}^n}{12h}.$$

Figure 3.8 shows the resulting Delta of a European put option. Through the numerical convergence method used to study the convergence observed in the call option in Section 3.1.2, we examine the convergence of the Delta with respect to a numerical reference solution. The results are seen in Figures 3.9 and 3.10. We also observe here that the numerical convergence order agrees well with the theoretical order of the schemes, with the new HOC scheme achieving convergence rates between three and four.

### Hedging Example 1 — Delta-neutral portfolio

We construct a Delta-neutral portfolio  $\Pi = P - \Delta S$  to measure the accuracy of the hedge, the value of this portfolio should not be affected by any change in the underlying asset. We conduct the test on a fine reference grid with mesh-size  $h_{\text{ref}} = 0.025$ , then we compare the performance of each subsequent mesh-size. For comparative purposes this test is also conducted using the second-order scheme central difference scheme.

We now examine the percentage error introduced into the value of each portfolio in comparison to the reference grid. This test is conducted by moving the asset price up

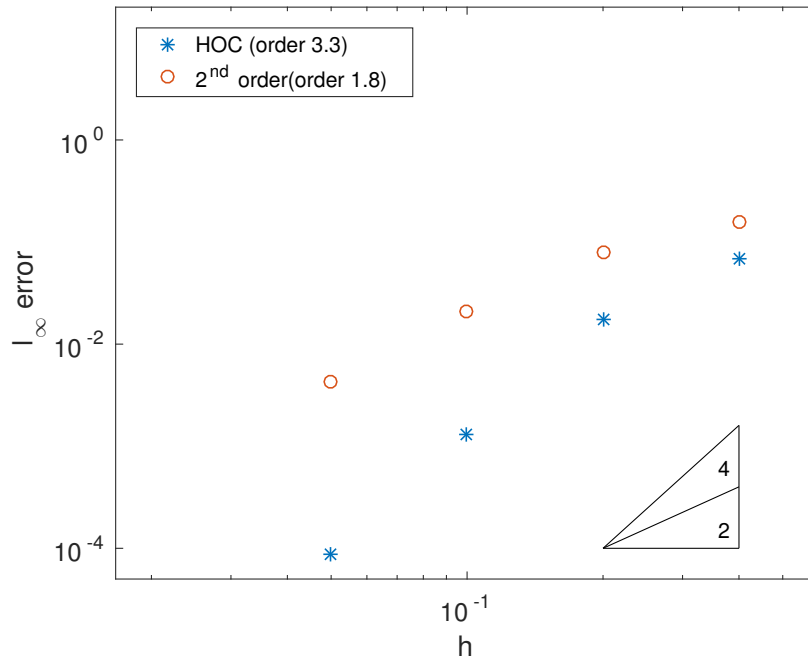


Figure 3.10: Convergence of  $l_\infty$ -error of Delta of a European put option priced under Bates' model with parameters: Strike  $K = 100$ , time to expiry  $T = 0.5$ .

Mesh Size	HOC	2nd order
$h = 0.4$	5.7649	10.3354
$h = 0.2$	0.3505	2.2765
$h = 0.1$	0.0083	0.5598
$h = 0.05$	$7.33 \cdot 10^{-4}$	0.1137

Table 3.4: Percentage error in the value of the Delta-hedged portfolio for a move down in the underlying.

or down by a fixed amount. The results for this experiment are shown in Table 3.4 and Table 3.5, with the parameters given in Table 2.1. We observe that the high-order scheme offers a better delta hedge, even on a coarser grid.

### 3.3.2 Vega

Vega measures the sensitivity of the option price with respect to changes in the volatility of the underlying asset, with the volatility given by the square root of the variance,  $\sqrt{\sigma}$ , i.e.

$$\text{Vega} = \frac{\partial V}{\partial(\sqrt{\sigma})}.$$

Mesh Size	HOC	2nd order
$h = 0.4$	4.6914	6.4067
$h = 0.2$	0.2980	1.0895
$h = 0.1$	0.0074	0.2417
$h = 0.05$	$7.86 \cdot 10^{-4}$	0.0493

Table 3.5: Percentage error in the value of the Delta-hedged portfolio for a move up in the underlying.

We examine whether the higher-order convergence achieved in the option price will also be represented in the vega of the option. Vega is calculated from the option price  $V(S, \sigma, t)$ , while the order of the scheme is maintained by using a fourth-order approximation formula.

$$\text{Vega} = \frac{\partial V}{\partial(\sqrt{\sigma})} = \frac{\partial y}{\partial(\sqrt{\sigma})} \frac{\partial V}{\partial y}$$

$$\text{Vega}_{i,j}^n = \frac{2\sqrt{\sigma_j}}{v} \left( \frac{\partial V}{\partial y} \right)_{i,j}^n = \frac{2\sqrt{\sigma_j}}{v} \frac{V_{i,j-2}^n - 8V_{i,j-1}^n + 8V_{i,j+1}^n - V_{i,j+2}^n}{12h}$$

Through the standard numerical convergence method defined in Section 3.1.2, we examine the convergence of vega with respect to a numerical reference solution.

The results of these experiments are seen in Fig. 3.12 and Fig. 3.13. We observe here that the experimentally determined convergence rates match well the theoretical order of each scheme. The errors at coarse grid,  $h = 0.4$ , are comparable, while on finer grids the high-order compact scheme gives orders of magnitude better accuracy on the same grids, achieving convergence rates of about fourth order.

As with all financial trading, options are subject to risk and managing this risk is key to success. One method of managing risk is to establish a hedge against the implied volatility of the underlying asset. This is achieved by creating a vega neutral option position, which will be not be sensitive to fluctuations in volatility.

### Hedging Example 2 — Hedging vega

An investment fund holds a long position in a non dividend paying stock, XYZ, which is currently trading at \$135. The investment fund wishes to secure an income from the position and writes some put options for XYZ with strike \$100. The investment fund now has a position with negative vega. To hedge this vega risk the investment fund creates a

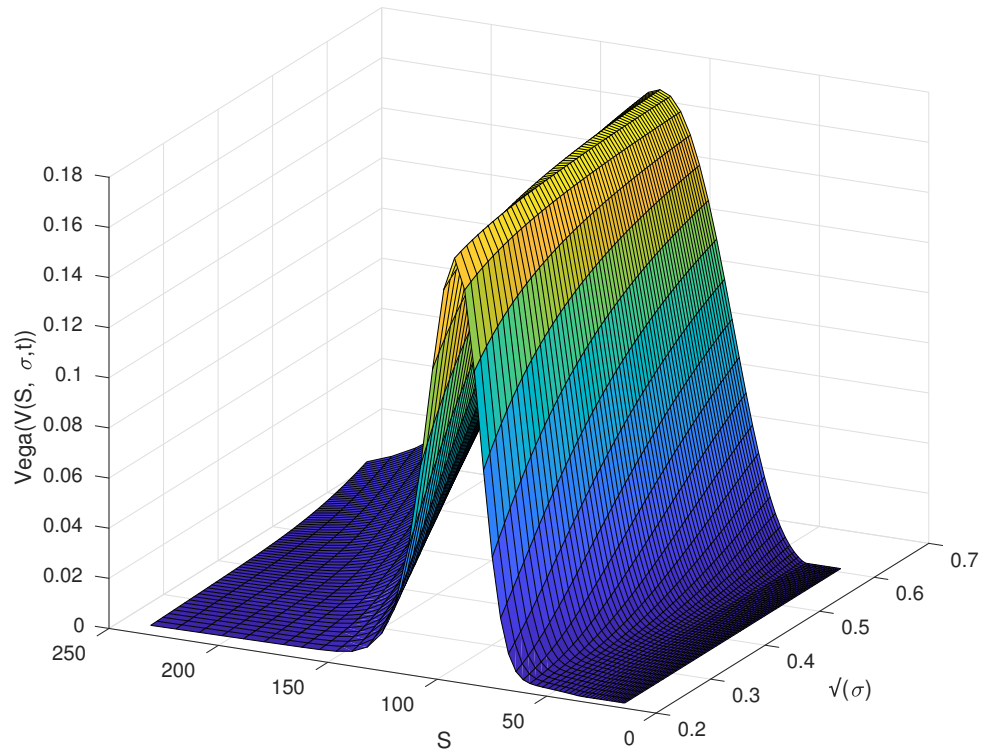


Figure 3.11: Vega of European put option priced under Bates' model with parameters: Strike  $K = 100$ , time to expiry  $T = 0.5$ .

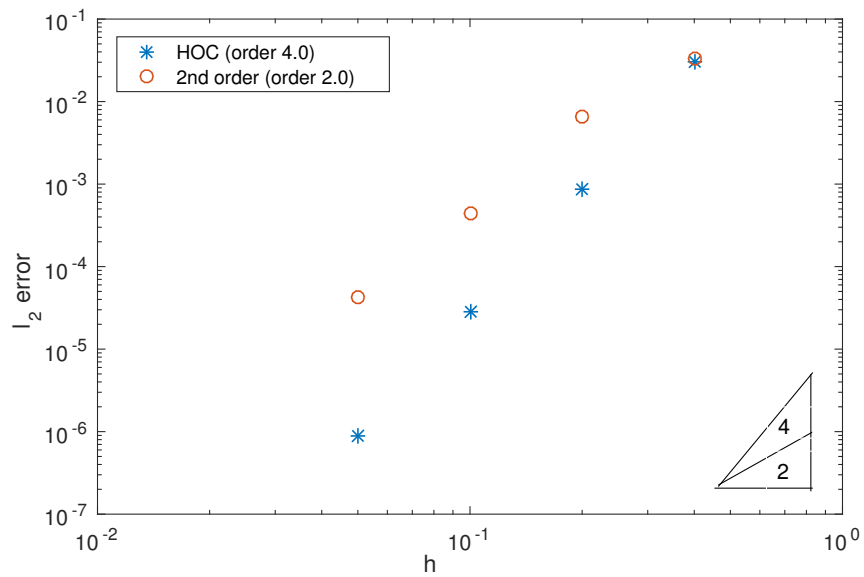


Figure 3.12: Convergence of  $l_2$ -error of the vega of a European put option priced under Bates' model with parameters: Strike  $K = 100$ , time to expiry  $T = 0.5$ .

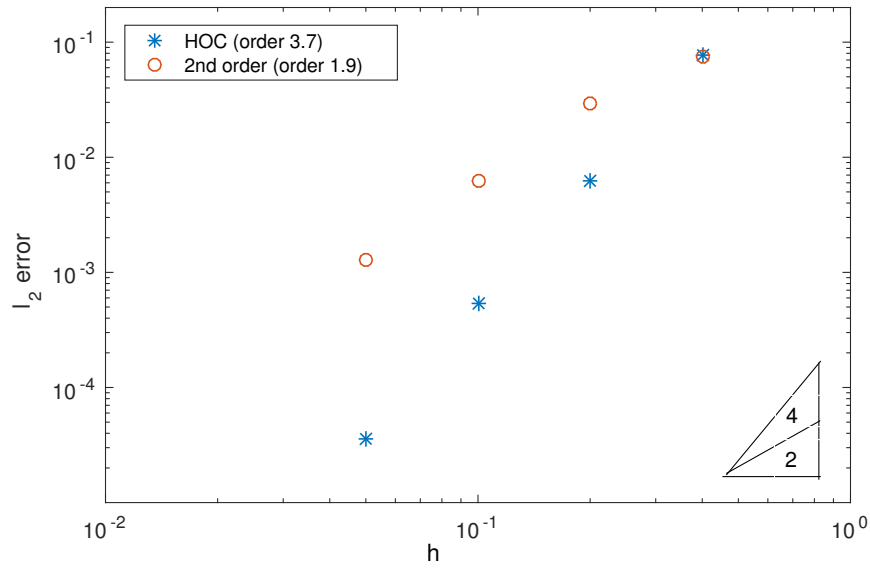


Figure 3.13: Convergence of  $l_\infty$ -error of the vega of a European put option priced under Bates' model with parameters: Strike  $K = 100$ , time to expiry  $T = 0.5$ .

Scheme	Mesh-size	Percentage error	Scheme	Mesh-size	Percentage error
HOC	0.4	33.3138	2 <sup>nd</sup> -order	0.4	62.0312
HOC	0.2	6.7519	2 <sup>nd</sup> -order	0.2	33.0638
HOC	0.1	0.6251	2 <sup>nd</sup> -order	0.1	7.4073
HOC	0.05	0.0400	2 <sup>nd</sup> -order	0.05	1.5364

Table 3.6: Percentage error in vega hedge ratio

ratio vertical put spread by buying put options with strike \$150, creating a payoff diagram as shown in Fig. 3.14.

We propose that using the HOC scheme the investment fund can utilise the high-order convergence in vega to achieve a more accurate vega hedge when constructing the ratio spread. To measure this we compare the ratio used for each mesh size,  $h$ , with the fine reference grid and examine the resulting percentage error.

The results for the high-order scheme and those for a comparative second-order scheme are shown in Table. 3.6. The high-order scheme significantly outperforms the second-order scheme at all mesh-sizes, suggesting that when entering a large position the HOC scheme will lead to a significant improvement in the vega hedge.

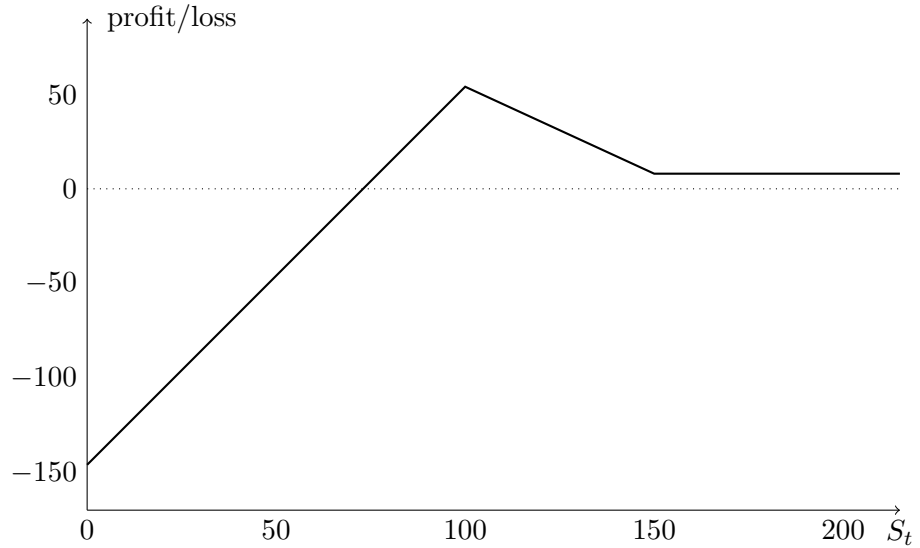


Figure 3.14: Payoff for ratio vertical put spread, examples include a 1:2 spread, where the trader writes two put options then goes long one put option with a higher strike price.

### 3.3.3 Gamma

Gamma is the second derivative of the option price with respect to the underlying asset. Gamma measures the rate of change in an option's delta, providing information on the convexity of the option's value in relation to the price of the underlying asset,

$$\Gamma = \frac{\partial^2 V}{\partial S^2}.$$

We calculate gamma using the option price  $V(S, \sigma, t)$ . To maintain the order of the scheme we use a fourth-order approximation formula.

$$\Gamma = \frac{\partial^2 V}{\partial S^2} = \frac{\partial^2 x}{\partial S^2} \frac{\partial^2 V}{\partial x^2}$$

$$\Gamma_{i,j}^n = \frac{1}{S_i^2} \left( \frac{\partial^2 V}{\partial x^2} \right)_{i,j}^n = \frac{1}{S_i^2} \frac{V_{i-2,j}^n - 16V_{i-1,j}^n + 30V_{i,j}^n - 16V_{i+1,j}^n + V_{i+2,j}^n}{12h^2}$$

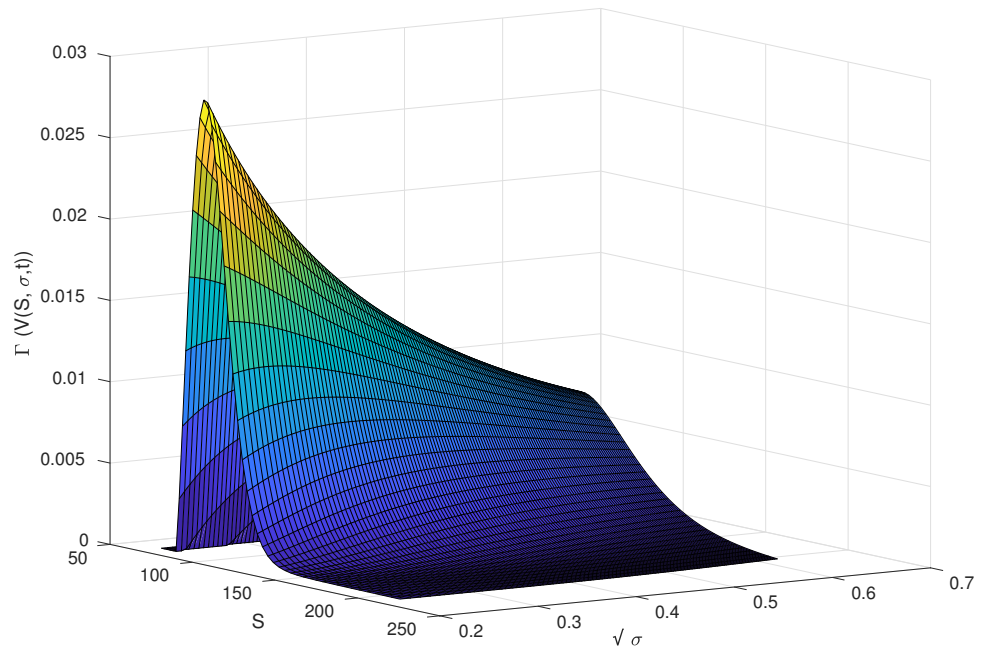


Figure 3.15: Gamma of European put option priced under Bates model' with parameters: Strike  $K = 100$ , time to expiry  $T = 0.5$ .

We conduct a numerical study to evaluate the rate of convergence of gamma, following the approach defined in Section 3.1.2. The results of these experiments are seen in Fig. 3.16 and Fig. 3.17.

The HOC scheme achieves convergence rates between three and four for the  $l_2$ - and  $l_\infty$ -errors, respectively. This is an improvement on the second-order scheme and suggests that the high-order scheme is beneficial when developing trading strategies which involve a gamma hedge.

Hedges of gamma risk are often accompanied by a delta hedge, with delta being the first derivative of the option price with respect to the underlying asset. A delta hedged portfolio is not subject to risk owing to a change in the price of the underlying asset, the gamma hedge is a re-adjustment of this delta hedge.

Delta-gamma hedging strategies often require frequent adjustments and hence are subject to high trading costs. However, if executed correctly they can enable the holder to exploit positions with positive theta, meaning the position is profitable over short time durations.

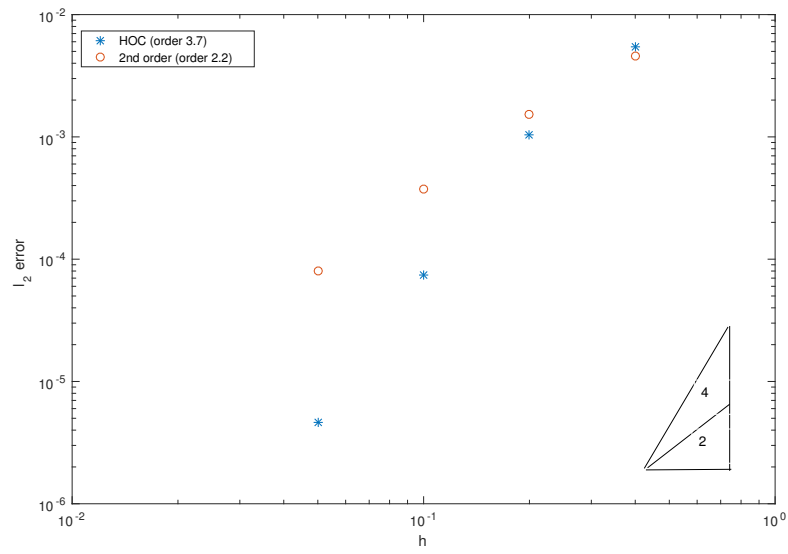


Figure 3.16: Convergence of  $l_2$ -error of gamma of a European put option priced under Bates' model with parameters: Strike  $K = 100$ , time to expiry  $T = 0.5$ .

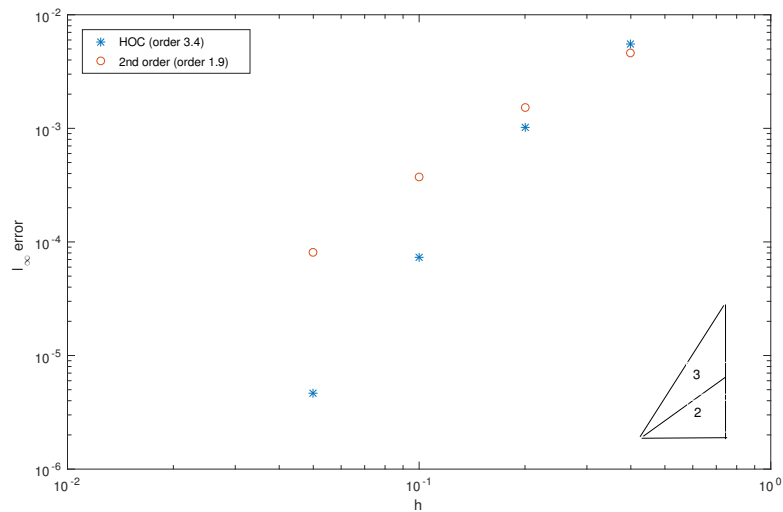


Figure 3.17: Convergence of  $l_\infty$ -error of gamma of a European put option priced under Bates' model with parameters: Strike  $K = 100$ , time to expiry  $T = 0.5$ .

### Hedging Example 3 — Hedging gamma

An analyst at an investment fund looks to create a strategy with positive theta against the funds currently held assets. They choose a ratio write spread, which involves writing options at a higher strike price than they are purchased. The analyst is wary of the positions risk related to move in the underlying asset and hence adjusts the ratio of short to long options to eliminate the net gamma.

The resulting position will have a delta value which must be hedged before the analyst can assess any profitability from the positive theta of the spread. The delta of the two option positions long and short is totalled and if positive or negative underlying assets are sold or bought, respectively.

The resulting theta is calculated and if positive the analyst can recommend the strategy as a short term trade for the investment fund.

We propose that using the HOC scheme the investment fund can utilise the high-order convergence in gamma to achieve a more accurate gamma hedge ratio. To measure this we compare the ratio used for each mesh size,  $h$ , with the fine reference grid and examine the resulting percentage error.

The results for the high-order scheme and those for a comparative second-order scheme are shown in Table. 3.7. The high-order scheme offers better results at all mesh-sizes, this improvement is particularly important in hedged positions which require repeat computation and regular adjustments.

Scheme	Mesh-size	Percentage error	Scheme	Mesh-size	Percentage error
HOC	0.4	14.8885	2 <sup>nd</sup> -order	0.4	25.1112
HOC	0.2	2.3323	2 <sup>nd</sup> -order	0.2	6.3482
HOC	0.1	0.1281	2 <sup>nd</sup> -order	0.1	1.3304
HOC	0.05	0.0081	2 <sup>nd</sup> -order	0.05	0.2674

Table 3.7: Percentage error in gamma hedge ratio

## 3.4 Summary of chapter

We have introduced the practice of hedging and given examples of strategies which are commonly used in today's derivative markets. Using the new HOC finite difference method

for option pricing in stochastic volatility jump models developed in Chapter 2, we have conducted numerical experiments to compare the scheme's hedging performance to standard finite difference methods. We confirm high-order convergence in the so called '*greeks*', the partial derivatives of the option price with respect to the underlying, with our experiments focussing on the Delta, vega and gamma of the option.

To further demonstrate the hedging properties of the new scheme, we give an example of a Delta hedged portfolio , which provides clear evidence that the high-order scheme is valuable for industry professionals seeking to calculate the relevant Delta accurately and requiring fastest computational time. We also include examples of trading strategies involving both the vega and gamma of the option, which confirm gains in the convergence and computation time. We believe this to be another tool which may be utilised by market participants attempting to achieve a more accurate hedged position.

## Chapter 4

# High-order compact finite difference scheme for option pricing in stochastic volatility with contemporaneous jump models

In any option pricing model based on the concept of a fundamentally arbitrage-free environment, invariably a compromise is made between the analytical and computational amenability of pricing and estimation. As a result of this compromise, a series of assumptions are made on the behavioural distribution of the underlying asset in an attempt to yield closed-form or nearly closed-form expressions for the price of derivatives [25].

The Black-Scholes model [11] made assumptions, including a constant volatility of the underlying asset in order to achieve a closed form solution for the price of European options. Where this assumption proved inconsistent with observed market prices, the stochastic volatility model proposed by Heston [47], was able to achieve a nearly closed-form expression for the price of European options, whilst offering the market observed variable volatility of the underlying asset.

To further this model to better reflect observed market prices, Bates added a jump-diffusion component [7], this inclusion had the effect of imposing far greater analytical and computational complexity and removing any closed-form expression except in highly restricted pricing cases. However, allowing the underlying asset to have jumps in returns, let the model generate large movements in the underlying asset capable of recreating market crashes, such as the Black Monday crash of 1987.

Despite Bates' addition of jumps in returns to the stochastic volatility model of Heston, Bates [8], and additionally Bakshi, Cao, and Chen [5] found that the sole addition of jumps in returns was not able to explain the historical shifts in volatility smiles implied by options on the S&P 500 index.

To fill the gap between the required volatility of volatility needed to reflect observed prices and the diffusive stochastic volatility featured in Bates' model, Duffie, Pan and Singleton proposed an ODE-based approach [25], which was based on the classification scheme of Dai and Singleton [22]. This approach allowed for stochastic-volatility models featuring correlated jumps in both returns and volatility, however, this was at the expense of any attempt to yield a closed-form or nearly closed-form expression for the option price.

The Duffie, Pan, Singleton model lets jumps in returns and volatility be either simultaneous, or have correlated stochastic arrival intensities, these models are named the SVCJ and SVJJ models, respectively. The SVCJ model in particular can be seen as an extension of the Bates model, and importantly both models the option price is given as the solution of a PIDE, see e.g. [20], for which we have shown HOC finite differences to be a suitable numerical method, see Chapter 2.

In this chapter we propose to extend the HOC implicit-explicit scheme derived for Bates' model in Chapter 2 to the SVCJ model. The derived scheme is fourth order accurate in space and second order accurate in time, and offers the first case of high-order convergence for this industry standard option pricing model.

This chapter is organised as follows. In the next section we recall the SVCJ model for option pricing, we discuss the implementation of the implicit-explicit scheme and note the adaptations to the previously derived scheme for option pricing under the Bates model. Section 4.2 is devoted to the numerical experiments, where we assess the performance of the new scheme. Section 4.3 offers a discussion in selection preference between the Bates and SVCJ models, where we comment on previous studies findings and relate these to recent market developments with a view to aiding financial practitioners in determining model selection. Section 4.4 summarises.

## 4.1 The SVCJ Model

The SVCJ model [25] is a stochastic volatility model which allows for jumps in both volatility and returns. Within this model the behaviour of the asset value,  $S$ , and its

variance,  $\sigma$ , is described by the coupled stochastic differential equations,

$$\begin{aligned} dS(t) &= \mu_S S(t)dt + \sqrt{\sigma(t)}S(t)dW_1(t) + S(t)dJ^S, \\ d\sigma(t) &= \kappa(\theta - \sigma(t))dt + v\sqrt{\sigma(t)}dW_2(t) + dJ^\sigma, \end{aligned}$$

for  $0 \leq t \leq T$  and with  $S(0), \sigma(0) > 0$ . Here,  $\mu_S = r - \lambda\xi_S$  is the drift rate, where  $r \geq 0$  is the risk-free interest rate. The two-dimensional jump process  $(J^S, J^\sigma)$  is a compound Poisson process with intensity  $\lambda \geq 0$ . The distribution of the jump size in variance is assumed to be exponential with mean  $v$ . In respect to jump size  $z^\sigma$  in the variance process,  $J + 1$  has a log-normal distribution  $p(z^S, z^\sigma)$  with the mean in  $\log z^s$  being  $\gamma + \rho_J z^\sigma$ , i.e. the probability density function is given by

$$p(z^S, z^\sigma) = \frac{1}{\sqrt{2\pi z^S \delta v}} e^{-\frac{z^\sigma}{v} - \frac{(\log z^S - \gamma - \rho_J z^\sigma)^2}{2\delta^2}}.$$

The parameter  $\xi_s$  is defined by  $\xi_s = e^{\gamma + \frac{\delta^2}{2}}(1 - \nu\rho_J)^{-1} - 1$ , where  $\rho_J$  defines the correlation between jumps in returns and variance,  $\gamma$  is the jump size log-mean and  $\delta^2$  is the jump size log-variance. The variance has mean level  $\theta$ ,  $\kappa$  is the rate of reversion back to mean level of  $\sigma$  and  $v$  is the volatility of the variance  $\sigma$ . The two Wiener processes  $W_1$  and  $W_2$  have constant correlation  $\rho$ .

#### 4.1.1 Partial Integro-Differential Equation

By standard derivative pricing arguments for the SVCJ model, we obtain the PIDE

$$\begin{aligned} \frac{\partial V}{\partial t} + \frac{1}{2}S^2\sigma \frac{\partial^2 V}{\partial S^2} + \rho v\sigma S \frac{\partial^2 V}{\partial S \partial \sigma} + \frac{1}{2}v^2\sigma \frac{\partial^2 V}{\partial \sigma^2} + (r - \lambda\xi_s)S \frac{\partial V}{\partial S} + \kappa(\theta - \sigma) \frac{\partial V}{\partial \sigma} \\ - (r + \lambda)V + \lambda \int_0^{+\infty} \int_0^{+\infty} V(S \cdot z^S, \sigma + z^\sigma, t) p(z^S, z^\sigma) dz^\sigma dz^S = 0, \end{aligned}$$

which has to be solved for  $S, \sigma > 0$ ,  $0 \leq t < T$  and subject to a suitable final condition, e.g.  $V(S, \sigma, T) = \max(K - S, 0)$ , in the case of a European put option, with  $K$  denoting the strike price.

Through the following transformation of variables

$$x = \log S, \quad \tau = T - t, \quad y = \sigma/v \quad \text{and} \quad u = \exp(r + \lambda)V$$

we obtain

$$\begin{aligned} u_\tau &= \frac{1}{2}vy \left( \frac{\partial^2 u}{\partial x^2} + \frac{\partial^2 u}{\partial y^2} \right) + \rho vy \frac{\partial^2 u}{\partial x \partial y} - \left( \frac{1}{2}vy - r + \lambda\xi_s \right) \frac{\partial u}{\partial x} \\ &+ \kappa \frac{(\theta - vy)}{v} \frac{\partial u}{\partial y} + \lambda \int_{-\infty}^{+\infty} \int_0^{+\infty} \tilde{u}(x + z^x, y + z^y, \tau) \tilde{p}(z^x, z^y) dz^y dz^x = \tilde{L}_D u + \tilde{L}_I u, \quad (4.1) \end{aligned}$$

which is now posed on  $\mathbb{R} \times \mathbb{R}^+ \times (0, T)$ , with  $\tilde{u}(x, y, \tau) = u(e^x, vy, \tau)$  and  $\tilde{p}(z^x, z^y) = ve^{z^x} p(e^{z^x}, z^y)$ .

The problem is completed by suitable initial and boundary conditions. In the case of a European put option we have initial condition  $u(x, y, 0) = \max(1 - \exp(x), 0)$ ,  $x \in \mathbb{R}$ ,  $y > 0$ .

### 4.1.2 Implicit-explicit high-order compact scheme

For the discretisation, we replace  $\mathbb{R}$  by  $[-R_1, R_1]$  and  $\mathbb{R}^+$  by  $[L_2, R_2]$  with  $R_1, R_2 > L_2 > 0$ . We consider a uniform grid  $Z = \{x_i \in [-R_1, R_1] : x_i = ih_1, i = -N, \dots, N\} \times \{y_j \in [L_2, R_2] : y_j = L_2 + jh_2, j = 0, \dots, M\}$  consisting of  $(2N + 1) \times (M + 1)$  grid points with  $R_1 = Nh_1$ ,  $R_2 = L_2 + Mh_2$  and with space step  $h := h_1 = h_2$  and time step  $k$ . Let  $u_{i,j}^n$  denote the approximate solution of (2.2) in  $(x_i, y_j)$  at the time  $t_n = nk$  and let  $u^n = (u_{i,j}^n)$ .

For the numerical solution of the PIDE we use the implicit-explicit HOC scheme presented in Chapter 2. The implicit-explicit discretisation in time is achieved through an adaptation of the Crank-Nicholson method, for which we shall define an explicit treatment for the two-dimensional integral operator,  $\tilde{L}_I$ .

The derivation of the finite difference scheme for the differential operator  $\tilde{L}_D$  mirrors that formed in Section 2.3, as does the implementation of initial and boundary conditions. In order to form the SVCJ model the coefficients used in the scheme are adjusted, with constant  $\xi_s$  replacing  $\xi_B$ .

### 4.1.3 Two-dimensional integral operator

We will approach the integral operator  $\tilde{L}_I$  for the SVCJ model in a similar manner to that of Bates' model. After the initial transformation of variables we have the integral operator in the following form,

$$\tilde{L}_I = \lambda \int_{-\infty}^{+\infty} \int_0^{+\infty} \tilde{u}(x + z^x, y + z^y, \tau) \tilde{p}(z^x, z^y) dz^y dz^x,$$

We make a final change of variables  $\zeta = x + z^x$  and  $\eta = y + z^y$ , with the intention of studying the value of the integral at the point  $(x_i, y_j)$ ,

$$I = \int_{-\infty}^{+\infty} \int_0^{+\infty} \tilde{u}(\zeta, \eta, \tau) \tilde{p}(\zeta - x_i, \eta - y_j) d\eta d\zeta \quad (4.2)$$

We numerically approximate the value of (4.2) over the rectangle  $(-R_1, R_1) \times (L_2, R_2)$ , with these values chosen experimentally.

$$\begin{aligned}
I_{i,j} &= \int_{-\infty}^{+\infty} \int_0^{+\infty} \tilde{u}(\zeta, \eta, \tau) \tilde{p}(\zeta - x_i, \eta - y_j) d\eta d\zeta \\
&\approx \int_{-R_1}^{R_1} \int_{L_2}^{R_2} \tilde{u}(\zeta, \eta, \tau) \tilde{p}(\zeta - x_i, \eta - y_j) d\eta d\zeta \quad (4.3)
\end{aligned}$$

To estimate the integral we require a numerical integration method of high order to match our finite difference scheme. Given the positive results achieved in Chapter 2 using the Simpson's rule to compute the integral operator in Bates' model, we take the decision to utilise the two dimensional composite Simpson's rule.

**Definition 4.1** *Two dimensional Simpson's rule*

*The double integral*

$$I = \int_a^b \int_c^d f(x, y) dx dy$$

can be approximated by applying Simpson's 1/3 rule twice, once for the  $x$  integration and once for the  $y$  integration with  $N$  partitions for both the  $x$  and  $y$  values.

$$\begin{aligned}
\int_a^b \int_c^d f(x, y) dx dy &\approx \frac{\Delta x \Delta y}{9} \left[ f(a, c) + f(a, d) + f(b, c) + f(b, d) \right. \\
&+ 4 \sum_{j=1}^n f(a, y_{2j-1}) + 2 \sum_{j=1}^{n-1} f(a, y_{2j}) + 4 \sum_{j=1}^n f(b, y_{2j-1}) + 2 \sum_{j=1}^{n-1} f(b, y_{2j}) \\
&+ 4 \sum_{i=1}^m f(x_{2i-1}, c) + 2 \sum_{i=1}^{m-1} f(x_{2i}, c) + 4 \sum_{i=1}^m f(x_{2i-1}, d) + 2 \sum_{i=1}^{m-1} f(x_{2i}, d) \\
&+ 16 \sum_{j=1}^n \left( \sum_{i=1}^m f(x_{2i-1}, y_{2j-1}) \right) + 8 \sum_{j=1}^{n-1} \left( \sum_{i=1}^m f(x_{2i-1}, y_{2j}) \right) \\
&\left. + 8 \sum_{j=1}^n \left( \sum_{i=1}^{m-1} f(x_{2i}, y_{2j-1}) \right) + 4 \sum_{j=1}^{n-1} \left( \sum_{i=1}^{m-1} f(x_{2i}, y_{2j}) \right) \right].
\end{aligned}$$

With the error of the integral bounded by

$$\frac{h^4}{180} (b-a)(d-c) \max_{\zeta \in [a,b], \eta \in [c,d]} |f^{(4)}(\zeta, \eta)|.$$

Allowing the integral in (4.3) to be evaluated using the two-dimensional Simpsons rule on a equidistant grid in  $x, y$  with spacing  $\Delta x = \Delta y$ , with  $m_x$  grid-points in  $(x_{min}, x_{max})$  and  $m_y$  grid-points in  $(y_j, y_{max})$ , where each interval has length mesh-size  $h/2$ , we have

$$\begin{aligned}
\bar{I}_{i,j} \approx & \frac{h^2}{36} \left[ \tilde{u}(x_{min}, y_{min}, \tau) \tilde{p}(x_{min} - x_i, y_{min} - y_j) + \tilde{u}(x_{min}, y_{max}, \tau) \tilde{p}(x_{min} - x_i, y_{max} - y_j) \right. \\
& + \tilde{u}(x_{max}, y_{min}, \tau) \tilde{p}(x_{max} - x_i, y_{min} - y_j) + \tilde{u}(x_{max}, y_{max}, \tau) \tilde{p}(x_{max} - x_i, y_{max} - y_j) \\
& + 4 \sum_{l=1}^{\frac{m_x}{2}} \tilde{u}(x_{min}, y_{2l-1}, \tau) \tilde{p}(x_{min} - x_i, y_{2l-1} - y_j) + 2 \sum_{l=1}^{\frac{m_x}{2}-1} \tilde{u}(x_{min}, y_{2l}, \tau) \tilde{p}(x_{min} - x_i, y_{2l} - y_j) \\
& + 4 \sum_{l=1}^{\frac{m_x}{2}} \tilde{u}(x_{max}, y_{2l-1}, \tau) \tilde{p}(x_{max} - x_i, y_{2l-1} - y_j) + 2 \sum_{l=1}^{\frac{m_x}{2}-1} \tilde{u}(x_{max}, y_{2l}, \tau) \tilde{p}(x_{max} - x_i, y_{2l} - y_j) \\
& + 4 \sum_{k=1}^{\frac{m_x}{2}} \tilde{u}(x_{2k-1}, y_{min}, \tau) \tilde{p}(x_{2k-1} - x_i, y_{min} - y_j) + 2 \sum_{k=1}^{\frac{m_x}{2}-1} \tilde{u}(x_{2k}, y_{min}, \tau) \tilde{p}(x_{2k} - x_i, y_{min} - y_j) \\
& + 4 \sum_{k=1}^{\frac{m_x}{2}} \tilde{u}(x_{2k-1}, y_{max}, \tau) \tilde{p}(x_{2k-1} - x_i, y_{max} - y_j) + 2 \sum_{k=1}^{\frac{m_x}{2}-1} \tilde{u}(x_{2k}, y_{max}, \tau) \tilde{p}(x_{2k} - x_i, y_{max} - y_j) \\
& + 16 \sum_{l=1}^{\frac{m_x}{2}} \left( \sum_{k=1}^{\frac{m_x}{2}} \tilde{u}(x_{2k-1}, y_{2l-1}, \tau) \tilde{p}(x_{2k-1} - x_i, y_{2l-1} - y_j) \right) \\
& + 4 \sum_{l=1}^{\frac{m_x-1}{2}} \left( \sum_{k=1}^{\frac{m_x-1}{2}} \tilde{u}(x_{2k}, y_{2l}, \tau) \tilde{p}(x_{2k} - x_i, y_{2l} - y_j) \right) \\
& + 8 \sum_{l=1}^{\frac{m_x-1}{2}} \left( \sum_{k=1}^{\frac{m_x}{2}} \tilde{u}(x_{2k-1}, y_{2l}, \tau) \tilde{p}(x_{2k-1} - x_i, y_{2l} - y_j) \right) \\
& \left. + 8 \sum_{l=1}^{\frac{m_x}{2}} \left( \sum_{k=1}^{\frac{m_x-1}{2}} \tilde{u}(x_{2k}, y_{2l-1}, \tau) \tilde{p}(x_{2k} - x_i, y_{2l-1} - y_j) \right) \right]
\end{aligned}$$

Which, with  $f$  representing the integral in (4.3), has error bounded by

$$\frac{h^4}{180} (R_2 - L_2)(2R_1) \max_{\zeta \in [-R_1, R_1], \eta \in [L_2, R_2]} |f^{(4)}(\zeta, \eta)|.$$

To compute this sum in the case of Bates' model, see Section 2.3.2, we computed the calculation explicitly at each time-step using a the matrix-vector equation, whereby a matrix is created which holds the probability terms and the weights applied by the Simpson's rule. This is multiplied by a vector containing the option price solution from the current time step  $u_t$ . After the initial time-step we extend this further by incorporating the solution at time-step  $u_{t-1}$ , which resulted in a scheme that is second-order in time.

The decision to follow this approach was driven by the need for a high-order numerical integration method. Had we required a second order method we may have chosen, for example the trapezoidal rule, and have been able to follow the method of Salmi et. al, which utilises the Toeplitz structure of the probability matrix [74]. Following this method

it is possible to embed the Toeplitz matrix into a Circulant matrix, which may be decomposed allowing a sequence of Fast Fourier Transforms (FFT) to compute the integral in a fast and efficient manner. The weights associated with the Simpson's rule render this approach unviable and hence lead to the creation of the dense matrix, a structure which is purposefully avoided in algorithmic calculations, as the memory requirements limit potential refinement in the pricing algorithm.

The complexity of this problem is intensified in the case of the two dimensional Simpson's rule, where we have a weight matrix  $W$ , with

$$W = \begin{bmatrix} 1 & 4 & 2 & 4 & 2 & \dots & 4 & 1 \\ 4 & 16 & 8 & 16 & 8 & \dots & 16 & 4 \\ 2 & 8 & 4 & 8 & 4 & \dots & 8 & 2 \\ \vdots & \vdots & \vdots & \vdots & \vdots & \ddots & \vdots & \vdots \\ 4 & 16 & 8 & 16 & 8 & \dots & 16 & 4 \\ 1 & 4 & 2 & 4 & 2 & \dots & 4 & 1 \end{bmatrix}.$$

The difficulty is compounded by the nature of a double integral problem, as these weightings apply to a matrix of elements and not an individual element as was the case in Bates' model. Attempting to implement this method to our integral leads to the block Toeplitz matrix  $T_{\bar{m}_y m_x}$ , which performs the integration over  $y$ .

$$T_{\bar{m}_y m_x} = \begin{pmatrix} T_0 & T_1 & \dots & T_{m_y-1} \\ T_{-1} & T_0 & \dots & T_{m_y-2} \\ \vdots & \ddots & \ddots & \vdots \\ T_{-(m_y-1)} & \dots & T_{-1} & T_0 \end{pmatrix}$$

The matrix  $T_{\bar{m}_y m_x}$  is populated with Toeplitz blocks  $T_\ell$ , containing elements  $T_{k,\ell}$ , which relate to the integration over the variable  $x$ .

$$T_\ell = \begin{pmatrix} T_{0,\ell} & T_{1,\ell} & \dots & T_{m_x-1,\ell} \\ T_{-1,\ell} & T_{0,\ell} & \dots & T_{m_x-2,\ell} \\ \vdots & \ddots & \ddots & \vdots \\ T_{-(m_x-1),\ell} & \dots & T_{-1,\ell} & T_{0,\ell} \end{pmatrix}$$

$$T_{k,\ell} = \tilde{p}(k\Delta(x), (\ell + m_y - 1)\Delta(y)),$$

By defining  $\bar{I} = (\bar{I}_1 \ \bar{I}_2 \ \dots \ \bar{I}_{m_x-1} \ \bar{I}_{m_x})^T$  and  $\bar{u} = (\bar{u}_1 \ \bar{u}_2 \ \dots \ \bar{u}_{m_x-1} \ \bar{u}_{m_x})^T$ , where  $\bar{I}_\ell = (\bar{I}_{1,\ell} \ \bar{I}_{2,\ell} \ \dots \ \bar{I}_{m_y-1,\ell} \ \bar{I}_{m_y,\ell})^T$  and  $\bar{u}_\ell = (\bar{u}_{1,\ell} \ \bar{u}_{2,\ell} \ \dots \ \bar{u}_{m_y-1,\ell} \ \bar{u}_{m_y,\ell})^T$ , we can compute  $\bar{I}$  by

$$\bar{I} = W T_{\bar{m}_y m_x} \bar{u}$$

When discretising the differential operator  $L_D$  we formed a uniform grid consisting of  $(2N + 1) \times (M + 1)$  grid points, with mesh size  $h_x = h_y$ . To discretise the integral operator over this grid using the Simpson's rule requires the use of the intermediate grid points, leading to the introduction of mesh-size  $h/2$ , and the required values of  $u_{i,j}$  to be approximated at the intermediate points through interpolation.

We employ a standard measure for designing end-user algorithms based on the memory requirements. We decide that requirements of over 4GB of RAM pose a significant barrier to non-organisational users, additionally we impose a strict rule that one individual matrix should not exceed half of this limit, which allows for a dense square matrix of order  $(16000 \times 16000)$ . For Bates' model, with a single integral, we required a dense matrix of order  $(4N + 1) \times (2M + 1)$ , rendering a value of  $N < 4000$  acceptable, which we consider not to be a significant limitation on the refinement of mesh size  $h$ . Comparatively, for the SVCJ model, the required block Toeplitz matrix  $T_{\bar{m}_y m_x}$  is a dense matrix of order  $(8N^2 + 1) \times (2M^2 + 1)$ . When imposing the 2GB limit on this matrix we arrive at an acceptable value of  $N \leq 11$ , which clearly poses a significant barrier to reducing mesh-size  $h$ , producing an accurate solution and achieving the mesh-size required to plot convergence results.

We propose an alternative approach, where we avoid the construction of a dense matrix through computation of the integral, as a product of the sums, at each time step. To ease this calculation we choose  $R_1, L_2$  and  $R_2$  experimentally, such that the value of the terms on the boundary can be considered negligible. Hence,

$$I_{i,j} \approx \frac{h^2}{36} \left[ 16 \sum_{l=1}^{\frac{m_x}{2}} \left( \sum_{k=1}^{\frac{m_x}{2}} \tilde{u}(x_{2k-1}, y_{2l-1}, \tau) \tilde{p}(x_{2k-1} - x_i, y_{2l-1} - y_j) \right) \right. \\ \left. + 4 \sum_{l=1}^{\frac{m_x-1}{2}} \left( \sum_{k=1}^{\frac{m_x-1}{2}} \tilde{u}(x_{2k}, y_{2l}, \tau) \tilde{p}(x_{2k} - x_i, y_{2l} - y_j) \right) \right. \\ \left. + 8 \sum_{l=1}^{\frac{m_x-1}{2}} \left( \sum_{k=1}^{\frac{m_x}{2}} \tilde{u}(x_{2k-1}, y_{2l}, \tau) \tilde{p}(x_{2k-1} - x_i, y_{2l} - y_j) \right) \right]$$

$$+ 8 \sum_{l=1}^{\frac{m_x}{2}} \left( \sum_{k=1}^{\frac{m_x-1}{2}} \tilde{u}(x_{2k}, y_{2l-1}, \tau) \tilde{p}(x_{2k} - x_i, y_{2l-1} - y_j) \right) \Big].$$

This computation imposes no additional memory demands on the algorithm, which is in agreement with the requirement for an end-user algorithm.

## 4.2 Numerical Experiments

We perform numerical studies to evaluate the rate of convergence and computational efficiency of the scheme. For comparison we include the results of a second-order central finite difference scheme, which follows the implicit-explicit approach of the HOC scheme. For a clear comparison of the effect of Simpson's rule in the HOC scheme, we evaluate the numerical integration with the two-dimensional trapezoidal rule, calculated explicitly as a product of the sums at each time step. The second-order finite difference scheme requires the inclusion of a Rannacher-style start up to combat stability issues [68].

The parameters for the numerical experiments, unless otherwise stated, are given in Table 4.1.

Parameter	Value
Strike Price	$K = 100$
Time to maturity	$T = 0.5$
Interest rate	$r = 0.05$
Volatility of volatility	$v = 0.1$
Mean reversion speed	$\kappa = 2$
Long-run mean of $\sigma$	$\theta = 0.01$
Correlation	$\rho = -0.5$
Jump Intensity	$\lambda = 0.2$
Jump size in returns log-variance	$\delta^2 = 0.16$
Jump size in returns log-mean	$\gamma = -0.5$
Jump size in volatility mean	$\nu = 0.2$

Table 4.1: Default parameters for numerical simulations associated with the SVCJ model.

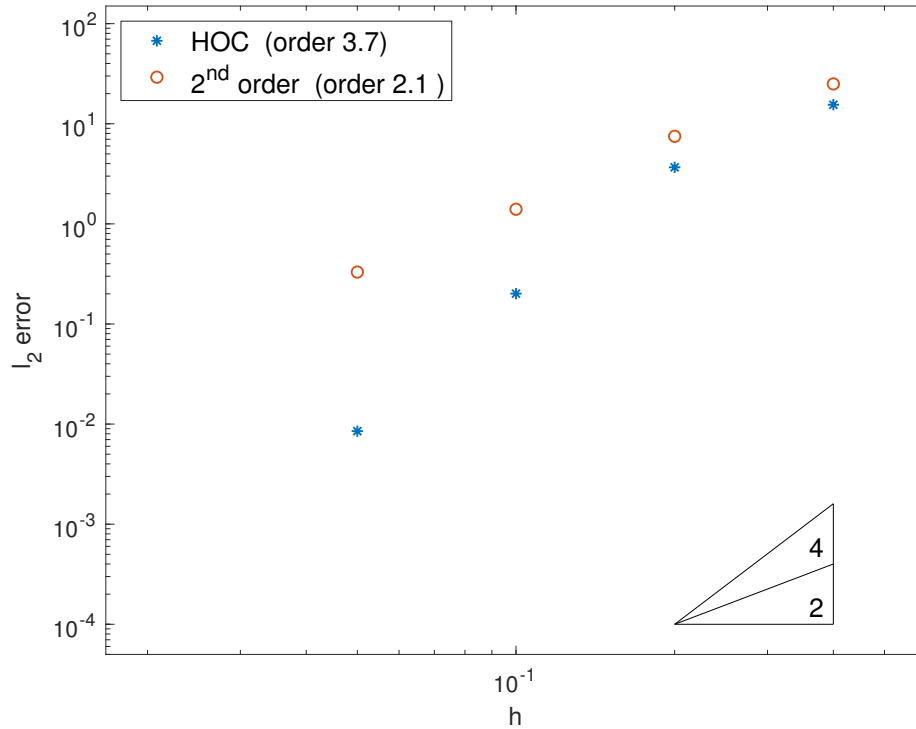


Figure 4.1:  $l_2$  error in European put option price under the SVCJ model taken at mesh-sizes  $h = 0.4, 0.2, 0.1, 0.05$ .

#### 4.2.1 Numerical convergence

For our convergence study we refer to both the  $l_2$ -error  $\epsilon_2$  and the  $l_\infty$ -error  $\epsilon_\infty$  with respect to a numerical reference solution on a fine grid with  $h_{\text{ref}} = 0.025$ . With the parabolic mesh ratio  $k/h^2$  fixed to a constant value we expect these errors to converge as  $\epsilon = Ch^m$  for some  $m$  and  $C$  which represent constants. From this we generate a double-logarithmic plot  $\epsilon$  against  $h$  which should be asymptotic to a straight line with slope  $m$ , thereby giving a method for experimentally determining the order of the scheme.

The numerical convergence results are included in Figure 4.1. We observe that the numerical convergence orders reflect the theoretical order of the schemes, with the new HOC scheme achieving convergence rates near fourth order.

#### 4.2.2 Computational efficiency comparison

We compare the computational time of the two schemes, looking at the time to obtain a given accuracy, taking into account matrix setups, factorisation and boundary condition evaluation. The timings depend obviously on technical details of the computer as well as on specifics of the implementation, for which care was taken to avoid unnecessary bias in

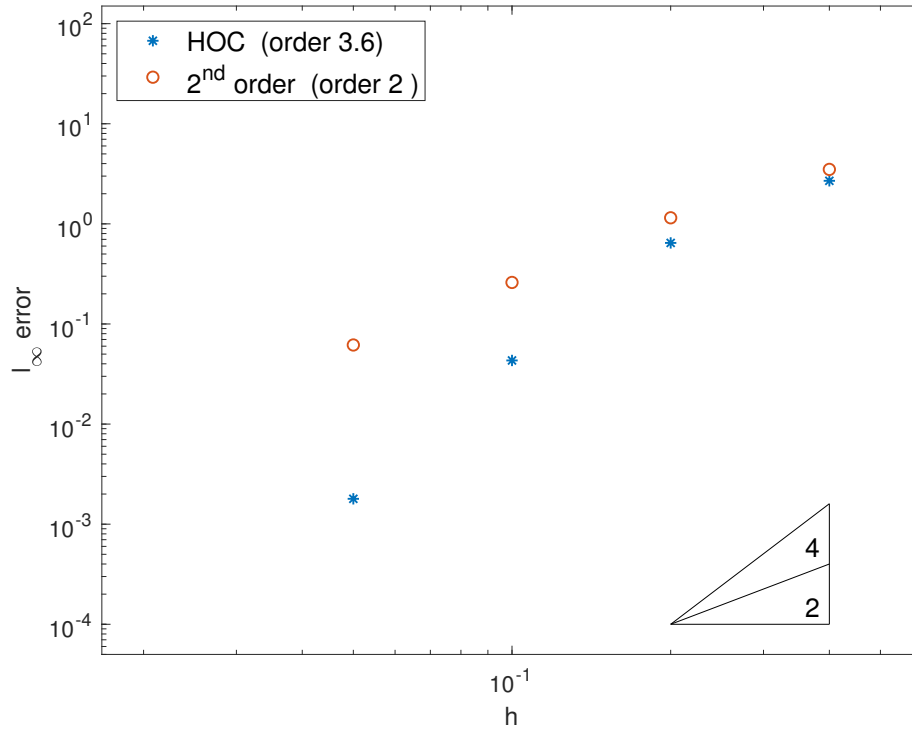


Figure 4.2:  $l_\infty$  error in European put option price under the SVCJ model taken at mesh-sizes  $h = 0.4, 0.2, 0.1, 0.05$ .

the results. All results were computed on the same laptop computer (2015 MacBook Air 11”).

The results are shown below in Table 4.2. The mesh-sizes used for this comparison are  $h = 0.4, 0.2, 0.1$  and  $0.05$ , with the reference mesh-size used being  $h_{\text{ref}} = 0.025$ .

The HOC scheme achieves higher accuracy, with a lower memory allocation, at all mesh sizes. This is a direct consequence of our persistence to produce a scheme with low memory demands, the second-order schemes increased demand is a result of the requirement of a Rannacher start-up. This beneficial results in terms of memory usage are, however, at the expense of computation time, where we attribute this increase in the HOC scheme as a result of the extra computational cost associated with the Simpson’s rule as compared to the trapezoidal rule.

In Figure 4.3, we include the results previously seen for the Bates model, see Chapter 2. This indicates the increase in computation time between the two models. Financial practitioners must base a decision of which model to implement on their requirements for

---

<sup>1</sup>Rather than total memory usage, increases in memory usage at each subsequent refinement from the base mesh size  $h = 0.4$  are given for each scheme.

Scheme	$h$	$l_2$ -error	$l_\infty$ -error	time (s)	memory (kB)
HOC	0.4	4.9321	1.5433	0.304	7096
	0.2	0.4361	0.1864	5.713	+812
	0.1	0.0394	0.0141	312.562	+4168
	0.05	0.0022	0.0009	21180.171	+17008
FD	0.4	8.1927	2.0370	0.372	7144
	0.2	1.9337	0.5820	3.592	+1420
	0.1	0.4772	0.1441	102.554	+5552
	0.05	0.1262	0.0347	3637.313	+23396

Table 4.2: Performance results for the HOC and second-order FD schemes for the SVCJ model<sup>1</sup>.

faster computational time, against their preference for a model which offers a more robust calibration setup.

We do stress, however, that with access to higher memory allocation it would be possible to achieve high-order convergence with a far reduced increase in computation time. This may be achieved by solving the numerical integration through use of the block-matrix structure described in Section 4.1.3 and computed through a matrix-vector product.

### 4.2.3 Numerical stability analysis

To assess the stability of the scheme we present a numerical stability analysis. We propose to test to what extent the parabolic mesh ratio  $k/h^2$  impacts the convergence of the scheme. If the effect is minimal this will allow numerically regular solutions to be obtained without restriction on the time step-size. We proceed to compute numerical solutions for varying values of the parabolic mesh ratio  $k/h^2$  and the mesh width  $h$ , then plot these against the associated  $l_2$ -errors to detect stability restrictions depending on  $k/h^2$ . This numerical test is performed for both the high-order and the second-order schemes, with the results shown in Figure 4.4 and Figure 4.5 respectively. We use default parameters from Table 4.1, and vary the parabolic mesh size from 0.1 to 1 in increments of 0.1. As was noted in Section 2.6.3 we draw the readers attention to the difference in the error scales between the two schemes.

The second-order scheme shows a mild dependence on the time-stepping, with a

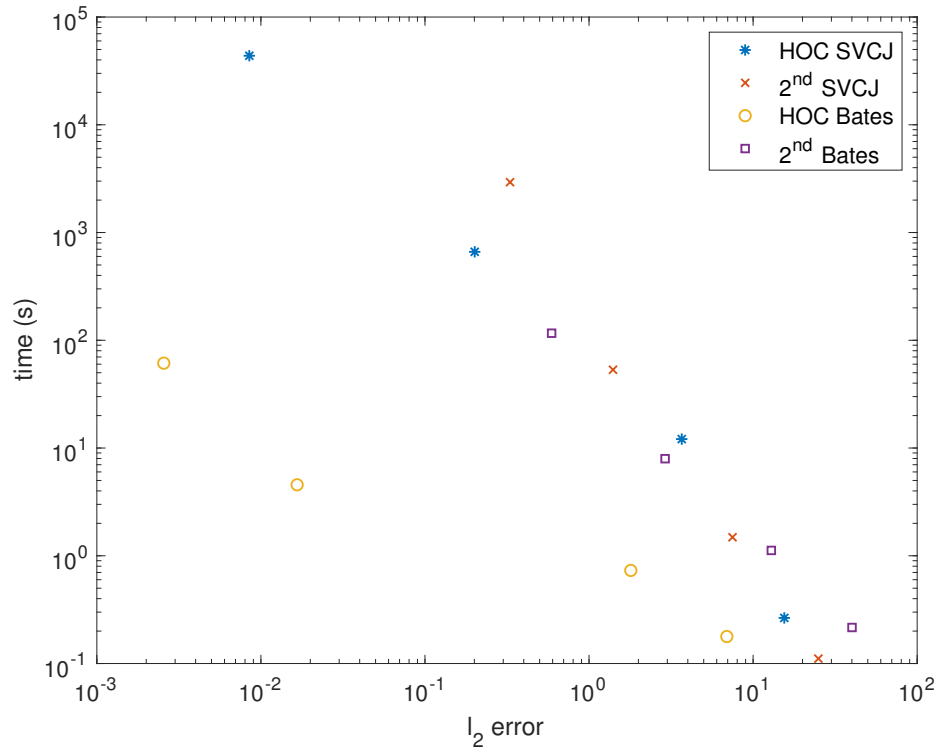


Figure 4.3: Computational efficiency comparison taken at mesh-sizes  $h = 0.4, 0.2, 0.1, 0.05$ .

stronger effect for larger mesh size  $h$ . The HOC scheme also shows a mild condition for larger mesh-size  $h$ , however this dissipates as  $h$  is reduced and on the finer meshes there appears to be negligible dependence on the parabolic mesh ratio. As there is no apparent stability restriction for the HOC scheme, we suggest parabolic mesh ratio at or above 0.5 are most useful, as this has potential to partially counteract the time increase seen in the HOC scheme.

The dependence of the parabolic mesh ratio we notice on coarser mesh sizes can be attributed to the implicit-explicit nature of the scheme. However, as the restriction on the time stepping for the new scheme is not severe, since the discretisation matrices do not change in time (the coefficients in the PIDE (4.1) do not depend on time). Hence, the sparse matrix factorisation is performed only once, and additional time steps do not require additional factorisations to solve the problem.

#### 4.2.4 Feller Condition

We examine the robustness of the new HOC scheme for the SVCJ model with respect to the Feller condition as we did for the Bates' model in Section 2.6.4. We study the

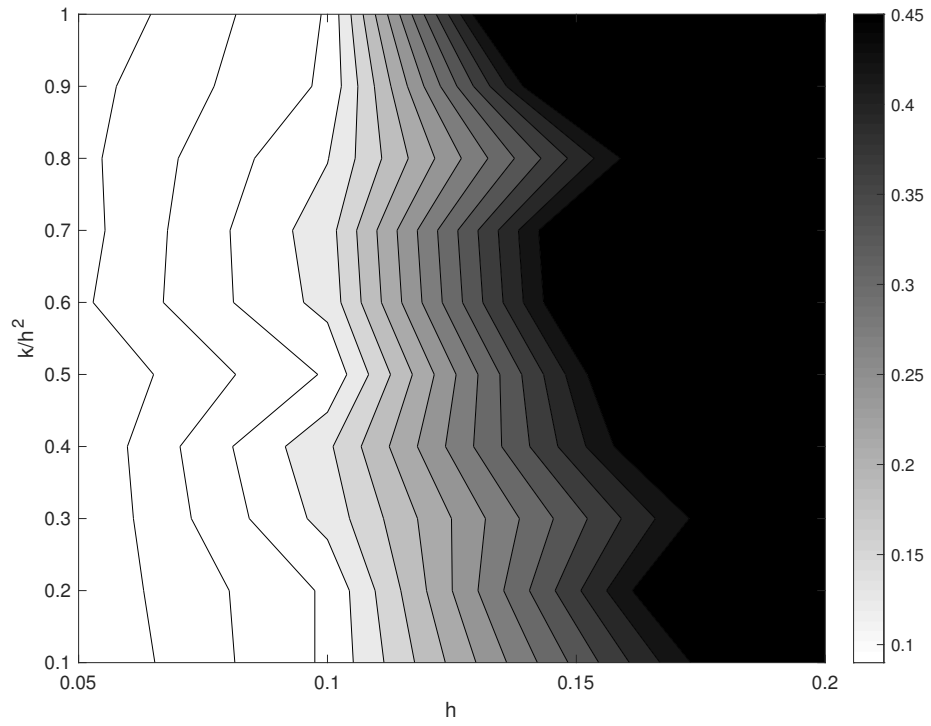


Figure 4.4: Contour plot of the  $l_2$ -error for the HOC scheme for the SVCJ model.

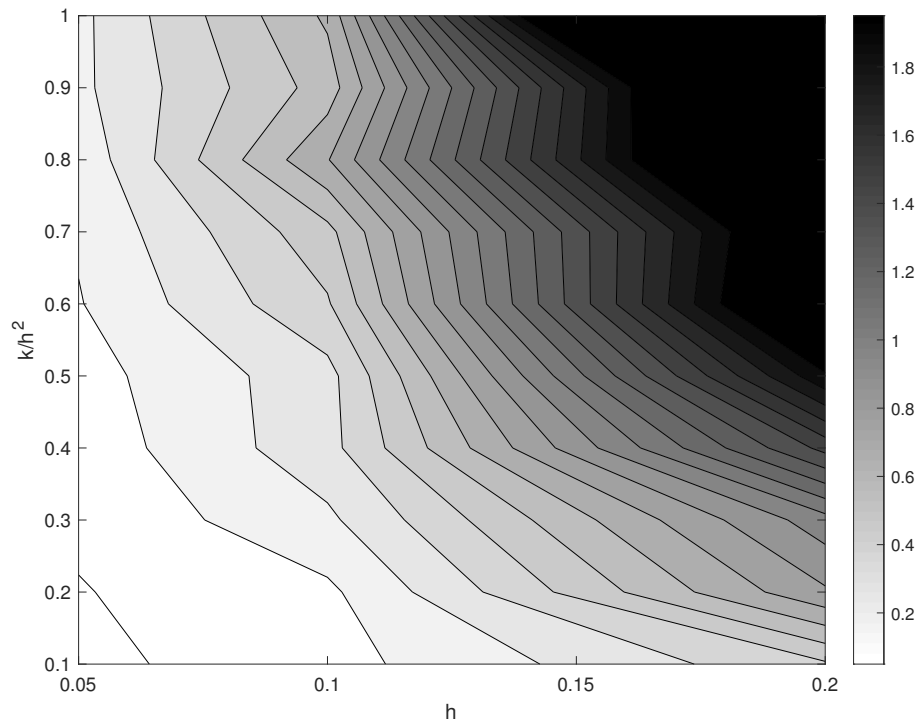


Figure 4.5: Contour plot of the  $l_2$ -error for second-order scheme for the SVCJ model.

convergence rates achieved when the Feller condition,  $2\kappa\theta \geq v^2$ , is not satisfied for the Cox-Ingersol-Ross (CIR) volatility process [21].

We use the default parameters defined in Table 4.1, with exceptions for long-run variance mean  $\theta$  and volatility of volatility  $v$ , which we alter to test the condition as shown in Table 2.3.

We study the  $l_2$  and  $l_\infty$  -error associated with each condition. The results are shown in Table 4.3, the  $l_2$ -error numerical convergence rates, obtained from a least squares fitted line as explained earlier, are 3.6, 3.6 and 3.7 for  $v = 0.7, 0.4$  and  $0.1$ , respectively. This leads us to confirm that the new HOC scheme performs well irrespective of the validity of the Feller condition.

Condition	$h$	$l_2$ -error	$l_\infty$ -error
$2\kappa\theta < v^2$	$h = 0.2$	3.6417	0.3623
	$h = 0.1$	0.3435	0.0409
	$h = 0.05$	0.0254	0.0031
$2\kappa\theta = v^2$	$h = 0.2$	2.0172	0.2683
	$h = 0.1$	0.1392	0.0257
	$h = 0.05$	0.0138	0.0024
$2\kappa\theta > v^2$	$h = 0.2$	0.7681	0.2748
	$h = 0.1$	0.0722	0.0260
	$h = 0.05$	0.0047	$1.97 \cdot 10^{-3}$

Table 4.3: Numerical convergence results for HOC scheme for the SVCJ model with varying Feller condition.

### 4.3 Bates/SVCJ model selection

Both the SVCJ and Bates' model offer high levels of calibration in comparison to standard stochastic volatility models. Many research papers has been conducted on the differences of the Heston model to Bates' model and the SVCJ model, with a focus on the calibration of the models parameters to observed market prices, particularly in times of market turbulence [16].

These studies offer a range of results regarding the necessity of the inclusion of jumps in returns, of jumps in volatility and furthermore the relationship between the jump pro-

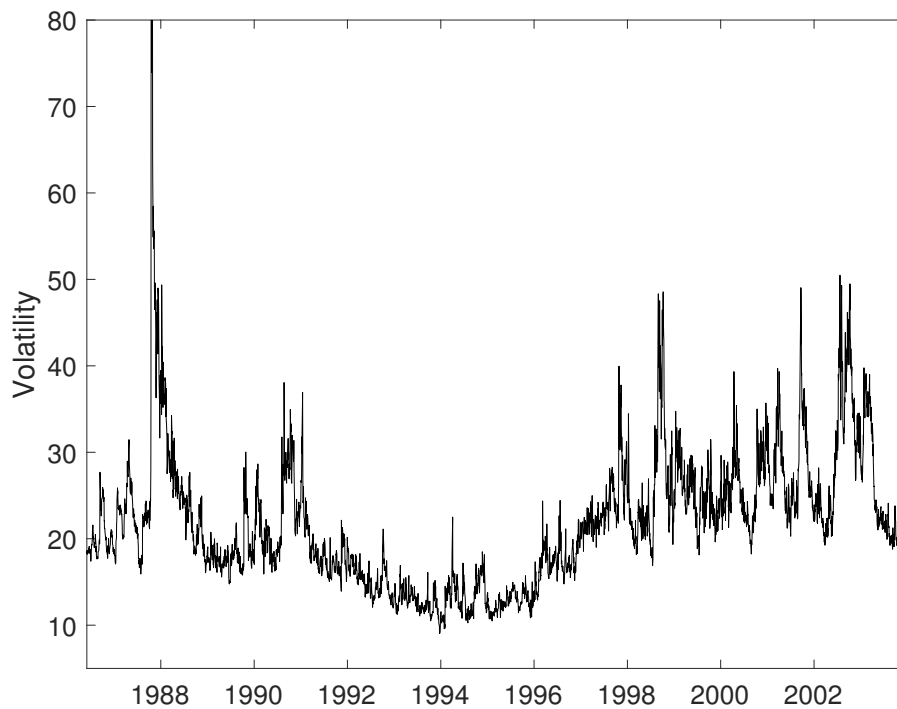


Figure 4.6: Time series of implied volatility as measured by the VIX<sup>2</sup> from 1987-2003, *Cboe*.

cesses. The studies of Bates [8] and Bakshi, Cao and Chen [5], offer contrasting opinions on the inclusion of jumps, with the former concluding that the benefits are economically small whereas the latter sees substantial benefits.

More recently, Broadie, Chernov and Johannes [16] conduct a study into model specification and risk premia, focussing on observed prices in futures options. They propose that where previous studies were unable to agree on the benefits of jump processes is related to differing test statistics and limited time periods of the data collection. Historically large market shocks have been observed to be infrequent and the existence of a shock within the data set will heavily determine the authors decision as to whether the inclusion of jumps is warranted.

Broadie et.al. use a larger set of data from S&P 500 futures options, with data from January 1987 to March 2003. This period features a range of market shocks, see Figure 4.6,

---

<sup>2</sup>VIX: On September 22, 2003, the Cboe made two key enhancements to the VIX methodology: Based on S&P 500 Options Prices. The new VIX will be based on prices of S&P 500 (SPX) options. Previously, the original-formula VIX was based on prices of the S&P 100 (OEX) Index Options, and Cboe will continue to calculate and disseminate the original-formula index to be known as the Cboe S&P 100 Volatility Index SM with the ticker VXO index.

and encompasses the time-periods which feature in the studies of Bates, Bakshi, Cao and Chen and the further studies of both Eraker and Pan [37].

The study of Broadie et.al. concludes that adding jumps to the Heston model improves the cross-sectional fit by almost 50%, which gives further weight to the work of Bakshi, Chao and Chen while offering a contrasting view to that of Bates, Pan and Eraker. Over the larger data set Broadie et.al. judge that Bates' and the SVCJ model perform similarly well. This is attributed to the importance of price jumps and stochastic volatility for describing the time series of returns or for pricing options [16].

This is not to dispute that jumps in volatility, albeit not to the same degree do offer an important addition to an option pricing model, both by further explaining the time series of returns [16] and secondly as their inclusion alleviates concerns over model misspecification, which was cause enough for Bates to suggest adding jumps in volatility [8].

In recent years, partly due to the emergence of algorithmic trading, jumps in both prices and volatility have become commonplace in financial markets. Algorithms have been blamed for exacerbating large moves, through programming which is focussed on following trends and in some cases following the behaviour of other algorithms [2]. The VIX index between 2003-2019, see Figure 4.7, shows frequent spikes occurring, which appear to be increasingly common after the 2008 financial crash and offering further weight to the argument for the SVCJ models benefit to current financial practitioners.

For optimal model selection, these studies and developments suggest that the SVCJ model is a clear choice. However, as we have shown in our numerical experiments, see Table 4.2, the computational demands imposed by the SVCJ model in terms of time or required memory allocation are a potential barrier to financial practitioners demanding the fastest computation time. While Bates' model offers a drastically faster alternative and an important improvement on purely stochastic volatility models, allowing Bates' model to serve as a highly effective model for option pricing.

For financial practitioners, model selection must also be based on their chosen markets dynamics, as with notable differences in the trading patterns of commodity futures, currency and stocks, variations should be expected in the performance of option pricing models. However, using either of the established quasi market-standard Bates' and SVCJ models, allows for excellent calibration to fit observed data while the HOC scheme presented in this thesis offers a robust, efficient and effective numerical method for the option price computation.

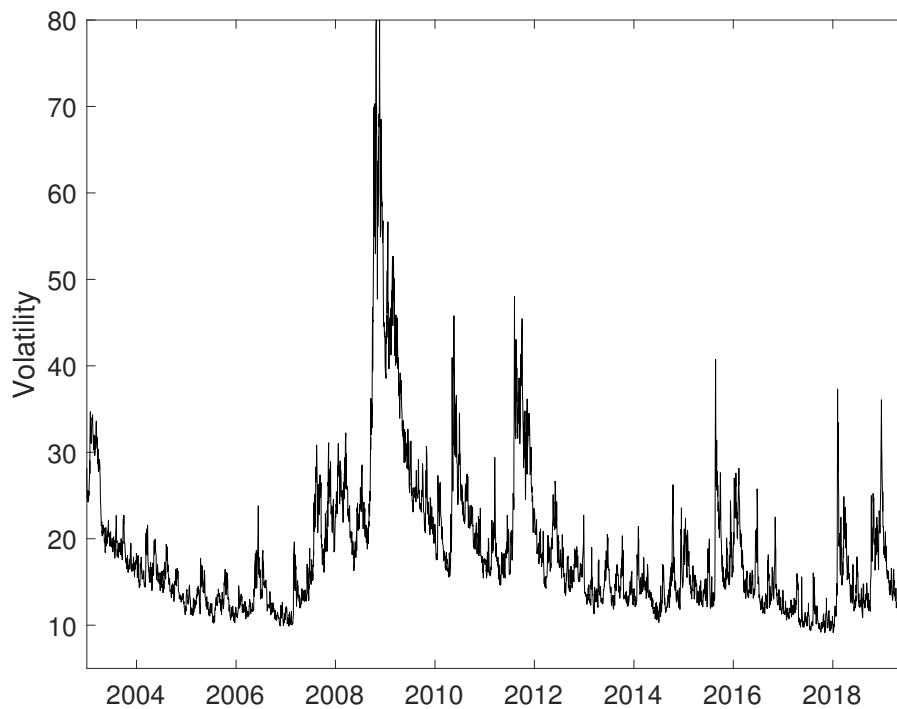


Figure 4.7: Time series of implied volatility as measured by the VIX index from 2003-2019, *Cboe*.

#### 4.4 Summary of chapter

We have derived a new HOC finite difference method for option pricing under the SVCJ model. Numerical experiments confirm high-order convergence in the option price without stability restrictions and confirm the scheme's acceptance of the Feller condition. The numerical method is based on an implicit-explicit scheme in combination with HOC finite difference stencils for solving the partial integro-differential equation. The two-dimensional jump term adds a complexity to the option pricing model, while the requirement of a high-order double numerical integration method increases the scheme's demand for memory and the computational time required to achieve high-order convergence.

As the availability of computer memory improves it should be expected that alternative methods will become possible for the solution of the double integral problem using high-order numerical integration methods, allowing for faster computational times, comparable to those seen for the HOC scheme for Bates' model, as shown in Chapter 2. We also note the opportunity for parallelisation in the problem and the potential for ADI methods to again improve computation time.

We finished by discussing what drives financial practitioners choices in selecting either

the Bates' or the SVCJ model. Focussing on the studies of Bates, Bakshi et.al, Pan, Eraker and Broadie et.al, we discuss the contradictory views of these studies and associate their findings with recent market developments and the emergence of algorithmic trading as the main liquidity provider in financial markets. We note the difference in computational time as an important driver in the selection process, with the HOC scheme for Bates' model offering pricing approximately  $10^3$  times faster when used on a fine grid (mesh-size  $h = 0.05$ ), and up to 40 times faster on a coarse grid (mesh-size  $h = 0.2$ ).

## Chapter 5

# Conclusion

This thesis is concerned with the derivation and implementation of high-order compact finite difference methods to solve the PIDEs arising from a class of option pricing models, stochastic volatility with jump models.

In Chapter 2, we employed standard derivative pricing arguments for the Bates model, to obtain the PIDE

$$\begin{aligned} \frac{\partial V}{\partial t} + \frac{1}{2}S^2\sigma \frac{\partial^2 V}{\partial S^2} + \rho v\sigma S \frac{\partial^2 V}{\partial S \partial \sigma} + \frac{1}{2}v^2\sigma \frac{\partial^2 V}{\partial \sigma^2} + (r - \lambda\xi_B)S \frac{\partial V}{\partial S} + \kappa(\theta - \sigma) \frac{\partial V}{\partial \sigma} - (r + \lambda)V \\ + \lambda \int_0^{+\infty} V(S\tilde{y}, v, t)p(\tilde{y}) d\tilde{y} = 0, \quad (5.1) \end{aligned}$$

which has to be solved for  $S, \sigma > 0$ ,  $0 \leq t < T$  and subject to a suitable final condition, e.g.  $V(S, \sigma, T) = \max(K - S, 0)$ , in the case of a European put option, with  $K$  denoting the strike price.

We transform the variables in 5.1, as an introductory step in the derivation of an implicit-explicit scheme based on the high-order finite difference method introduced by Düring et.al for option pricing in the Heston model [28].

The implicit-explicit scheme combines the treatment of the derivative operator using HOC finite difference stencils, with our chosen fourth order numerical integration method, the Simpson's rule, for the integral operator.

The scheme is completed with necessary smoothing of the initial condition, which in this example is the payoff of a European put option. This follows from [59], where it is proposed that a sufficiently smooth initial condition is required to yield high-order convergence. The resulting scheme uses a Crank-Nicolson time discretisation and is fourth order in space and second order in time.

In the results section we conduct numerical experiments to assess the convergence and computational efficiency of the new HOC scheme. In order to form a comparative study

we introduce a second-order finite difference method discretisation and both second and high-order finite element formulation.

The results confirm the theoretical order of the scheme, with convergence of order 4 in both the  $l_2$  and  $l_\infty$  norms, which are estimated from the slope of a least squares fitted line. This is to the best of the author's knowledge the first high-order scheme for this highly popular option pricing model.

Compared to finite element methods, it is very parsimonious in terms of memory requirements and computational effort, since it achieves high-order convergence without requiring additional unknowns (unlike finite elements with higher polynomial order).

At the same time, the new HOC scheme is very efficient, requiring only one initial  $LU$ -factorisation of a sparse matrix to perform the option price valuation. It can also be useful to upgrade existing implementations based on standard finite differences in a straightforward manner to obtain a highly efficient option pricing code.

For trading professionals, the new HOC scheme offers the ability to more accurately compute option prices, in faster time and with less memory requirements. These improvements will allow both individuals and institutions more confidence in their ability to offer tighter market spreads, in more varied and volatile market conditions, and lead to an increase in volume across options markets globally.

In Chapter 3 we introduce the practice of hedging, a key use of financial derivatives. We confirm high-order convergence for the HOC scheme with initial condition the payoff of a European call option. This allows us to study examples of hedging strategies, which are commonly used in today's derivative markets. We focus on the straddle and butterfly strategies, where a trader buys and sells a combination of options to form a payoff which is hedged to certain changes in the underlying asset.

In the results section we again use the HOC finite difference method for option pricing in stochastic volatility jump models developed in Chapter 2, to conduct numerical experiments to compare the scheme's hedging performance to standard finite difference methods. We confirm high-order convergence in the so called '*greeks*', the partial derivatives of the option price with respect to the underlying, with our experiments focussing on the Delta, vega and gamma of the option.

To further demonstrate the hedging properties of the new scheme, we give an example of a Delta hedged portfolio, which provides clear evidence that the high-order scheme is valuable for industry professionals seeking to calculate the relevant Delta accurately and requiring fastest computational time. We also include examples of trading strategies

involving both the vega and gamma of the option, which confirm gains in the convergence and computation time. We believe this to be another tool which may be utilised by market participants attempting to achieve a more accurate hedged position.

In Chapter 4, we implement standard derivative pricing arguments for the SVCJ model, to obtain the PIDE

$$\begin{aligned} \frac{\partial V}{\partial t} + \frac{1}{2}S^2\sigma \frac{\partial^2 V}{\partial S^2} + \rho v\sigma S \frac{\partial^2 V}{\partial S \partial \sigma} + \frac{1}{2}v^2\sigma \frac{\partial^2 V}{\partial \sigma^2} + (r - \lambda\xi_s)S \frac{\partial V}{\partial S} + \kappa(\theta - \sigma) \frac{\partial V}{\partial \sigma} \\ - (r + \lambda)V + \lambda \int_0^{+\infty} \int_0^{+\infty} V(S.z^S, \sigma + z^\sigma, t)p(z^S, z^\sigma) dz^\sigma dz^S, \quad (5.2) \end{aligned}$$

which has to be solved for  $S, \sigma > 0$ ,  $0 \leq t < T$  and subject to a suitable final condition, e.g.  $V(S, \sigma, T) = \max(K - S, 0)$ , in the case of a European put option, with  $K$  denoting the strike price.

We follow the same transformation of variables we applied in Chapter 2 to equation (5.2). We complete the HOC finite difference scheme with a suitable adaption to the derivative operator to fit the SVCJ model. The complexity of the SVCJ model is entwined in it's double integral for the jump term, where the underlying asset now features correlated jumps in both returns and volatility.

We attempt to implement the numerical integration in the manner suggested in [74], however, we find the memory requirements of the two-dimensional Simpson's composite rule are prohibitive to reduction of the mesh-size required to form an accurate pricing algorithm. In order to combat the memory allocation issue we compute the integral directly at each time-step, which removes the requirement to store a dense matrix and allows for the algorithm to fit within the pre-imposed 4GB RAM limit.

We conduct numerical experiments, which confirm high-order convergence in the option price without stability restrictions and confirm the scheme's acceptance of the Feller condition. This is to the best of the author's knowledge the first high-order scheme for this complex option pricing model.

We discuss what drives financial practitioners choices in selecting either Bates' or the SVCJ model, with a focus on recent market developments. To aid financial practitioners in determining model selection we compare the computational time of the two schemes, with the HOC scheme for Bates' model offering pricing approximately  $10^3$  times faster when used on fine grids, and up to 40 times faster on coarse grids.

For further research we consider the American option pricing problem for Bates' model, which will require solving a free boundary problem involving the PIDE (5.1). This can in principle be approached by combining the HOC scheme presented in this paper with

standard methods like projected successive overrelaxation (PSOR) or penalty methods. The key challenge, however, will be to retain high-order convergence of the scheme in view of limited regularity across the free boundary.

As a second extension, and with Moore's law in mind, as the availability of computer memory improves over the coming years it should be expected that alternative methods will become possible for the solution of the double integral problem using high-order numerical integration methods, allowing for progressively faster computational times. We also note the opportunity for parallelisation in the problem and the potential for a combination with high-order alternating direction implicit methods [33] methods and with sparse grids methods [46, 31], which along with providing an interesting research topic also offer potential for improved computation time and further memory efficiencies.

# Bibliography

- [1] Y. Achdou and O. Pironneau. Computational methods for option pricing. In: *Frontiers in Applied Mathematics Volume 30*, SIAM, Philadelphia, PA, 2005.
- [2] S. Amaro, Sell-offs could be down to machines that control 80% of the US stock market, fund manager says [online], viewed 8th Sept 2019, <<https://www.cnbc.com/2018/12/05/sell-offs-could-be-down-to-machines-that-control-80percent-of-us-stocks-fund-manager-says.html>>.
- [3] L. Andersen and J. Andreasen. Jump-Diffusion Processes: Volatility Smile Fitting and Numerical Methods for Option Pricing, *J. Review of Derivatives Research* **4**, 231-262, 2000.
- [4] L. Bachelier. Théorie de la spéculation (Thesis), *Annales scientifiques de l'École Normale Supérieure, Sér.* **3** (17), 21-88, 1900. (English Translation:- In: *The Random Character of Stock Market Prices*, P.H. Cootner, (ed.) pp.17-78, MIT Press, Cambridge, Mass., 1964.)
- [5] G. Bakshi, C. Cao, and Z. Chen. Empirical performance of alternative option pricing models, *Journal of Finance*, **52**, 2003-2049, 1997.
- [6] O.E. Barndorff-Nielsen and N. Shephard. Non-Gaussian Ornstein-Uhlenbeck based models and some of their uses in financial economics, *Journal of the Royal Statistical Society*, **63**, 167-241, 2001.
- [7] D.S. Bates. Jumps and stochastic volatility: Exchange rate processes implicit Deutsche mark options, *Rev. Financ. Stud.* **9**, 637-654, 1996.
- [8] D.S. Bates. Post-'87 Crash fears in S&P 500 futures options, *Journal of Econometrics* **94**, 181-238, 2000.
- [9] E. Benhamou, E. Gobet and M. Miri. Time Dependent Heston Model, *SIAM J. Finan. Math.* **1**, 289-325, 2010.

- [10] G. Berikelashvili, M.M. Gupta, and M. Mirianashvili. Convergence of fourth order compact difference schemes for three-dimensional convection-diffusion equations, *SIAM J. Numer. Anal.*, **45**, 443-455, 2007.
- [11] F. Black and M. Scholes. The pricing of options and corporate liabilities. *J. Polit. Econ.* **81**, 637-659, 1973.
- [12] T. Bollerslev, R.F. Engle and D.B. Nelson. Arch Models. In: *Handbook of Econometrics, Volume IV*, D.L McFadden et al. (eds) pp.2960–3038, Elsevier Science B.V, North Holland, 1994.
- [13] M. Briani, R. Natalini and G. Russo. Implicit-explicit numerical schemes for the jump-diffusion processes, *Calcolo* **44**, 33-57, 2007.
- [14] M. Briani, L. Caramellino and A. Zanette. A hybrid approach for the implementation of the Heston model, *IMA J. Manag. Math.* **28**(4), 467-500, 2017.
- [15] M. Briani, L. Caramellino, G. Terenzi and A. Zanette. On a hybrid method using trees and finite-differences for pricing options in complex models. Preprint, arXiv:1603.07225, 2016.
- [16] M. Broadie, M. Chernov and M. Johannes. Model Specification and Risk Premia: Evidence from Futures Options, *J. Of Finance*, **62** (3), 1453-1490, 2007.
- [17] D.M. Causon and C.G. Mingham. *Introductory Finite Difference Methods for PDEs*, Ventus, Academic Press, 2010.
- [18] C. Chiarella, B. Kang, G. Meyer and A. Ziogas. The evaluation of American option prices under stochastic volatility and jump-diffusion dynamics using the method of lines. *Int. J. Theor. Appl. Finan.* **12**, 393, 2009.
- [19] N. Clarke and K. Parrott. Multigrid for American option pricing with stochastic volatility. *Appl. Math. Finance* **6**(3), 177-195, 1999.
- [20] R. Cont and P. Tankov. *Financial Modelling with Jump Processes*, Chapman & Hall/CRC, Boca Raton, FL, 2004.
- [21] J.C. Cox, J. Ingersoll and S. Ross. A theory of the term structure of interest rates. *Econometrica*, **53**, 385-407, 1985.
- [22] Q. Dai, K.J. Singleton. Specification Analysis of Affine Term Structure Models, *The J. Finance*, **55** (5), 1943-1978, 2002.

- [23] E. Derman and I. Kani. Riding on a smile, *Risk*, **7** (2), 32-39, 1994.
- [24] H. Deusch. Arbitrage in bullion, coins, bills, stocks, shares and options, **2**, Effingham Wilson, London, 1910.
- [25] D. Duffie, J. Pan and K. Singleton. Transform analysis and asset pricing for affine jump-diffusions, *Econometrica*, **68**(6), 1343-1376, 2000.
- [26] D. Duffie. Numerical Analysis of Jump Diffusion Models: A Partial Differential Equation Approach, Technical Report, Datasim, 2005.
- [27] S.R. Dunbar, Stochastic Processes and Advanced Mathematical Finance [online], viewed 9th Sept 2019, < <http://www.math.unl.edu/~sdunbar1/MathematicalFinance/Lessons/BrownianMotion/Definition/definition> >.
- [28] B. Düring and M. Fournié. High-order compact finite difference scheme for option pricing in stochastic volatility models, *J. Comp. Appl. Math.* **236**, 4462-4473, 2012.
- [29] B. Düring, M. Fournié and C. Heuer. High-order compact finite difference scheme for option pricing in stochastic volatility models on non-uniform grids, *J. Comp. Appl. Math.* **271**, 247-266, 2014.
- [30] B. Düring, M. Fournié, and A. Rigal. High-order ADI schemes for convection-diffusion equations with mixed derivative terms. In: *Spectral and High Order Methods for Partial Differential Equations - ICOSAHOM'12*, M. Azañez et al. (eds.), pp.217–226, Lecture Notes in Computational Science and Engineering 95, Springer, Berlin, Heidelberg, 2013.
- [31] B. Düring, C. Hendricks and J. Miles. Sparse grid high-order ADI scheme for option pricing in stochastic volatility models. In: *Novel Methods in Computational Finance*, M. Ehrhardt et al. (eds.), pp.295–312, Mathematics in Industry 25, Springer, Cham, 2017.
- [32] B. Düring and C. Heuer. High-order compact schemes for parabolic problems with mixed derivatives in multiple space dimensions, *SIAM J. Numer. Anal.* **53**(5), 2113-2134, 2015.
- [33] B. Düring and J. Miles. High-order ADI scheme for option pricing in stochastic volatility models, *J. Comput. Appl. Math.* **316**, 109-121, 2017.

- [34] B. Düring and A. Pitkin. Efficient hedging in Bates model using high-order compact finite differences. In: *Recent Advances in Mathematical and Statistical Methods for Scientific and Engineering Applications, Volume 259*, R. Makarov (eds.) pp.489–498. Springer Verlag, 2018.
- [35] B. Düring and A. Pitkin. High-order compact finite difference scheme for option pricing in stochastic volatility jump models, *J. Comput. Appl. Math.*, **355**, 201-217, 2019.
- [36] B. Düring and A. Pitkin. High-order compact finite difference scheme for option pricing in stochastic volatility with contemporaneous jump models. In: *Progress in Industrial Mathematics at ECMI 2018*, I. Faragó, F. Izsák and P.L. Simon (eds.) pp.365–371, Springer Verlag.
- [37] B. Eraker, M. Johannes and N. Polson. The Impact of Jumps in Volatility and Returns, *J. of Finance* **58** (3), 1269-1300, 2003.
- [38] M. Fakharany, R. Company and L. Jódar. Positive finite difference schemes for a partial integro-differential option pricing model. *Appl. Math. Comp.* **249**, 320-332, 2014.
- [39] J. Gatheral. *The Volatility Surface: A Practitioner's Guide*. John Wiley & Sons, New York, NY, 2006.
- [40] O. Gelderblom and J. Jonker. Amsterdam as the cradle of modern futures and options trading, 1550?1630. In: *The origins of value: the financial innovations that created modern capital markets*, W.M. Goetzmann et al. (eds.), pp.189–205, Oxford University Press, Oxford, 2005.
- [41] M.B. Giles and R.J. Carter. Convergence analysis of Crank-Nicholson and Rannacher time-marching, *J. Comput. Financ.* **9**, 89-102, 2006
- [42] N. Gugole. Merton Jump-Diffusion model versus the Black and Scholes approach for the log-returns and volatility smile fitting, *Int. J. Pure and Appl. Math.*, **109** (3), 719-736, 2016.
- [43] M.M. Gupta, R.P. Manohar, and J.W. Stephenson, A single cell high order scheme for the convection-diffusion equation with variable coefficients, *Int. J. Numer. Methods Fluids*, **4**, 641-651, 1984.

- [44] M.M. Gupta, R.P. Manohar, and J.W. Stephenson, High-order difference schemes for two-dimensional elliptic equations, *Numer. Methods Partial Differential Equations*, **1**, 71-80, 1985.
- [45] E.G. Haug. The History of Option Pricing and Hedging. In: *Vinzenz Bronzin's Option Pricing Models*, W. Hafner et. al. (eds.), pp 471-486, Springer, Berlin, Heidelberg, 2009.
- [46] C. Hendricks, C. Heuer, M. Ehrhardt and M. Günther. High-order ADI finite difference schemes for parabolic equations in the combination technique with applications in finance, *J. Comput. Appl. Math.* **316**, 175-194, 2017.
- [47] S.L. Heston. A closed-form solution for options with stochastic volatility with applications to bond and currency options. *Rev. Financ. Stud.* **6**(2), 327-343, 1993.
- [48] L. Holz. Die Prämien-geschäfte. Doctoral dissertation, Universität Rostock. Rostock, 1905.
- [49] K.J. in't Hout and S. Foulon. ADI finite difference schemes for option pricing in the Heston model with correlation. *Int. J. Numer. Anal. Mod.* **7**, 303–320, 2010.
- [50] N. Hilber, A. Matache and C. Schwab. Sparse wavelet methods for option pricing under stochastic volatility. *J. Comput. Financ.* **8**(4), 1-42, 2005.
- [51] J.C. Hull and A. White. The Pricing of Options on Assets with Stochastic Volatilities, *Journal of Finance*, **42**, 281-300, 1987.
- [52] J.C. Hull and A. White. Hedging the risks from writing foreign currency options, *Journal of International Money and Finance*, **6**, 131-152, 1987.
- [53] J.C. Hull and A. White. An Analysis of the Bias in Option Pricing Caused by a Stochastic Volatility. In: *Advances in Futures and Options Research: Volume 3*, Greenwich, CT, JAI Press, 1988.
- [54] S. Ikonen and J. Toivanen. Efficient numerical methods for pricing American options under stochastic volatility. *Numer. Methods Partial Differential Equations* **24**(1), 104-126, 2008.
- [55] K. Itô. Stochastic integral, *Proc. Imp. Acad.*, **20**(8), 519-524, 1944.
- [56] C. Johnson. Numerical solution of partial differential equations by the finite element method, Cambridge University Press, Cambridge, 1990.

- [57] S. Karaa and J. Zhang. Convergence and performance of iterative methods for solving variable coefficient convection-diffusion equation with a fourth-order compact difference scheme, *Comput. Math. Appl.*, **44**, 457-479, 2002.
- [58] S.G. Kou. A Jump-Diffusion Model for Option Pricing, *Journal of Management Science*, **48** (8), 955-1101, 2002.
- [59] H.O. Kreiss, V. Thomée and O. Widlund. Smoothing of initial Data and Rates of Convergence for Parabolic Difference Equations, *Comm. Pure Appl. Math.* **23**, 241-259, 1970.
- [60] A.L. Lewis. *Option valuation under stochastic volatility*. Finance Press, Newport Beach, CA, 2000.
- [61] A. Melino and S.M. Turnbull. Pricing foreign currency options with stochastic volatility, *Journal of Econometrics*, **45** (1), 239-265, 1990.
- [62] R.C. Merton. Theory of Rational Option Pricing, *The Bell J. Econ. Management Science*, **4** (1), 141-183, 1973.
- [63] R.C. Merton. Option pricing when underlying stock returns are discontinuous. *J. Financ. Econ.* **3**(1-2), 125-144, 1976.
- [64] M. Moran, Extended Trading Hours Planned for March in SPX and VIX Options [online], viewed 8th Sept 2019, <<https://www.cboe.com/blogs/options-hub/2015/02/06/extended-trading-hours-planned-spx-vix-options>>.
- [65] S.A. Nelson. The A B C of options and arbitrage. The Wall Street Library, New York, 1904.
- [66] A. Pitkin and B. Düring (2019), "C++ implementation of "High-order compact finite difference scheme for option pricing in stochastic volatility jump models"", Mendeley Data, v1 <http://dx.doi.org/10.17632/964tyzmwrn.1>
- [67] D. Poole. Linear Algebra: A Modern Introduction. Thomson Brooks, 2006.
- [68] R. Rannacher. Finite element solution of diffusion problems with irregular data, *Numer. Math.*, **43**, 309-327, 1984.
- [69] E. Renault and N. Touzi. Option hedging and implied volatilities in a stochastic volatility model, *Mathematical Finance*, **6**, 279-302, 1996.

- [70] S.M. Ross. Introduction to Probability Models, 8th Edition, Academic Press, 2003.
- [71] M.J. Ruijter and C.W. Oosterlee. Two-dimensional Fourier cosine series expansion method for pricing financial options, *SIAM J. Sci. Comp.* **34**(5), 642–671, 2012.
- [72] E.W. Sachs and A.K. Strauss. Efficient solution of a partial integro-differential equation in finance, *Appl. Numer. Math.* **58**, 1687-1703, 2008.
- [73] S. Salmi and J. Toivanen. An IMEX-scheme for pricing options under stochastic volatility with jumps, *Appl. Numer. Math.* **84**, 33-45, 2014.
- [74] S. Salmi, J. Toivanen and L. von Sydow. An IMEX-scheme for pricing options under stochastic volatility models with jumps, *SIAM J. Sci. Comp.*, **36**(5), B817-B834, 2014.
- [75] P.A. Samuelson. Mathematics of speculative price, *SIAM Review*, **15**, 1-42, 1973.
- [76] L.O. Scott. Option Pricing When the Variance Changes Randomly: Theory, Estimation, and an Application, *Journal of Financial and Quantitative Analysis*, **22**, 419-438, 1987.
- [77] W.F. Spitz and G.F. Carey. A high-order compact formulation for the 3D Poisson equation, *Numer. Methods Partial Differential Equations*, **12**, 235-243, 1996.
- [78] W.F. Spitz and G.F. Carey. Extension of high-order compact schemes to time-dependent problems, *Numer. Methods Partial Differential Equations*, **17**, 657-672, 2001.
- [79] C. Sprenkle. Warrant prices and indicators of expectations and preferences, In: *The Random Character of Stock Market Prices*, pp.412–417, MIT Press, Cambridge, Mass., 1967.
- [80] L. von Sydow, J. Toivanen and C. Zhang. Adaptive finite difference and IMEX time-stepping to price options under Bates Model, *Int. J. Comput. Math.*, **92**(12), 2515-2529, 2015.
- [81] D. Tavella and C. Randall. *Pricing Financial Instruments: The Finite Difference Method*. John Wiley & Sons, 2000.
- [82] S.H. Wang. Jump diffusion model. In: *Encyclopedia of Finance* Lee C.F. Lee et al. (eds.), Springer, Boston, MA, 2006.
- [83] N. Wiener. Optics and the theory of stochastic processes, *J. Opt. Soc. Am.*, **43**(17), 225-228, 1956.

- [84] P. Wilmott. Derivatives. The Theory and Practice of Financial Engineering, John Wiley & Sons, Chichester, UK, 1998.
- [85] W. Zhu and D.A. Kopriva. A spectral element approximation to price European options with one asset and stochastic volatility. *J. Sci. Comput.* **42**(3), 426-446, 2010.
- [86] R. Zvan, P.A. Forsyth and K.R. Vetzal. Penalty methods for American options with stochastic volatility. *J. Comp. Appl. Math.* **91**(2), 199-218, 1998.

## Appendix A

# Derivation of the Black-Scholes partial differential equation

In this appendix we show the derivation of the PDE of the Black-Scholes model from [84]. Recalling the Black-Scholes model we have,

$$dS(t) = \mu S(t)dt + \sigma S(t)dW(t), \quad (\text{A.1})$$

where  $\mu$  is the constant drift,  $\sigma$  is the constant volatility of the asset  $S$  and  $dW$  is a Wiener process. With the use of Lemma 1.1, we have

$$dV = \left( \mu S \frac{\partial V}{\partial S} + \frac{1}{2} \sigma^2 S^2 \frac{\partial^2 V}{\partial S^2} + \frac{\partial V}{\partial t} \right) dt + \sigma S \frac{\partial V}{\partial S} dW. \quad (\text{A.2})$$

If we now create a portfolio  $P$  with structure  $P = V - \alpha S$ , we get

$$dP = dV - \alpha dS. \quad (\text{A.3})$$

Substituting (A.1) and (A.2) into (A.3), we have

$$dP = \sigma S \left( \frac{\partial V}{\partial S} - \alpha \right) dW + \left( \mu S \frac{\partial V}{\partial S} + \frac{1}{2} \sigma^2 S^2 \frac{\partial^2 V}{\partial S^2} + \frac{\partial V}{\partial t} - \alpha \mu S \right) dt.$$

To create a risk-free portfolio  $\Pi$  we may choose  $\alpha = \frac{\partial V}{\partial S}$ . Hence, without arbitrage

$$d\Pi = r\Pi dt$$

follows, and we have

$$d\Pi = \left( \frac{\partial V}{\partial t} + \frac{1}{2} \sigma^2 S^2 \frac{\partial^2 V}{\partial S^2} \right) dt.$$

Through comparing these two equations and the use of  $\Pi = V - \frac{\partial V}{\partial S} S$ , we now obtain the Black-Scholes partial differential equation, where

$$\frac{\partial V}{\partial t} + \frac{\sigma^2 S^2}{2} \frac{\partial^2 V}{\partial S^2} + rS \frac{\partial V}{\partial S} - rV = 0.$$

## Appendix B

# Derivation of the Heston partial differential equation

In this appendix we show the derivation of the PDE from the Heston model, as seen in [39]. Recalling the Heston model we have,

$$\begin{aligned} dS(t) &= \mu S(t)dt + \sqrt{\sigma(t)}S(t)dW^{(1)}(t), \\ d\sigma(t) &= \kappa\sigma(t)(\theta - \sigma(t))dt + v\sigma(t)dW^{(2)}(t), \end{aligned}$$

with correlation  $\rho$ , such that  $dW^{(1)}(t)dW^{(2)}(t) = \rho dt$ .

To derive the PDE from the Heston model, we first form a portfolio of one option  $V = V(S, \sigma, t)$ ,  $\Delta$  units of the asset  $S$  and  $\phi$  units of another option  $U = U(S, \sigma, t)$ . This value of this portfolio is

$$\Pi = V + \Delta S + \phi U$$

with  $\Pi = \Pi_t$ . By assuming the portfolio is self-financing, the change in the portfolio value is

$$d\Pi = dV + \Delta dS + \phi dU \tag{B.1}$$

By applying the two-dimensional lemma of Itô, Lemma 1.2, and differentiating with respect to the variables  $t$ ,  $S$  and  $\sigma$ , we have

$$dV = \frac{\partial V}{\partial t}dt + \frac{\partial V}{\partial S}dS + \frac{\partial V}{\partial \sigma}d\sigma + \frac{1}{2}\sigma S^2 \frac{\partial^2 V}{\partial S^2}dt + \frac{1}{2}v^2\sigma \frac{\partial^2 V}{\partial \sigma^2}dt + \rho v\sigma S \frac{\partial^2 V}{\partial S \partial \sigma}dt.$$

We continue by applying Itô's Lemma to  $U$ , before substituting these two expressions into (B.1), yielding,

$$\begin{aligned} d\Pi = & \left\{ \frac{\partial V}{\partial t} + \frac{1}{2}\sigma S^2 \frac{\partial^2 V}{\partial S^2} + \frac{1}{2}v^2\sigma \frac{\partial^2 V}{\partial \sigma^2} + \rho v\sigma S \frac{\partial^2 V}{\partial S \partial \sigma} \right\} dt \\ & + \phi \left\{ \frac{\partial U}{\partial t} + \frac{1}{2}\sigma S^2 \frac{\partial^2 U}{\partial S^2} + \frac{1}{2}v^2\sigma \frac{\partial^2 U}{\partial \sigma^2} + \rho v\sigma S \frac{\partial^2 U}{\partial S \partial \sigma} \right\} dt \\ & + \left\{ \frac{\partial V}{\partial S} + \phi \frac{\partial U}{\partial S} + \Delta \right\} dS + \left\{ \frac{\partial V}{\partial \sigma} + \phi \frac{\partial U}{\partial \sigma} \right\} d\sigma. \quad (\text{B.2}) \end{aligned}$$

In order for the portfolio to be hedged against movements in the underlying asset and against moves in volatility, the final two terms in (B.2) must be zero, hence we have

$$\phi = -\frac{\frac{\partial V}{\partial \sigma}}{\frac{\partial U}{\partial \sigma}} \quad \text{and} \quad \Delta = -\phi \frac{\partial U}{\partial S} - \frac{\partial V}{\partial S}.$$

Furthermore, the portfolio must earn the risk-free rate  $r$ . Therefore,  $d\Pi = r\Pi dt$ . Combining these results with the values of  $\phi$  and  $\Delta$  gives the change in the value of the risk-free portfolio as

$$\begin{aligned} d\Pi = & \left\{ \frac{\partial V}{\partial t} + \frac{1}{2}\sigma S^2 \frac{\partial^2 V}{\partial S^2} + \frac{1}{2}v^2\sigma \frac{\partial^2 V}{\partial \sigma^2} + \rho v\sigma S \frac{\partial^2 V}{\partial S \partial \sigma} \right\} dt \\ & + \phi \left\{ \frac{\partial U}{\partial t} + \frac{1}{2}\sigma S^2 \frac{\partial^2 U}{\partial S^2} + \frac{1}{2}v^2\sigma \frac{\partial^2 U}{\partial \sigma^2} + \rho v\sigma S \frac{\partial^2 U}{\partial S \partial \sigma} \right\} dt \end{aligned}$$

which can be written as  $d\Pi = (A + \phi B)dt$ . Hence, we have

$$A + \phi B = r(V + \Delta S + \phi U).$$

Substituting for  $\phi$  and re-arranging gives (B.3), which enables further manipulation.

$$\frac{A - rV + rS \frac{\partial V}{\partial S}}{\frac{\partial V}{\partial \sigma}} = \frac{B - rU + rS \frac{\partial U}{\partial S}}{\frac{\partial U}{\partial \sigma}} \quad (\text{B.3})$$

The left-hand side of (B.3) is a function of  $V$  only, and the right-hand side if a function of  $U$  only. We can therefore write (B.3) as a function  $f(S, \sigma, t)$  of  $S$ ,  $\sigma$  and  $t$ . Heston, specified that we set this function as  $f(S, \sigma, t) = -\kappa(\theta - \sigma) + \lambda(S, \sigma, t)$ , where  $\lambda(S, \sigma, t)$  is the price of volatility risk. Substituting  $f(S, \sigma, t)$  into the left-hand side of (B.3), then substituting for  $B$ , and rearranging produces the Heston PDE expressed in terms of the price  $S$

$$\frac{\partial V}{\partial t} + \frac{1}{2}\sigma S^2 \frac{\partial^2 V}{\partial S^2} + \rho v\sigma S \frac{\partial^2 V}{\partial S \partial \sigma} + \frac{1}{2}v^2\sigma \frac{\partial^2 V}{\partial \sigma^2} + rS \frac{\partial V}{\partial S} + \kappa(\theta - \sigma) \frac{\partial V}{\partial \sigma} - rV = 0. \quad (\text{B.4})$$

This is Equation (6) of Heston [47], which can yield closed-form solutions under certain restrictions. To achieve this, Heston assumes that the characteristic function for the logarithm of the terminal asset price,  $x = \ln S_T$ , are of the form

$$f(\phi; x, v) = \exp(C(\tau, \phi) + D(\tau, \phi)v_0 + i\phi x)$$

where  $C$  and  $D$  are coefficients and  $\tau = T - t$  is the time to maturity.

## Appendix C

# Derivation of the Bates partial intergro-differential equation

In this appendix we show the derivation of the PIDE from Bates' model, as seen in [20]. Recalling Bates' model we have,

$$dS(t) = \mu_B S(t)dt + \sqrt{\sigma(t)}S(t)dW_1(t) + S(t)dJ, \quad (\text{C.1})$$

$$d\sigma(t) = \kappa(\theta - \sigma(t))dt + v\sqrt{\sigma(t)}dW_2(t), \quad (\text{C.2})$$

We allow the no-arbitrage condition to fix the drift of the risk neutral process: under the risk neutral probability  $\mu = r - \lambda$ , and apply Itô's Lemma to (C.1) to obtain the equation for the log-price  $x(t) = \ln S(t)$ .

$$dx(t) = (r - \lambda\xi_B)dt + \sqrt{\sigma(t)}dW_1(t) + dJ$$

To obtain the PIDE, we follow the method of Heston [47] as described in Appendix B, by first computing the characteristic function of the continuous component of  $x^c(t)$  of  $x(t)$ . Letting

$$f(x, \sigma, t) = E \left\{ e^{iux^c(t)} \mid x^c(t) = x, \sigma(t) = \sigma \right\}$$

and applying Itô's Lemma to  $M(t) = f(x, \sigma, t)$ , yields

$$\begin{aligned} dM(t) = & \left( \frac{1}{2}\sigma(t)\frac{\partial^2 f}{\partial x^2} + \rho v\sigma(t)\frac{\partial^2 f}{\partial x\partial\sigma} + \frac{1}{2}v^2\sigma(t)\frac{\partial^2 f}{\partial\sigma^2} + (r - \lambda\xi_B)\frac{\partial f}{\partial x} \right. \\ & \left. + \kappa(\theta - \sigma(t))\frac{\partial f}{\partial\sigma} + \frac{\partial f}{\partial t} \right) dt + \sqrt{\sigma}\frac{\partial f}{\partial x}dW_1(t) + \theta\sqrt{\sigma}\frac{\partial f}{\partial\sigma}dW_2(t). \quad (\text{C.3}) \end{aligned}$$

Next, since  $f(x, \sigma, t)$  is a martingale, by setting the drift term in (C.3) to zero, we obtain

$$\frac{\partial f}{\partial t} + \frac{1}{2}\sigma \frac{\partial^2 f}{\partial x^2} + \rho v \sigma \frac{\partial^2 f}{\partial x \partial \sigma} + \frac{1}{2}v^2 \sigma \frac{\partial^2 f}{\partial \sigma^2} + (r - \lambda \xi_B) \frac{\partial f}{\partial x} + \kappa(\theta - \sigma) \frac{\partial f}{\partial \sigma} = 0. \quad (\text{C.4})$$

Finally, we convert back to the asset price  $S = e^{x(t)}$  and since jump terms are homogeneous and independent from the continuous part, we can add the integral describing the jump-term with Gaussian distribution and obtain Bates' PIDE for the price of an option  $V$ .

$$\begin{aligned} \frac{\partial V}{\partial t} + \frac{1}{2}S^2 \sigma \frac{\partial^2 V}{\partial S^2} + \rho v \sigma S \frac{\partial^2 V}{\partial S \partial \sigma} + \frac{1}{2}v^2 \sigma \frac{\partial^2 V}{\partial \sigma^2} + (r - \lambda \xi_B) S \frac{\partial V}{\partial S} + \kappa(\theta - \sigma) \frac{\partial V}{\partial \sigma} - (r + \lambda)V \\ + \lambda \int_0^{+\infty} V(S\tilde{y}, v, t) p(\tilde{y}) d\tilde{y} = 0 \end{aligned}$$

## Appendix D

### Code

The codes for the C++ implementation of the high-order compact and second-order finite difference schemes utilised in Chapter 2 are available online through Mendeley Data <http://dx.doi.org/10.17632/964tyzmwrn.1> [66]. The implementation requires both GSL2.1 or higher and UMFPACK libraries.